

**Advances in lipopolyplexes as efficient non-viral carrier for  
nucleic acid delivery**

Dissertation

zur

Erlangung des Doktorgrades

der Naturwissenschaften

(Dr. rer. nat.)

dem

Fachbereich Pharmazie der  
Philipps-Universität Marburg

vorgelegt von

**Hirva Shah**

aus Gujarat, India

Marburg/Lahn **2023**

Erstgutachter: **Prof. Dr. Udo Bakowsky**

Zweitgutachter: **Prof. Dr. Frank Runkel**

Eingereicht am: **23.01.2023**

Tag der mündlichen Prüfung am: **07.03.2023**

Hochschulkenziffer: 1180

**Advances in lipopolyplexes as efficient non-viral carrier for  
nucleic acid delivery**

Thesis

Submitted in the fulfilment of the requirement of degree of

Doctor of Natural Science (Dr.rer.nat.)

Equivalent to

Doctor of Philosophy (Ph.D.)

To

The Faculty of Pharmacy

University of Marburg

by

**Hirva Shah**

from Gujarat, India

Marburg/Lahn **2023**

First Supervisor: **Prof. Dr. Udo Bakowsky**

Second Supervisor: **Prof. Dr. Frank Runkel**

Date of Submission: **23.01.2023**

Defense date: **07.03.2023**

Hochschulkennziffer: 1180

# EIDESSTATTLICHE ERKLÄRUNG

Ich versichere, dass ich meine Dissertation

## **„ Advances in lipopolyplexes as efficient non-viral carrier for nucleic acid delivery“**

selbständig ohne unerlaubte Hilfe angefertigt und mich dabei keiner anderen als der von mir ausdrücklich bezeichneten Quellen bedient habe. Alle vollständig oder sinngemäß übernommenen Zitate sind als solche gekennzeichnet.

Die Dissertation wurde in der jetzigen oder einer ähnlichen Form noch bei keiner anderen Hochschule eingereicht und hat noch keinen sonstigen Prüfungszwecken gedient.

Marburg, den 23.01.2023



.....  
**(Hirva Shah)**

# AUTHOR'S DECLARATION

I declare that this thesis titled

**„ Advances in lipopolyplexes as efficient non-viral carrier for nucleic acid delivery“**

has been written entirely by myself and is a record of work performed by myself. The research was carried out at the Institut für Pharmazeutische Technologie und Biopharmazie, University of Marburg, under supervision of Professor Udo Bakowsky.

This thesis has not been submitted in any form elsewhere for a higher degree.

Marburg, 23.01.2023



---

**(Hirva Shah)**

## ACKNOWLEDGEMENTS

My profound and sincere gratitude to my research supervisor Prof. Dr. Udo Bakowsky for his invaluable guidance during my whole Ph.D. research work. His continuous support, and advice helped me in all phases of research. I am thankful for his motivation and patience during my work. His indispensable scientific knowledge has led discussion towards solutions and had brought a new perspective in my way of scientific work.

I would also like to thank Dr. Shashank Reddy Pinnapireddy for fruitful scientific discussions and his willingness to help during my research work. A sincere thanks to Dr. Konrad Engelhardt for his scientific discussion, problem solving approach and support, which facilitate my work. I would like to express sincere thanks Dr. Muhammad Umair Amin for his scientific discussion and constant support during my research work. I am grateful to Dr Jens Schäfer, Dr. Jana Brüßler, and Dr. Eduard Preis for their invaluable and sensible advise.

I would like to acknowledge Mrs. Eva Maria Mohr for her support and motivation throughout my research work. A special thanks to Julia Michaelis for her guidance and eagerness to help. A special thanks to all scholars of research group Bakowsky, with whom I had fun in the last four years. Special thanks to Dr. Imran Tariq, Dr. Alice Abu Dayyih, Sascha Hubing, Ahmed M. Abdelsalam, Abdallah M. Ayoub, Tan Shi, Jan Schulze, and Julia Janina Schüer.

I am grateful to my spiritual mentor and my beloved parents, whose blessings and guidance gave me strength in whatever I pursue. Most importantly, I would like to thank my husband, Jaimin Modi for his support, encouragement, and patience during my research work.

Die vorliegende Arbeit entstand auf Anregung und unter Leitung von

*Herrn Prof. Dr. Udo Bakowsky*

am Institut für Pharmazeutische Technologie

und Biopharmazie der Philipps-Universität

Marburg



# INDEX

<b>1. Introduction</b>	<b>9</b>
1.1 Gene therapy	9
1.2 DNA based therapeutics	10
1.3 Biological barriers in gene delivery	12
1.3.1 Extracellular barriers	12
1.3.2 Blood-tissue barriers	14
1.3.3 Intracellular barriers	15
1.4 Endolysosomal escape	18
1.5 Study method of the endocytosis	19
1.5.1 Pre-treatment with pathway inhibitors	19
1.5.2 Codelivery of biomarker	20
1.5.3 Colocalization with a fluorescent fusion protein	20
1.5.4 Immunofluorescent labelling	20
1.6 Stimuli mechanism for endosomal escape	20
1.7 Formulation design strategies for endosomal escape	21
1.8 Non-viral carriers for gene delivery	23
1.8.1 Cationic liposomes	24
1.8.2 Lipoplexes	24
1.8.3 Lipid nanoparticles	26
1.8.4 Solid lipid nanoparticles	27
1.8.5 Polyplexes	28
1.8.6 Lipopolyplexes	29
1.9 Physical methods for transfection	32
1.9.1 Basic principle in sonoporation	32
1.9.2 Basic principle in photochemical internalization	35
1.10 Aim and scope	37
1.11 Objectives	39
<b>2. Materials &amp; Methods</b>	<b>40</b>
2.1 Materials	40
2.1.1 List of materials	40
2.1.2 DPPC	43

2.1.3	DPPG	43
2.1.4	PEG40S	43
2.1.5	DSPE-PEG2000-cyanur	44
2.1.6	Cholesterol	44
2.1.7	IPEI	45
2.1.8	pCMV-Luc	45
2.1.9	pCMV-GFP	46
2.1.10	Hypericin	46
2.1.11	Anti-transferrin antibody	46
2.2	Preparation method	47
2.2.1	Preparation of ultrasound-active lipopolyplexes	47
2.2.2	Preparation of hypericin lipopolyplexes	48
2.2.3	Preparation of antibody conjugated formulation	49
2.3	Characterization methods	51
2.3.1	Dynamic light scattering	51
2.3.2	Laser Doppler anemometry	51
2.3.3	Atomic force microscopy	51
2.3.4	Gel retardation assay	51
2.3.5	Characterization of ultrasound contrast	52
2.3.6	Characterization of photosensitizer loaded formulation	53
2.4	In-vitro cell culture experiments	55
2.4.1	Maintenance and harvesting of cell lines	55
2.4.2	Ultrasound mediated gene delivery	55
2.4.3	Photosensitizer induced gene delivery	59
2.4.4	Selective phototransfection	61
<b>3.</b>	<b>Results &amp; Discussion - Ultrasound - mediated gene delivery</b>	<b>63</b>
3.1	Characterization of ultrasound-active contrast vesicles	63
3.1.1	Ultrasound contrast measurements	63
3.1.2	Average particle size and zeta potential	63
3.1.3	AFM	65
3.2	Characterization of polyplexes and lipopolyplexes	67
3.2.1	N/P ratio optimization	67
3.2.2	Average particle size and zeta potential	68

3.2.3	AFM	69
3.3	In-vitro cell culture evaluation	70
3.3.1	Transfection efficiency	70
3.3.2	Cell viability	72
3.3.3	Ultrasound-mediated transfection	74
3.3.4	LDH release	76
3.3.5	GFP expression	77
3.3.6	Effect of ultrasound on cellular uptake	77
3.3.7	Ultrasound mediated transfection in 3D cell culture	79
<b>4.</b>	<b>Result &amp; Discussion - Photosensitizer induced gene delivery</b>	<b>82</b>
4.1	Characterization of liposomes	82
4.1.1	Entrapment efficiency of hypericin	82
4.1.2	Average particle size and zeta potential	83
4.1.3	TEM	85
4.2	Characterization of polyplexes, lipopolyplexes and hypericin lipopolyplexes	86
4.2.1	N/P ratio optimization	86
4.2.2	Average particle size and zeta potential	87
4.2.3	AFM	88
4.2.4	Fluorescence quenching	89
4.2.5	Photostability of encapsulated plasmid	91
4.3	In-vitro cell culture evaluation	92
4.3.1	Transfection efficiency	92
4.3.2	Cell viability	93
4.3.3	Phototransfection	96
4.3.4	Photocytotoxicity	98
4.3.5	Cellular uptake of hypericin lipopolyplexes	100
4.3.6	Intracellular reactive oxygen species measurements	101
<b>5.</b>	<b>Result &amp; Discussion - Selective phototransfection</b>	<b>104</b>
5.1	Characterization of conjugated hypericin lipopolyplexes	104
5.1.1	Average particle size and zeta potential	104
5.2	In-vitro cell culture evaluation	104

5.2.1	TfR receptor expression in HepG2 cells	104
5.2.2	Ligand mediated cellular uptake	106
5.2.3	GFP expression	107
<b>6.</b>	<b>Summary</b>	<b>109</b>
<b>7.</b>	<b>Zusammenfassung</b>	<b>114</b>
<b>8.</b>	<b>Appendix</b>	<b>119</b>
8.1	References	119
8.2	Abbreviation	135
8.3	Research Output	138
8.3.1	Publication	138
8.3.2	Conference and Workshops	138
8.4	Curriculum Vitae	139

## LIST OF FIGURES

<i>Figure 1. Schematic presentation of DNA non-viral vector delivery.....</i>	<i>10</i>
<i>Figure 2. Schematic presentation of clathrin-mediated endocytosis process.....</i>	<i>19</i>
<i>Figure 3. Formulation and design of cationic liposomes and lipoplexes.....</i>	<i>26</i>
<i>Figure 4. Formulation and design of lipid nanoparticles and solid lipid nanoparticles.....</i>	<i>28</i>
<i>Figure 5. Formulation and design of lipopolyplexes.....</i>	<i>30</i>
<i>Figure 6. Mechanism of sonoporation by cavitation process.....</i>	<i>33</i>
<i>Figure 7. Ultrasound-mediated transfection.....</i>	<i>34</i>
<i>Figure 8. Mechanism of photosensitizer-induced photochemical reactions.....</i>	<i>36</i>
<i>Figure 9. Graphical abstract. Ultrasound-mediated gene delivery.....</i>	<i>37</i>
<i>Figure 10. Graphical abstract: Photosensitizer induced gene delivery.....</i>	<i>38</i>
<i>Figure 11. Thin-film hydration method for preparation of liposome.....</i>	<i>47</i>
<i>Figure 12. Ethanol injection method for preparation of photosensitizer loaded liposome.....</i>	<i>48</i>
<i>Figure 13. Schematic presentation of flow model used for determining the ultrasound contrast.....</i>	<i>53</i>
<i>Figure 14. Ultrasound contrast measurements of ultrasound-active contrast vesicles.....</i>	<i>64</i>
<i>Figure 15. Ultrasound contrast measurements of ultrasound-active lipopolyplexes.....</i>	<i>64</i>
<i>Figure 16. AFM micrograph of ultrasound-active contrast vesicles.....</i>	<i>66</i>
<i>Figure 17. Comparison of ultrasound-active contrast vesicles with standard UCA.....</i>	<i>67</i>
<i>Figure 18. Optimization of N/P ratio.....</i>	<i>68</i>
<i>Figure 19. AFM micrographs of ultrasound-active lipopolyplexes.....</i>	<i>70</i>
<i>Figure 20. Transfection efficiency of polyplexes (lPEI/pDNA complexes) and lipopolyplexes.....</i>	<i>71</i>
<i>Figure 21. Cell viability of cells incubated with polyplexes (lPEI/pDNA complexes) and lipopolyplexes.....</i>	<i>73</i>
<i>Figure 22. Ultrasound-mediated transfection efficiency of ultrasound-active lipopolyplexes.....</i>	<i>75</i>
<i>Figure 23. LDH release upon ultrasound-mediated transfection.....</i>	<i>76</i>
<i>Figure 24. Visualization of GFP expression.....</i>	<i>77</i>
<i>Figure 25. Effect of post-transfection ultrasound treatment on the cellular uptake.....</i>	<i>78</i>
<i>Figure 26. Transfection efficiency of ultrasound-active lipopolyplexes in 3D - cell culture... </i>	<i>80</i>
<i>Figure 27. Absorbance spectra of hypericin liposomes.....</i>	<i>82</i>
<i>Figure 28. Colloidal stability of hypericin liposomes.....</i>	<i>85</i>

<i>Figure 29. Visualization of hypericin liposomes using TEM.</i> .....	86
<i>Figure 30. Entrapment of pDNA in polyplexes by gel electrophoresis.</i> .....	86
<i>Figure 31. Physicochemical characterization of hypericin lipopolyplexes.</i> .....	88
<i>Figure 32. AFM micrograph of hypericin formulation...</i> .....	89
<i>Figure 33. Determination of complex integrity by % fluorescence quenching assay.</i> .....	90
<i>Figure 34. Photostability of encapsulated pDNA by gel electrophoresis.</i> .....	91
<i>Figure 35. Transfection efficiency of lipopolyplexes.</i> .....	92
<i>Figure 36. Cell viability of cells incubated with hypericin liposomes and photoirradiated....</i>	93
<i>Figure 37. Cell viability of cells treated with hypericin lipopolyplexes and photoirradiated.</i>	95
<i>Figure 38. Photochemical induced transfection efficiency of hypericin lipopolyplexes in HepG2 cells.</i> .....	98
<i>Figure 39. Photocytotoxicity of hypericin lipopolyplexes.</i> .....	99
<i>Figure 40. Cellular uptake of hypericin lipopolyplexes.</i> .....	101
<i>Figure 41. Intracellular reactive oxygen species measurement...</i> .....	103
<i>Figure 42. Cellular binding and uptake of FITC-labelled transferrin conjugate.</i> .....	105
<i>Figure 43. Ligand mediated cellular uptake.</i> .....	106
<i>Figure 44. Visualization of GFP expression.</i> .....	107

## LIST OF TABLES

<i>Table 1. FDA approved DNA/RNA based therapeutics .....</i>	<i>11</i>
<i>Table 2. Applicability of DNA delivery system .....</i>	<i>17</i>
<i>Table 3. Strategies to improve endosomal escape .....</i>	<i>22</i>
<i>Table 4. Modification of lipopolyplexes for gene delivery.....</i>	<i>31</i>
<i>Table 5. Commercially available ultrasound contrast agents .....</i>	<i>35</i>
<i>Table 6. Physicochemical properties of the formulations.....</i>	<i>65</i>
<i>Table 7. Physicochemical properties of ultrasound-active lipopolyplexes.....</i>	<i>69</i>
<i>Table 8. Physicochemical properties of hypericin liposomes.....</i>	<i>84</i>
<i>Table 9. IC50 values of hypericin liposomes at different irradiation energies.....</i>	<i>94</i>

## **LIST OF EQUATIONS**

<i>Equation 1. Formula for calculation of N/P ratio -----</i>	<i>48</i>
<i>Equation 2. Formula for calculation of F/P ratio in FITC labelled transferrin -----</i>	<i>50</i>
<i>Equation 3. Formula for calculation of hypericin entrapment efficiency -----</i>	<i>54</i>
<i>Equation 4. Formula for calculation of % fluorescence quenching-----</i>	<i>54</i>
<i>Equation 5. Formula for calculation of irradiation duration -----</i>	<i>59</i>
<i>Equation 6. Formula for calculation of % cytotoxicity -----</i>	<i>60</i>



## 1. Introduction

### 1.1 Gene therapy

Gene therapy has been regarded as a potential strategy to cure various ailments including inherited genetic disorders (such as haemophilia, severe combined immunodeficiency, cystic fibrosis), infectious diseases (SARS CoV 2) or acquired diseases such as cancer. Gene therapy aims to radically treat the causes of the diseases instead of only relieving the symptoms. In 2003, the first gene therapy approved by FDA against cancer was Gendicine, which was commercially available to treat head and neck squamous cell carcinoma.<sup>1,2</sup> Given the improvement and diversity of genetic tool kits and over 3000 clinical gene therapy trials, and investments in the gene-therapy market, the next decade indeed looks bright and promising for gene therapies for human disorders.<sup>3</sup> However, employing nucleic acids as therapeutics is challenging because they are susceptible to degradation by nucleases, contribute to immune activation and have unfavourable physicochemical characteristics that prevent facile transmission into cells. Safe and effective nucleic acid therapeutics, therefore, require sophisticated delivery platform technologies.<sup>4,5</sup>

Currently, about 2400 completed or ongoing clinical gene therapy trials based on viral gene delivery systems have been reported worldwide (September 2020).<sup>3</sup> Among these trials, 26% account for Advs, 12% for AAVs, 23% for retroviral, 15% for lentiviral, 14% for poxviral, 4% for HSVs and finally 6% for other viral gene delivery systems.<sup>3</sup> The viral vectors typically offer higher transduction efficiency. However, considerable technical concerns remain to be addressed. Currently, safety issues and immune system reactions are major challenges in viral vector-based gene therapy. On the other hand, the non-viral delivery vehicles are non-integrative and less efficient compared to other gene therapeutic toolkits but have the potential to address many of the challenges of viral vectors, particularly concerning safety issues.<sup>6</sup> About 900 completed or ongoing trials on non-viral gene delivery comprises 56% account for pDNA, 7% for therapeutic mRNA, 6% for RNAi technology, less than 1% for DNAi technology, 15% for ASOs, 1% for miRNA mimic, 3% for aptamers, and finally, 12% for CpG-ODN.<sup>3</sup> Development of engineered viral strains, development of new viral vectors, and improvement of non-viral gene delivery methods could overcome pre-existing immunity and enhance the efficiency of

gene therapy in clinical practice. Furthermore, improving the systemic half-life of gene therapies would increase therapeutic durability.<sup>7</sup>

## 1.2 DNA based therapeutics

These potent therapeutics include plasmids containing transgenes, oligonucleotides, aptamers, ribozymes and DNAzymes. Plasmids are high molecular weight, double-stranded DNA constructs containing transgenes, which encode specific proteins.<sup>1</sup> On a molecular level, plasmid DNA molecules can be considered prodrugs that upon cellular internalization employ the DNA transcription and translation apparatus in the cell to biosynthesize the therapeutic entity, known as protein. The mechanism of action of plasmid DNA requires that the plasmid molecules gain access to the nucleus after entering the cytoplasm. The entry of plasmid molecules into the nucleus through the nuclear pores is a challenging process.<sup>8</sup> The design and engineering of a plasmid DNA molecule contain typically regulatory signals such as promoter and enhancer sequences (Figure 1). The promoter, a vital sequence, offers recognition sites for the RNA polymerase to initiate the transcription process. Higher efficiency can be obtained by engineering the plasmid with strong tissue or tumor specific promoters.

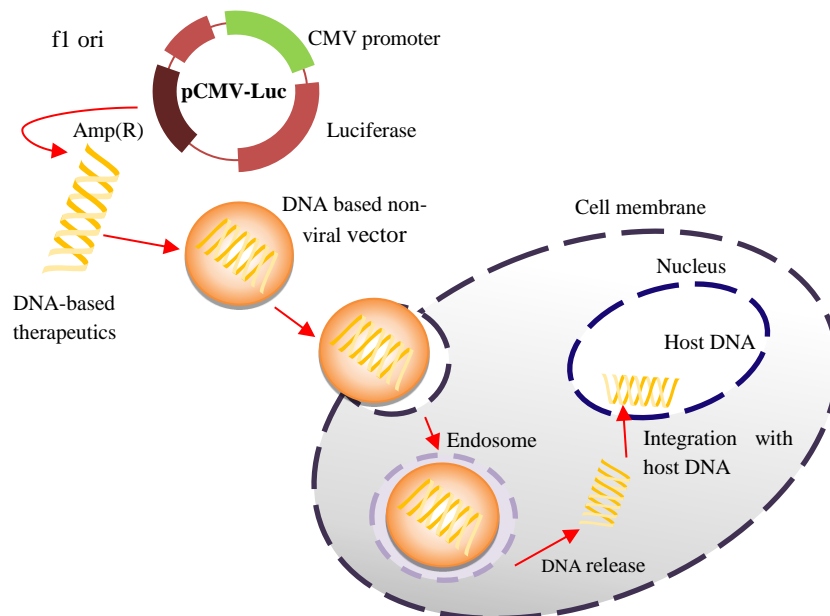


**Figure 1. Schematic presentation of DNA non-viral vector delivery.** An exogenous plasmid (e.g. pCMV-Luc) encapsulated in the non-viral vector undergoes cellular uptake by mammalian cells (mostly diseased cells) via the endocytosis process followed by integration with host DNA in the nucleus.

Commonly used promoter sequences are derived from viral origins such as cytomegalovirus (CMV).<sup>9</sup> The enhancers are regions on the plasmid DNA that enhance the production of the gene of interest by as much as several hundred times. It can be tissue-specific and can be present on the plasmid locus either upstream or downstream from the promoter region. The transcription can be substantially improved by the choice of suitable enhancers.<sup>10</sup> Table 1 enlists some approved DNA therapeutics for specific diseases.

**Table 1. FDA approved DNA/RNA based therapeutics**

<b>Drug candidate</b>	<b>Type of DNA-based therapeutics</b>	<b>Molecular Basis of action</b>
Gendicine	Plasmid	Adenovirus encoding the tumor suppressor p53 gene for head and neck squamous cell carcinoma <sup>11</sup>
Vitravene	siRNA	Inhibitor of immediate-early region 2 (IE2) of human cytomegalovirus for Cytomegalovirus retinitis in AIDS patients <sup>12</sup>
Affinitak	siRNA	Inhibitor of protein kinase c- alpha (PKC- alpha) expression for non-small cell lung cancer <sup>13</sup>
Alicaforsen	siRNA	Inhibitor of intracellular adhesion molecule 1 (ICAM-1) in Crohn's disease <sup>14</sup>
Genasense	siRNA	Inhibitor of B cell leukaemia/lymphoma 2 (Bcl-2) protein in chronic lymphomatic leukaemia. <sup>15</sup>
Comirnaty	mRNA	mRNA translated to produce a modified SARS-CoV-2 spike (S) protein antigen,
mRNA-1273	mRNA	which is recognized by the host immune system. <sup>16</sup>

### 1.3 Biological barriers in gene delivery

The delivery of therapeutics to the desired biological site of action and at required rates is limited by numerous biological barriers depending on route of administration. The biological barriers include the skin, mucosal membranes, blood-brain barrier, and cell and nuclear membrane. Overcoming biological barriers constitutes a key hurdle in the field of gene delivery. While these barriers serve the natural protective function in the body, they limit the delivery of therapeutics into the body.<sup>17,3</sup>

#### 1.3.1 Extracellular barriers

Extracellular barriers towards the gene delivery system are encountered from the injection site of the nanocarrier until the genetic material reaches the cell membrane of desired cells and is endocytosed inside the cell. Extracellular barriers make the transferring of extrinsic genes difficult in the body.

##### *a. Mononuclear phagocytic system*

In vivo, certain serum proteins promote the recognition and uptake of nanoparticles by macrophages of the mononuclear phagocytic system (MPS), i.e., opsonins. The nanoparticles may be opsonized by blood proteins following which they can be recognized by the cells of the mononuclear phagocyte system (MPS) and cleared from circulation. However, based on the immunogenicity of the non-viral gene delivery system, some researchers have exploited this property target immune cells such as tumor-associated macrophages and dendritic cells.<sup>18,4</sup> The total combination of monocytes, mobile macrophages, fixed tissue macrophages, and a few specialized endothelial cells in the bone marrow, spleen, and lymph nodes compose the mononuclear phagocytic system or the reticuloendothelial system.<sup>19</sup>

##### *b. Extravasation*

The extravasation of nanocarriers is a function of their size and the permeabilities of the vascular layers. With exception of the liver, the body tissues are difficult to extravasate from the blood capillaries because of the small gaps between nonfenestrated endothelial cells (< 5 nm). Moreover, the vascular endothelial layer is one of its most significant barriers and represents a semi-permeable layer of cells which lines the inner walls of the blood vessels and along with the glycocalyx, a proteoglycan layer, serves to control the

permeability of solutes and macromolecules across blood vessels. The glycocalyx ‘coat’ imparts a negative charge to the endothelial cell membrane and thus physicochemical characteristics have been implicated to affect extravasation into tumor microspace.<sup>17, 20</sup>

*c. Enhanced permeability retention*

Nanoparticles can passively target tumor tissues because of the enhanced permeability and retention (EPR) effect which is caused by leakiness of neovasculature and insufficient lymphatic drainage in tumors. Rapid tumor growth leads to angiogenesis with pore diameter ranging from 100 nm to 800 nm, which allows molecules or particles larger than 40 kDa to extravasate from blood vessels and accumulate in tumor tissues, providing a huge opportunity for preferential tumor accumulation of nanomedicine. The passive tumor targeting can be designed based on the enhanced permeability retention (EPR effect) of the tissue.<sup>20</sup>

*d. Heterogeneity of enhanced permeability retention (EPR)*

EPR effect is a very heterogenous phenomenon. Its presence and magnitude depend on the type of tumor under consideration, whether the lesion is of primary or metastatic origin and the characteristics of the individual patient. Within a given tumor, the accumulation of nanoparticle therapeutics may be heterogenous owing to internal tissue composition and characteristics. For less well-vascularized lesions, the efficiency of accumulation tends to be higher for smaller particles, however the influence of particle sizes diminishes as the lesion vascularization and leakiness increase. The species under investigation will also affect the conclusion and findings of EPR effect.<sup>21</sup>

*e. Mucous barrier*

Along with the cellular constitution, the barriers also have non-cellular elements that are essential barriers to protect the organ. Majorly, these non-cellular barriers are mucous barrier. Mucus is a complex barrier synthesized by secretory cells, specifically goblet cells. The major constituents of mucus are water (95–99%) and mucin, a high molecular weight glycoprotein that can be found either bound to membranes or in a secretory form. Depending on the mucus composition, the diffusion of nanoparticles having particle size (100 nm) was more restricted in colonic and tracheal tissue than in the small intestinal mucosal tissue. The diffusion was least restricted in oestrus-phase vaginal tissue.<sup>19, 22</sup>

### 1.3.2 Blood-tissue barriers

The blood-tissue barrier have a well-defined anatomic substrate: endothelium or epithelium near the vicinity of the capillary. Epithelia with barrier function typically have a dense intercellular junction and few pinocytotic vesicles. The exclusion of macromolecules from the tissue is called the blood-tissue barrier. Common examples for barriers are the blood-brain, the blood-placenta-, the blood-retina-, the blood-air- and the blood-thymus -barrier. These barriers express many transporters for the selective transport and for the exchange of molecules.

#### *a. Blood-brain barrier*

A highly controlled microenvironment is required to promote the normal function of the central nervous system. These biological barriers are established by different cells at three key interfaces: the blood-brain barrier (BBB), blood-cerebrospinal fluid barrier (BCB) and the arachnoid barrier.<sup>23</sup> BBB, considered as the largest interface for blood-brain exchange, consists of surface area per average adult between 12 and 18 m<sup>2</sup>. It plays a critical role in protecting the brain parenchyma from blood-borne agents and providing a significant obstacle to the entry of drugs and other exogenous compounds into the central nervous system.<sup>24</sup> BBB is formed by microvascular endothelial cells lining the cerebral capillaries penetrating the brain and spinal cord. These include the following: (1) the expression of tight junctions (TJs), sealing the paracellular pathways between adjacent endothelial cells, thus preventing the unregulated passage of polar (water-soluble) molecules between the blood and the brain; (2) the absence of fenestrations; (3) the lack of pinocytic activity and the expression of active transport mechanisms to regulate the passage of essential molecule (including nutrients and essential amino acids) while blocking the passage of potentially undesired substance (both endogenous and xenobiotics).<sup>25</sup>

#### *b. Air-blood barrier*

Alveolar walls present in the lung is the site of gas-exchange. Its structure supports passive diffusion of the respiratory gases by spreading the pulmonary capillary bed over an immense surface area and by having an extremely thin air-blood barrier. The pulmonary lining fluid at the alveolar region reduces significantly in thickness (0.09 – 0.8 μm) and is composed pulmonary surfactant. Pulmonary surfactant is a lipid/protein

complex essential to keep the airspaces of mammalian lung open.<sup>26</sup> Below the surfactant layer, the lung epithelial cells (type I and type II pneumocytes) and the underlying endothelial cells form the air-blood barrier.<sup>27</sup> The pulmonary surfactant in the alveolar region and the mucus layer in the conducting airways constitute the pulmonary lining liquid, which can be considered the major non-cellular pulmonary barrier to inhaled therapeutics. Alveolar macrophages patrol the air spaces in the deep lung and have the ability to efficiently clear inhaled particles in the 1–5  $\mu\text{m}$  size range. Thus, alveolar macrophages pose a significant barrier to therapeutic particles reaching the alveolar space.<sup>28</sup>

### **1.3.3 Intracellular barriers**

Earlier the focus has been on delivery to the target cells and transcription to optimize transfection and gene therapy. However, over the past few years intracellular trafficking of plasmids is more than just a black box and its one of the major barriers to effective gene delivery.

#### *a. Cellular membrane*

When nanocarrier surf onto the surface of the cell membrane, cellular uptake may occur through endocytosis or membrane fusion. The nanocarrier internalizes the intracellular space depending solely on its interaction with the cell membrane.<sup>29</sup> Various models have been used to study these interactions and it has been seen that surface charge, hydrophobicity and size play prominent roles.<sup>30</sup> The nanocarrier internalized by cells mainly through endocytosis can be divided into clathrin-mediated endocytosis (CME), caveolae-mediated endocytosis (CavME), phagocytosis, macropinocytosis, and clathrin/caveolae-independent endocytosis. In contrast, membrane fusion is a direct translocation of nanocarrier into the cytoplasm, resulting in efficient drug delivery to the cytoplasm without endosomal entrapment and enzymatic degradation<sup>31</sup> The physicochemical properties of nanocarrier including size, charge, lipid composition, surface modification are important factors in determination of endocytosis pathway of cellular uptake.<sup>19</sup>

*b. Endosomal membrane*

Followed by endocytosis process, the nanocarriers are enveloped by endosomal membrane and undergo maturation with the gradual acidification of the lumen, i.e., transition from early endosomes to recycling/multivesicular late endosomes, during which the wrapped nanocarrier is released and directed to the cytoplasm. Unfortunately, the late endosomes prefer to transport their preys to lysosomes for further degradation. The key to successful cytosolic delivery of therapeutics is to escape the endosomal/lysosomal pathway<sup>32</sup>.

*c. Cytoplasmic trafficking*

The cytoplasm resembles a reversible gel-sol system which is composed of multiple cytoskeletal elements including microfilaments, microtubules and lattice work that is constantly remodelling itself in response to a variety of internal and external stimuli.<sup>33</sup> The cytoplasm is a mesh-like cytoskeletal network and macromolecular crowding in which only particles with a diameter less than 50 nm can diffuse freely.<sup>34</sup> Microinjected DNA fragments > 2000 bp in length show no translational diffusion through cytoplasm. It was found that only small DNA fragments (< 250 bp) diffused rapidly to the nucleus by Brownian motion after microinjection into the cytoplasm.<sup>35</sup> Besides size-dependent geometrical constraints, non-specific interaction between nanocarriers and intracellular constituents, such as vesicles, organelles, and internal membranes, is another important factor decelerating cytoplasmic diffusion.

*d. Nuclear membrane*

The nuclear membrane acts as an envelope which regulates all traffic of macromolecules, including proteins, DNAs, RNAs and oligonucleotides between the cytosol and the nucleus. The final obstacle for successful transfection except for DNA-based cargo is entry into the nucleus from the cytoplasm. The nuclear transport is a major barrier in non-dividing cells. The non-viral gene therapy is greatly limited by the lower nuclear membrane permeability of therapeutic nucleic acid. These biological barriers and the methods to overcome the challenges for efficient DNA delivery have been tabularised in Table 2.



**Table 2. Applicability of DNA delivery system**

<b>Challenges</b>	<b>Method of overcoming the challenges</b>
DNA charge, shape, and size	Complexing the DNA with polycationic polymer helps to decrease the size and neutralizes the negative charge <sup>36</sup>
Serum nuclease degradation	Encapsulation of DNA in nanocarrier decreases the interaction of DNA with nucleases <sup>37</sup>
<b>Extracellular barriers</b>	
Physical instability of DNA delivery system	Steric stabilization by PEGylation of lipid or polymeric nanocarrier improves colloidal stability <sup>38</sup>
RES and hepatic clearance	
Extravasation	Direct tissue injection of the DNA-polycation nanocarrier <sup>36</sup>
Poor biodistribution and cellular targeting	Ligand-attached DNA nanocarrier delivery systems for target cells having overexpressed receptors alters pharmacokinetics favorably <sup>38</sup>
<b>Intracellular barriers</b>	
Endosomal escape and lysosomal degradation of DNA	Use of fusion lipids such as DOPE, endosomolytic agents such as chloroquine enhances DNA release from the endosomes <sup>39</sup>
Trafficking of DNA through cytoplasm	Nano-carrier enhances nuclear entry <sup>39</sup>
Nuclear transport	Sequence-specific nuclear import of plasmid DNA e.g., SV40 DNA sequence is employed for transfection during cell division. Transcription factors containing nuclear localization signals (NLS) also facilitates the process. <sup>40</sup>
Biological immune barrier	DNA sequences that cause immune response can be altered to remove the immune factor <sup>41,42</sup>
Scale-up barrier	Critical process parameters affecting the scale-up and production of gene delivery product are monitored. <sup>43</sup>

## 1.4 Endolysosomal escape

Endocytosis is a major pathway for cellular uptake of nanocarrier having a nanometer size. Poor endosomal escape of non-viral systems poses a major challenge for the intracellular delivery of nucleic acids. A lipid-based nanocarrier enters the eukaryotic cells majorly by clathrin-mediated endocytosis process (Figure 2). The endocytic pathway involves the formation of intracellular vesicles that transforms into various endocytic compartments. There are a series of maturation and fusion steps that are hypothesized to occur as the endosomes transform from early endosomes (pH 6.3) to lysosomes (pH 4.7).<sup>20, 44</sup> The inability to escape endosomes, the non-viral carrier follows the conventional endocytic route, trafficking first into early endosomes, then into late endosomes, and finally into lysosomes where it is enzymatically degraded. The lysosomal enzymes degrade the cargo and hence the efficiency of the gene delivery system is lowered.<sup>20, 45</sup>

Endosomes are dynamic, specialized compartments and undergo morphological and biological changes accompanied by vesicle trafficking. Molecular trafficking and sorting along the endocytic pathway are regulated by the protein named, Rab, small GTPases, which are critically important membrane association proteins. Rab proteins have corresponding host organelles; therefore, they are often regarded as markers of different endosomal compartments. The Rabs function as molecular switches that alternate between two conformational states: the activated GTP-bound form and the GDP-bound inactivated form.<sup>46</sup> The early endosome acts as a major sorting station, permitting the newly vacated receptors to recycle back to the cell surface for reuse. As mentioned, some membrane receptors along with membrane-bound lipids are transferred to recycling endosomes, returning to the plasma membrane, and this process is regulated by Rab4 and Rab11.<sup>47</sup> Further, the dissociated ligands are directed and transported to late endosome and finally to lysosomes for degradation. The transformation from early to late endosome is regulated by critical regulatory protein Rab 7 whereas the clathrin-coated vesicles and early endosomal vesicles possess significant Rab5 protein.<sup>48, 49</sup>

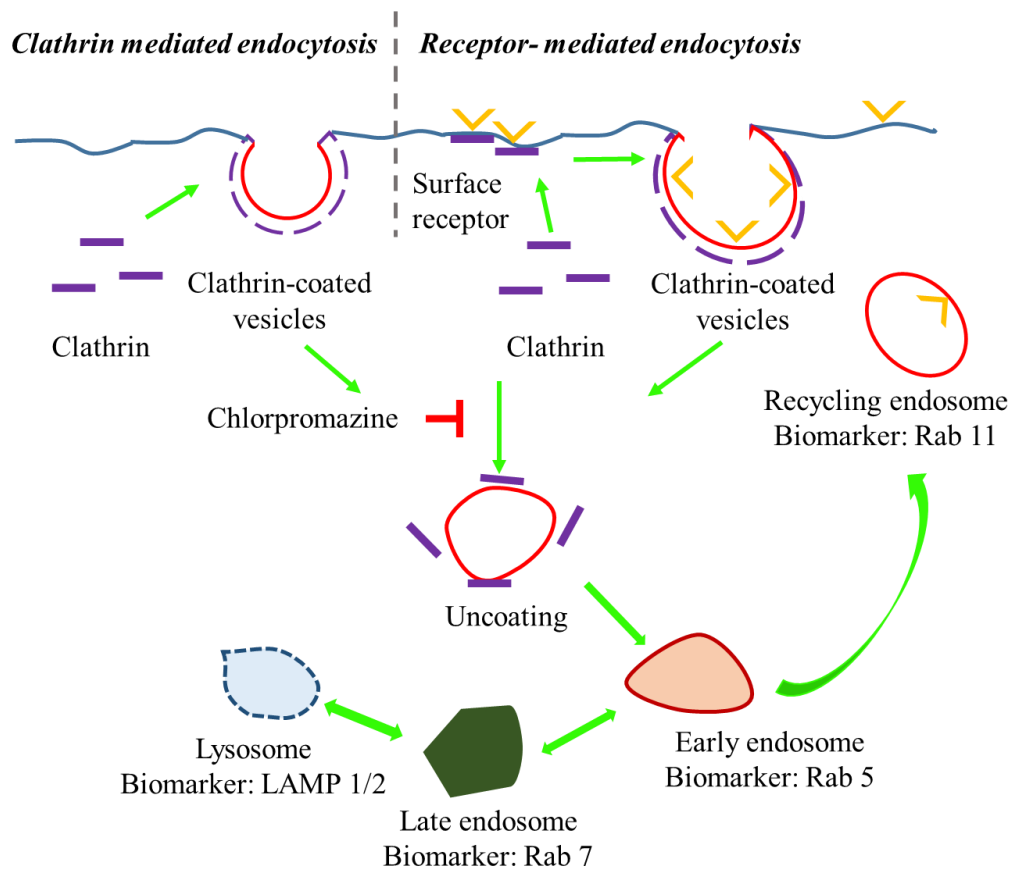


**Figure 2. Schematic presentation of clathrin-mediated endocytosis process.** Endocytosis is a cellular process that involves macromolecules being taken up through a plasma membrane-derived vesicle called an endosome. The figure sketches a classical clathrin-mediated endocytosis pathway along with the specific inhibitor and biomarkers of intracellular vesicles<sup>50, 51</sup>

## 1.5 Study method of the endocytosis

Recently few approaches have been developed to unveil the intracellular trafficking of non-viral nucleic acid delivery systems. The uptake of nanoparticles into cells is typically investigated by fluorescently labelling materials and measuring uptake using fluorescence microscopy such as by confocal laser scanning microscopy or flow cytometry.

### 1.5.1 Pre-treatment with pathway inhibitors

The chemical inhibitors of endocytosis, at non-toxic concentration, are widely used to study the involvement of specific uptake routes. For example, chlorpromazine inhibits the formation of the clathrin-coated pit for endocytosis. In presence of effective concentration of chlorpromazine, cellular internalization of nanocarrier is hindered. The

study involved comparison of the effect of an endocytosis inhibitor on the uptake of the specific nanocarrier with the effect on the uptake of reference substances.<sup>32</sup>

### **1.5.2 Codelivery of biomarker**

The utilization of marker cargo for specific route of endocytosis is one the method to study the endocytosis process. The study on colocalization of a nanocarrier with reference substances determine route of entry of a nanocarrier. Transferrin is a bona fide cargo for the clathrin-mediated endocytosis pathway.<sup>52</sup> Cholera toxin B is often used as a marker cargo for caveolar-mediated endocytosis.<sup>53</sup>

### **1.5.3 Colocalization with a fluorescent fusion protein**

Using DNA recombinant technology, the GFP gene combines with another gene that produces a protein of interest and is then transfected into a cell. If the cell produces the green fluorescence, it is inferred that the cell expresses the target gene as well. The fluorescent fusion proteins (FPs) can be visualized by fluorescence microscopy or flow cytometry and can serve as probes of environments within living cells. The addition of targeting and retention sequences to FPs can be exploited to highlight specific cellular organelles and to follow their dynamics. The colocalization studies using overexpression of fluorescent fusion proteins of key endocytic regulators or immunostaining for these regulators can help determine pathway for cellular uptake of nanocarriers.<sup>54</sup>

### **1.5.4 Immunofluorescent labelling**

Rab proteins are associated with intracellular membrane trafficking and have been identified to localize to specific domains on endocytic compartments. Rab5 and Rab 7 are used as a marker for early endosomes and late endosomes, respectively. The cellular internalization and intracellular distribution of nanocarrier have been studied by immunolabelling of the endocytic compartments. It was accomplished with specific fluorescent-tagged for endocytic markers antibodies.<sup>32, 55</sup>

## **1.6 Stimuli mechanism for endosomal escape**

Tumor tissues are distinctly separate from healthy tissue based on various factors such as pH, extracellular and intracellular enzymes and permeability of blood vessels.<sup>56</sup>

Accordingly, non-viral carriers can be developed to respond to these factors for tumor-specific gene release. Through an intrinsic or extrinsic trigger, various mechanisms have been promising for the efficient early endosomal escape of nanocarrier. The nanocarrier, containing therapeutic cargo, are fabricated using stimuli-responsive biomaterials.<sup>44</sup> The redox-sensitive or pH-sensitive bonds were introduced into the nanocarrier which releases the cargo upon the endocytosis by an in-situ stimuli mechanism.<sup>57</sup> Some studies have reported successful gene delivery by chemical modification of the polymer and lipids which are used to formulate the carrier system. In addition, physical triggers such as light, ultrasound, magnetic fields and electrical fields can also be applied to facilitate a non-viral carrier to be internalized by cancer cells and release cargo.<sup>56,58</sup> Trigger-responsive non-viral carriers demonstrate on-demand gene release, this avoiding off-target healthy cells and efficiently releasing nucleic acid in the cytoplasm of cancer cells.

### **1.7 Formulation design strategies for endosomal escape**

An ideal nucleic acid delivery system should fulfil several criteria such as non-toxicity, biocompatibility, and biodegradability, and offer protection to nucleic acids from enzymatic degradation. The nucleic acids are negatively charged, hydrophilic macromolecules and are incapable of crossing the plasma membrane unassisted.<sup>6</sup> To achieve successful transfection, an effective nucleic acid delivery system must be able to perform several functions: (i) entrap or encapsulate nucleic acid, (ii) protect nucleic acids from enzymatic degradation, (iii) promote cellular uptake, (iv) release nucleic acids into the cytoplasm, (v) promote nuclear entry (for pDNA delivery).<sup>59,21</sup> A delivery system must overcome a series of extracellular and intracellular barriers that are described earlier in Section 1.3. The different strategies to design and develop non-viral carriers and their underlying endosomal escape mechanism are listed in Table 3.

**Table 3. Strategies to improve endosomal escape**

Strategy	Mechanism	Polymers/Lipids	Formulation
<b>Polymer-based formulation</b>			
Proton sponge effect	Acidification of endosome cause osmotic swelling	PEI, PAMAM and PLL (polymers with pKa close to endosomal/lysosomal pH)	Polyplexes, dendriplexes <sup>60</sup>
<b>Lipid-based formulation</b>			
Flip-flop mechanism	Anionic lipids of the endosomal membrane laterally diffuse into the cationic lipoplexes	Cationic lipids: DOSPA, DOTAP, DOTMA	Lipoplexes composed of lipid mixture with cationic lipids <sup>1</sup>
Membrane fusion	Inverted hexagonal phase disrupts bilayer membrane structure of endosomes and lead to membrane fusion	DOPE is used as fusogenic lipid	Lipoplexes composed of lipid mixture with non-bilayer forming lipids <sup>61</sup>
<b>Peptide-based formulation</b>			
Pore formation	Pore-forming peptide integrated with the phospholipid vesicles	Pore-forming peptides such as GALA (pH-sensitive, pore-forming peptide)	Conjugation of the peptide with nucleic acid or onto the surface of nanoparticles containing nucleic acid. <sup>62</sup>
<b>Other mechanism</b>			
Codelivery with lysosomotropic agent	Osmotic swelling of endosomal vesicles	Chloroquine, Ammonium chloride	Codelivery of therapeutics with chloroquine <sup>63</sup>

Codelivery with photosensitizer	Light-induced generation of ROS and lipid oxidation	Photosensitizer; TPPS, m-THPC, curcumin, hypericin	Codelivery of therapeutics with free or photosensitizer loaded nanoparticle. <sup>64</sup>
Ultrasound	Ultrasound exposure destabilizes endocytosed bubble liposome	Liposome entrapping echo-contrast gas-perfluorocarbon	Bubble liposome <sup>65</sup>
Heat	Higher temperature (hyperthermia) disrupts endocytosed thermosensitive liposome	Thermosensitive lipids DSPC, DPPC.	Thermosensitive liposome <sup>66</sup>

## 1.8 Non-viral carriers for gene delivery

For a decade, viral vectors are replaced with non-viral vectors over the advantage of non-immunogenicity and biocompatibility of non-viral carriers formulations. The non-viral vectors possess an average particle size range in nanometer and higher encapsulation of nucleic acids. In most instances, these non-targeted nanocarriers are taken up by cancer cells via an enhanced permeability and retention effect.<sup>6,60</sup> Some surface-modified carriers are developed that possess a stealth surface made of a water-soluble polymer such as poly (ethylene glycol) (PEG). Unlike, passive tumor targeting driven by EPR-phenomenon, these carriers showed higher retention in the systemic circulation. However, the highly hydrophilic surface failed to attend optimal cellular uptake within the cancer cells. This effect is referred to as the PEG dilemma. To overcome this hurdle, the site-specific delivery of genes was designed by attachment of targeting ligands such as peptides, proteins, antibodies, or small molecules on the surface of the non-viral carriers. This modification promises enhanced in-vivo cellular internalization of the nanocarrier.<sup>67</sup> These targeting ligands enable the non-viral carrier to bind to cell surface receptors and enter cells via the receptor-mediated endocytic route.<sup>68</sup> The widely utilized non-viral carriers for gene therapy are discussed in following section.

### **1.8.1 Cationic liposomes**

Liposomes are a versatile drug delivery system and are widely exploited for their biocompatibility. The phospholipids self-assemble in an aqueous medium and form a vesicle known as liposomes, that has an aqueous core and phospholipid bilayer as a shell.<sup>69</sup> The influence of the solubility of nucleic acid in the aqueous phase favours its encapsulation in the hydrophilic core of the liposomes. (Figure 3A).

Cationic liposomes (CL) are dominantly composed of a cationic lipid along with neutrally charged lipids. These cationic lipids are frequently composed of a positively charged head group bridged by a linker group to a hydrophobic tail of phospholipid. Hence, CLs possess positive surface charge, which promotes interaction with negatively charged biomolecules such as nucleic acid. The monovalent lipids such as DOTAP, DOTMA DC-Chol and DMRIE condense more efficiently with DNA.<sup>70</sup> The highly charged complexes in which DNA is completely sequestered and condensed, exhibit a homogeneous size distribution (mean diameter of 100 – 450 nm).<sup>71</sup> However, the impact of adsorption of plasma proteins on CLs results into aggregation, charge neutrality and size enlargement, leading to their in-vivo instability.<sup>19</sup> The positive charge of CLs contributes to their interaction with cells and endosomal escape, but also inevitably leads to opsonisation, and rapid clearance by RES.<sup>72</sup>

PEGylation is a more effective approach to improve colloidal stability and preventing the negative effect of increased immunogenicity and toxicity of CLs in the body. However, the stealth effect of PEGylated CLs is not conducive to cellular uptake and endosomal escape.<sup>73</sup> Alternatively, the targeting ligands such as folate, transferrin, and cyclic Arg-Gly-Asp (cRGD) peptides are exploited to enhance tumor-targeted delivery. The specific morphology and structure orientation occurs due to employed preparation method. The reverse-phase evaporation followed by sonication or the sonication-extrusion method is commonly used.<sup>74</sup>

### **1.8.2 Lipoplexes**

The nucleic acids such as DNA, siRNA, miRNA and As-ODN are effectively condensed by lipids via electrostatic interaction to form complexes called 'lipoplexes'. The lipid composition is usually composed of cationic lipids, neutral helper lipids like cholesterol, and phosphatidylethanolamine (PE) lipids.<sup>60</sup> (Figure 3B) The composition of lipids



mainly consists of cationic lipids such as DOTAP, DOTMA along with DPPC or DSPC and helper lipid such as DOPE and cholesterol.<sup>75</sup> The physicochemical properties, as well as transfection efficiency of lipoplexes, depend on the ratio between the charged lipid and nucleic acid molecules.<sup>75</sup> Further, the transfection efficiency is attributed to the ability of DOPE to undergo a transition from a bilayer to a hexagonal configuration under acidic pH, which may facilitate fusion with or destabilization of target endosomal membranes. However, DOPE-dominated lipoplexes (e.g., DOTAP/DOPE molar ratios at 1:3) existed in a hexagonal phase completely that would destabilize lipoplexes and easily release their cargo before uptake.<sup>61, 76, 77</sup> The studies have shown that despite its excellent in-vitro transfection results, DOPE is unsuitable for improving in-vivo gene delivery.

Cholesterol has also been employed as a co-lipid to prepare more stable complexes than those containing DOPE. Cholesterol-rich lipoplexes could partially induce fusion-driven cellular uptake and facilitate endosomal destabilization. Lipoplexes enter the cells via endocytosis or membrane fusion. The studies have shown that the effect of lipoplex size on the endocytosis pathway, where smaller lipoplexes (around 270 nm) preferred CavME pathway and larger lipoplexes (around 500 nm) preferred CME pathway. For instance, the lipoplexes prepared with lipid composition DOTAP/DNA are observed preferably to enter the cells via clathrin-mediated endocytosis while the lipoplexes prepared using DMRIE-C follow the caveolin pathway<sup>78,79</sup> When administered intravenously, the serum cause inactivation and this leads to rapid elimination from the blood. Moreover, due to the positive charge cause activation of the immune system and lead to the aggregate formation.<sup>60</sup>

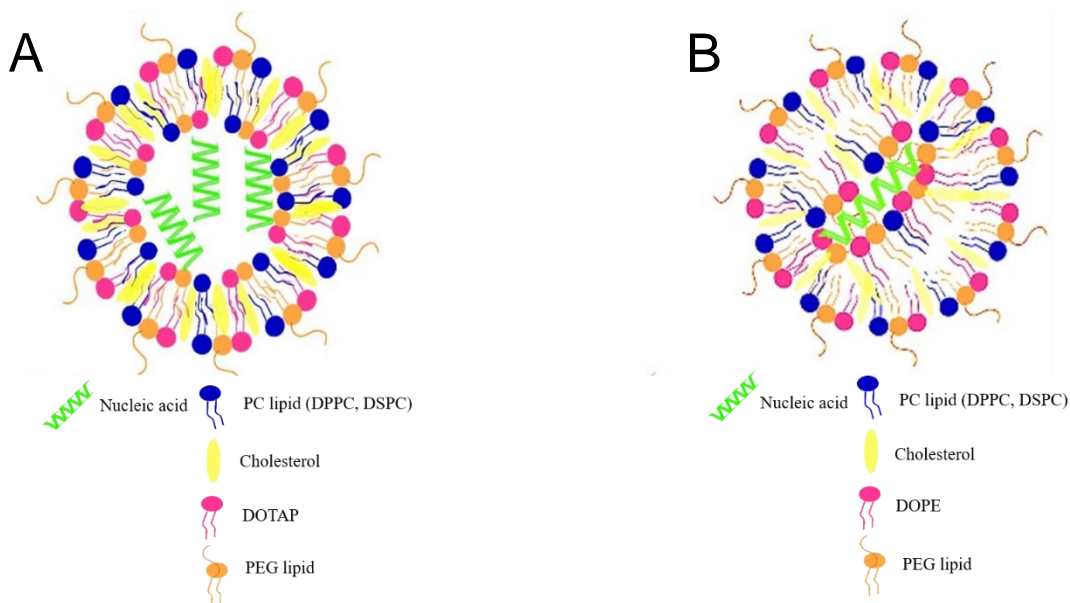


**Figure 3. Formulation and design of cationic liposomes and lipoplexes.** (A) The liposomes are vesicles with phospholipid bilayer passively encapsulating the exogenous oligonucleotide. (B) The lipoplexes are complexes formed between cationic liposomes and oligonucleotides. The main composition of formulation, which resembles the cell membrane, are phospholipid, cholesterol, and neutral helper lipids.

### 1.8.3 Lipid nanoparticles

In 1995, lipid nanoparticles were approved as drug delivery platform for small molecules (doxorubicin or amphotericin B) by FDA. Recently, LNP have been thoroughly investigated and successfully entered the clinic for delivery of mRNA, siRNA for cancer or genetic disorders. Lipid nanoparticles comprising ionizable lipids, cholesterol for particle stability, a helper phospholipid for lipid bilayer structure maintenance and polyethylene glycol (PEG) -derivative for decreased in-vivo interaction with plasma proteins and enhanced circulation time (Figure 4A).<sup>80</sup> The ionizable lipid such as DODAP, DODMA are employed, which carries a positive charge at low pH so that it interacts with negatively charged biomolecule. However, it becomes neutral at physiological pH which eliminates the side-effects.<sup>16</sup> In particularly, LNPs for nucleic acid are optimized for different lipid composition, tuning physicochemical parameters and for scaling up from a few mL to 200 mL/min. The emergence of microfluidic mixing method revolutionized the preparation of lipid nanoparticles. Microfluidics involves the manipulation of fluids through channels of at least one dimension in the microscale.<sup>81</sup> The lipid nanoparticles were prepared using lipids dissolved in ethanol, which are injected or

slowly dropped into a buffer solution containing nucleic acids. A pump is used to mix lipids dissolved in ethanol with nucleic acids dissolved in buffer using a T-shaped mixer. Rapid mixing of the two components occurs at the intersection. This results in an abrupt rise in the polarity of the organic solution and the assembly of lipid nanoparticles with the entrapped nucleic acid.<sup>82</sup> However, the LNPs eluting from that early microfluidic device are unstable until further stabilization is carried out by a second dilution in a neutral buffer solution. This method has been routinely reported to result in a high encapsulation efficiency of nucleic acid (~95%) as well as a small particle size (< 150 nm) and narrow size distribution.<sup>83</sup> It can easily have achieved by controlling the chip design, lipid concentration, and lipid flow rate.<sup>84</sup>

LNP–siRNA manufacturing required a rapid, reproducible procedure. This was accomplished through an ethanol-loading technique that involved mixing preformed LNP (at pH 4) with nucleic acids in the presence of high ethanol concentrations (~40% v/v). Rapid-mixing techniques produced LNP– siRNA systems with high entrapment efficiencies (>85%) and narrow size distributions.<sup>81</sup>

#### **1.8.4 Solid lipid nanoparticles**

Solid lipid nanoparticles (SLN), a suitable alternative as carriers, are aqueous colloidal dispersions, produced in solution using solid lipidic material, which comprises lipid matrix and surfactants and co-surfactants (Figure 4B). SLNs are microemulsion or nanoemulsion produced by techniques such as high-pressure homogenization and solvent emulsification-evaporation.<sup>85</sup> Depending on the procedure of preparation the particle obtained usually in the submicron range (10 - 1000 nm).<sup>86</sup> The cargo-free SLNs are often in the nanoscale ranges 50 – 200 nm. Following, the addition of nucleic acids, ‘lipoplexes’ with sizes up to approximately 500 nm are obtained. A variety of lipid compounds (i.e., lipids or appropriate solid fatty acids) have been used as wax solid lipid matrix in the preparation of SLNs including Compritol 888 ATO, cetylpalmitate, stearic acid, cholesteryl oleate, glyceryl trioleate, soya lecithin and glyceryl monostearate.

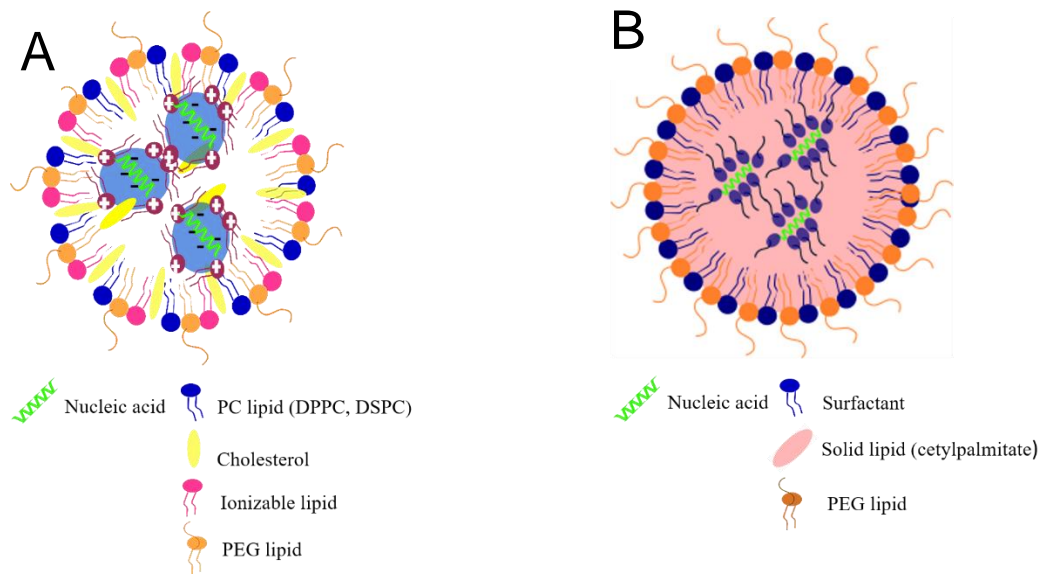


**Figure 4. Formulation and design of lipid nanoparticles and solid lipid nanoparticles.** Lipid vesicles typically having single phospholipid outer layer encapsulating the interior, which can be either (A) aqueous; known as lipid nanoparticles or (B) non-aqueous; known as solid lipid nanoparticles. They can strongly condense the negatively charged oligonucleotide with ionizable lipid. The lipid nanoparticles are composed of phospholipid, cholesterol, helper lipids and pH-sensitive lipids. The composition may or may not contain polyethylene glycol (PEG) lipid.

To accommodate the negatively charged nucleic acids, cationic SLNs are prepared by including positively charged co-surfactant such as benzalkonium chloride (BA), cetylpyridinium chloride (CPC), cetrimide (CTAB) in their formulation.<sup>87</sup> The combination of cationic and matrix lipids seems imperative as it may exert a significant impact on transfection efficiency.<sup>88,89</sup> SLN lipoplexes containing cationic lipids capable of adopting the H<sub>I</sub> structure promote nucleic acid delivery and transfection. It suggested that adoption of non-bilayer structures of the lipoplex is instrumental in endosome membrane destabilization and hence in nucleic acid delivery. By inclusion of a helper lipid such as DOPE that may promote and facilitate endosomal escape.<sup>90,91</sup>

### 1.8.5 Polyplexes

A cationic polymer such as polyethylenimine (PEI), poly(L-lysine), PLL, and chitosan binds with the naked plasmid and forms a condensed nanoparticle, known as polyplex. The polyplexes are formed by a strong electrostatic interaction between the cationic polymer and negative charged nucleic acid (Figure 5). The most used polymer is

polyethylenimine, which has a strong positive charge. This positive charge offers high buffering properties and simultaneously increase  $\text{Cl}^-$  ions concentration. This results into osmotic swelling and eventually bursting of endosomes. Subsequently, it helps the cargo to escape the endosome compartment after its internalization.<sup>92</sup>

Though, PEI is considered a golden standard for transfection of gene carriers, has been reported to be cytotoxic to the cells. PEI is synthesized by acid-catalysed ring-opening of aziridine monomers resulting in linear PEI (lPEI) which have secondary amines in the backbone and primary amines at the polymer end whereas the branched PEI (bPEI) which have primary, secondary and tertiary amine groups in ratio 1:2:1.<sup>92</sup> N/P ratio is the crucial factor taken into consideration that affects the overall efficacy of the polyplex (PEI/pDNA complex). N/P ratio is the molar ratio of nitrogen atoms within imine groups of polyethylenimine to phosphorous atoms comprising in phosphate group of nucleic acid. While the formation of polyplexes, the right balance should be maintained with polymer concentration, molecular weight, and pH of the medium.<sup>63</sup> Polyplexes enter the cells via the endocytosis (both caveolar and clathrin-dependent) pathway. Polyethylenimine circumvents the endolysosomal degradation by 'proton sponge effect'. The transfection efficiency of linear PEI is higher than branched PEI.<sup>93</sup> PEI-based transfection is being modified by grafting the polymer with PEG. A sufficient high-density PEG molecules prevent opsonisation which prevents rapid clearance from the blood stream.<sup>94</sup> There is also reduced cytotoxicity as well as transfecting efficiency due to shielding of the polyplex surface by PEG.<sup>60,95</sup> It is worth underlining that, even in vitro conditions, prolonged exposure of cells to PEI/DNA complexes may significantly impair cellular proliferation and viability.<sup>96</sup>

### **1.8.6 Lipopolyplexes**

Suitable delivery vehicles for genetic material are lipid-based and polymer-based nanocarriers. By combining these two vehicles, a lipid-polymer hybrid is formed, known as lipopolyplexes (LPP), where the inner core contains the DNA complexed with the polymer (polyplexes) and the outer surface is made of a lipid monolayer/ bi-layer (Figure 5). The study, that coined the term 'lipopolyplexes', compared the physicochemical properties, in-vitro transfection efficiencies and cytotoxicity of the ternary complexes composed of cationic, neutral or anionic liposomes.<sup>97</sup> The basic composition typically

includes a condensed nucleic acid either with polycationic polymer (such as PEI, forming polyplexes) or with a highly ordered polymer called dendrimer (such as PAMAM, forming dendriplexes). Further, these complexes were combined with cationic, anionic or neutral liposomes to form lipopolyplexes or lipodendriplexes respectively.<sup>98</sup>

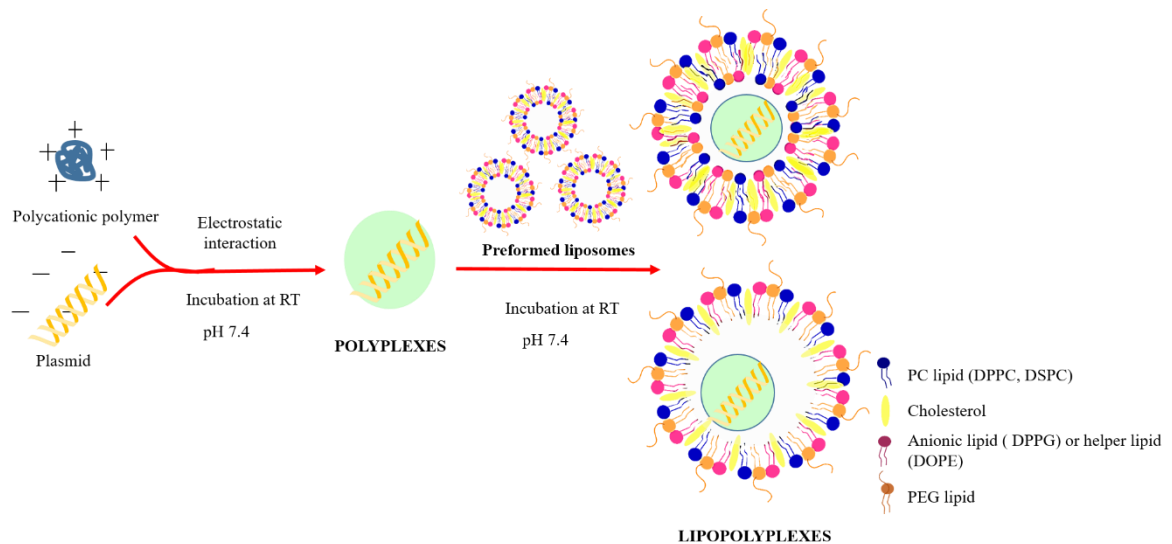


**Figure 5. Formulation and design of lipopolyplexes.** Lipopolyplexes is a ternary complex prepared with two steps where first the polyplexes are formed by electrostatic interaction between nucleic acid and polycationic polymer. Subsequently, these polyplexes are further incubated with liposomes to form lipopolyplexes.

Lipopolyplexes have colloidal stability, biocompatibility, higher transfection efficiency and lower cytotoxicity. It was reported that the cytotoxicity that is imparted by the cationic nature of the polymer is shielded by the lipid layer, which reduces the overall surface charge of the carrier.<sup>99,100</sup> The lipopolyplexes comprising a low-molecular-weight polyethylenimine (PEI) and the phospholipid DPPC were explored for therapeutic siRNA delivery in tumor-bearing mice.<sup>101</sup> Combination of both lipid vesicles and polyplexes shows many advantageous features as nucleic acid carrier systems. The presence of a lipid bilayer surrounding polyplexes not only prevents the interaction of such complexes with anionic components of serum but also prevents their spontaneous aggregation, maintaining the colloidal stability and biological activity of the carrier, when stored as a suspension for longer periods.<sup>102</sup>

The non-viral vector has the advantage of combining polyplexes as well as lipoplexes and showed promoted cellular uptake as well as endosomal escape of its payloads. Some of the recent advances in lipopolyplexes based formulations are listed in Table 4. The thesis is focused on the preparation of modified lipopolyplexes that exhibits the enhanced transfection efficiency by an external trigger.

**Table 4. Modification of lipopolyplexes for gene delivery**

<b>Formulation</b>	<b>Transfection efficiency</b>	<b>Remarks</b>
<b>Unmodified polymer-based LPPs</b>		
SAINT-5/DOPE-poly-l-lysine-DNA complexes	2-fold to 4-fold increase in transfection efficiency	Poly-l-lysine-coated ensures importance of the condensed state of DNA in its translocation <sup>103</sup>
Liposome-coated PEI F25-LMW/DNA complexes	Increase in transfection efficiency compared to non-lipidised polyplexes	liposomal with negative charge and rigid phenotype, i.e., DPPC, DPPC/cholesterol (85:15) and DPPC/DPPG (92:8) favoured transfection <sup>97</sup>
DOCSPER: DOSPER /bPEI 25kDa/DNA	5- fold to 400-fold increase in transfection efficiency	Addition of cationic liposome to polyplexes <sup>104</sup>
DOTAP/PBAE/DNA	Increase in transfection efficiency	LPP was compared with lipofectin and polyplexes <sup>105</sup>
DOTAP/chitosan/DNA	20-fold increase in transfection efficiency	Chitosan caused rapid nuclear localization <sup>106</sup>
<b>Modified polymer-based LPPs</b>		
DOTAP:Chol/IPEI-acrylate/DNA	Increase in efficiency compared to unmodified LPPs	LPP with IPEI 250kDa showed the highest transfection efficiency but high cytotoxicity <sup>107</sup>
Man-LPD100	2-3 fold increase in transfection efficiency compared to LPD	Both PLL and liposome were mannosylated histidylated <sup>108</sup>
DOTAP:Chol/PAA-6-bromo HA/DNA	Increase in transfection efficiency	The highest transfection efficiency was observed in the modified PAA 15-LPP <sup>109</sup>
<b>Reverse LPP</b>		
CHEDLA/PEI-TA/DNA	Increase in transfection efficiency	TA anchored PEI to the surface of the liposome <sup>110</sup>

<b>Modified lipids in LPPs</b>		
His-Chol:Rhod-DOPE/bPEI/DNA	Increase in transfection efficiency	Lipid coating having histidylated cholesterol was on polyplexes <sup>111</sup>
DOTMA/DOPE/Peptide/DNA	Increase in transfection efficiency	The peptide component has condensation with DNA and an integrin targeting sequence.

## 1.9 Physical methods for transfection

Various methods have been proposed and commonly used as the physical method for non-viral gene delivery system. Each method requires specific physical forces such as electric, magnetic, ultrasonic or laser and specific tools for the transfection process. These physical methods for gene delivery include needle injection, gene gun, sonoporation, photoporation (laser-based transfection), magnetofection and hydroporation.<sup>112</sup>

### 1.9.1 Basic principle in sonoporation

Apart from a therapeutic delivery platform, a few techniques such as magnetic resonance imaging, photoacoustic imaging and bioluminescence imaging have been promising methods for imaging techniques for guided delivery and to determine the local activity. Ultrasound imaging is more feasible for future clinical applications because it is non-invasive, cost-effective, widely available, portable device. It allows molecular imaging and real-time guided imaging without any ionizing radiation effect. For a decade medical ultrasound has attracted attention as a potential energy for use with thernostic system. Ultrasound-mediated bioeffects are reported to be caused by the cavitation process. Acoustic cavitation involves the growth and collapse of pre-existing gas bubbles in the liquid, when subjected to ultrasound.

There is a noticeable application of a gas-filled lipid or polymeric vesicle, a microbubble. These microbubbles are vesicles encapsulating volatile liquid such as perfluorocarbon, which turn into gas-filled vesicles at body temperature upon administration. Upon the exposure of ultrasound in presence of a microbubble, an acoustic field is generated and results in the formation of transient pores on the biological membrane for a microsecond duration. The cavitation bubbles are the result of oscillations which occurs because of the effect of maximum temperature and pressure reached, just before they collapse. The



described process is termed sonoporation (Figure 6).<sup>113,114</sup> Cavitation bubbles may exhibit sustained growth and oscillations over several cycles (stable cavitation) or violent growth and collapse in less than a cycle (transient or inertial cavitation). These bubbles grow when subjected to low frequency and implode at higher frequencies due to compression. The effect of ultrasound on cell membrane permeability depends on a variety of intensities (or pressure amplitudes) and frequencies.<sup>115</sup>

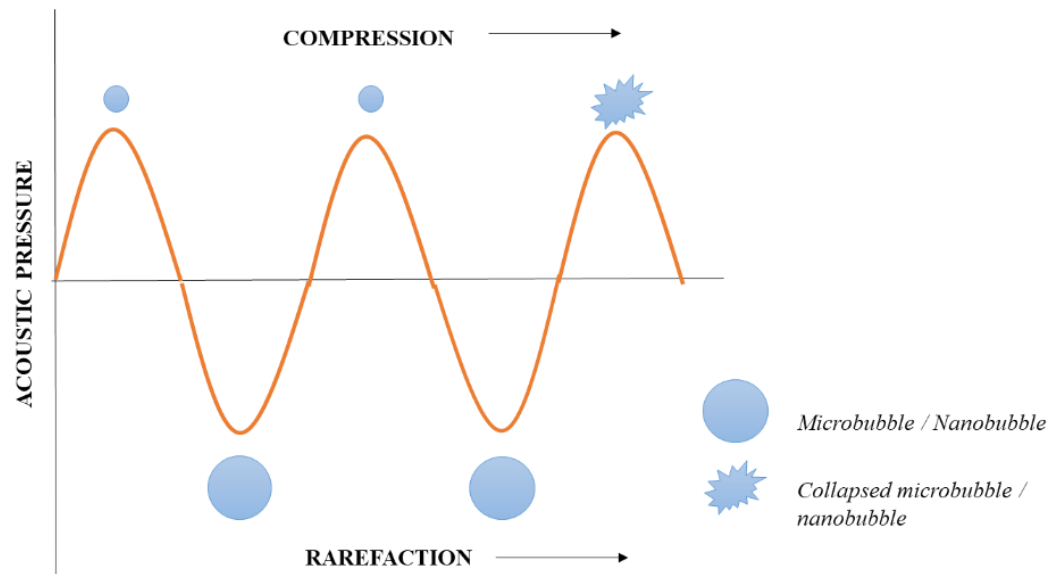


**Figure 6. Mechanism of sonoporation by cavitation process.** The cavitation process is caused by exposure to the ultrasound waves. The figure describes the change in microbubble or nanobubble (rarefaction and compression) caused by ultrasound waves at higher pressure. It induces the collapse of the microbubble or nanobubble and jet streaming towards the cell membrane.

Clinically, ultrasound contrast agents have been utilized to left-ventricular opacification/endocardial border delineation, and detection and characterization of liver and breast masses. Unfortunately, the intrinsic poor structural stability (life-cycle ~ 5-12 mins) and micrometre-scale particle size limit their application as imaging. Therefore, many efforts have been focused on the design and fabrication of rigid nano-sized vesicles with relatively high structural stability as well as echogenic properties.<sup>116</sup> Recently, sonosensitive nanoparticle, which encapsulates genetic material and exhibits reduced particle size, has been developed.<sup>117,118</sup> The ultrasound-stimuli influences two profound rate-limiting steps in endocytosis process of nanocarriers (Figure 7). The approach asserts of utilization of ultrasound waves that destabilizes and disrupts the endosomal membrane

because of cavitation effect caused due to presence of microbubble/nanobubble or sonosensitive nanoparticle. Another approach emphasis the permeability of the cell membrane is reportedly increased at low-frequency ultrasound exposure in presence of microbubble/nanobubble or sonosensitive nanoparticle. When such nanocarrier is supposedly near to the cell membrane but not yet internalized, the cellular internalization of vesicles is subsequently enhanced due to temporary pore formation by ultrasound.

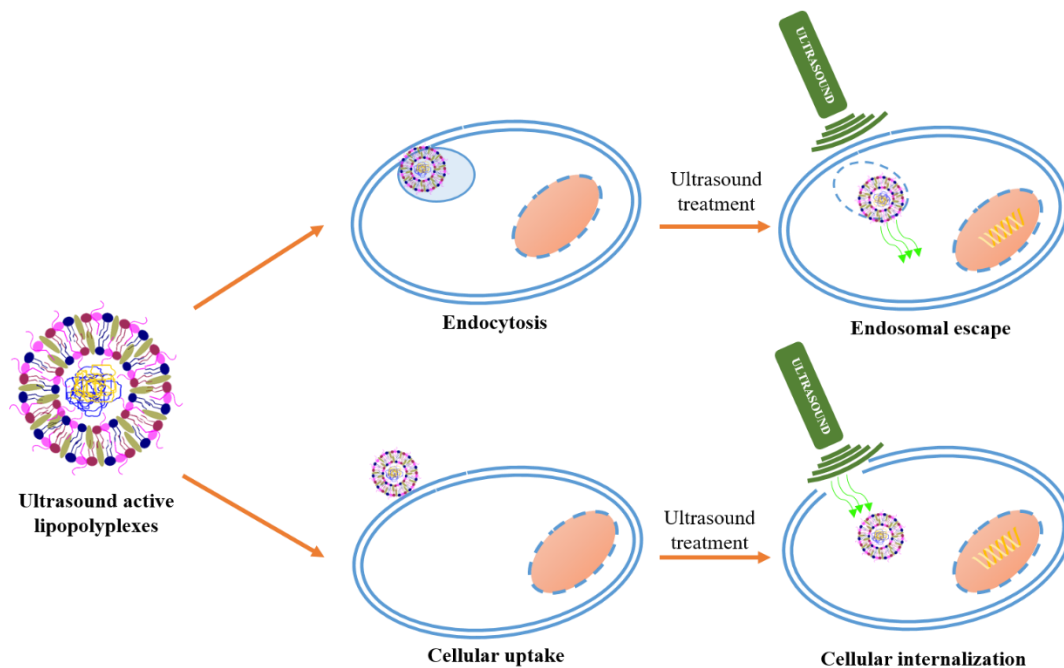


**Figure 7. Ultrasound-mediated transfection.** The figure depicts two possibilities where ultrasound treatment could affect the transfection efficiency of the ultrasound-active formulation in the cancer cells. 1) Ultrasound exposure enhances the endosomal escape of the nanocarrier in cancer cell (above). 2) Ultrasound exposure promotes the cellular internalization of the nanocarrier in cancer cell (below).

Contrast-enhanced ultrasound permits real-time visualization of contrast enhancement patterns in various organs. Commercially available ultrasound contrast agents (UCA) are listed in Table 5. An in-vivo study using SonoVue<sup>®</sup> with low fixed MI values (<0.1) was performed at full clinical doses and half clinical doses: i.e., 34  $\mu\text{L}/\text{kg}$  and 17  $\mu\text{L}/\text{kg}$  for SonoVue<sup>®</sup>. The results showed that, for the conditions used in this study, SonoVue<sup>®</sup> showed contrast enhancements at full clinical dose whereas, the contrast enhancement was short-lived at half clinical doses. The latter result emphasizes the utilization of higher dose of the contrast agent, if strong late-phase enhancement is needed.<sup>116</sup>

**Table 5. Commercially available ultrasound contrast agents<sup>119</sup>**

<b>Ultrasound contrast agent</b>	<b>Manufacturer</b>	<b>Shell</b>	<b>Ultrasound contrast</b>
<b>Echovist</b>	Bayer	Galactose	Air
<b>Albunex</b>	Molecular Biosystem	Albumin	Air
<b>Optison</b>	GE Healthcare	Albumin	Perfluoropropane
<b>SonoVue</b>	Bracco	Phospholipids	Sulfur hexafluoride
<b>Definity</b>	Lantheu	Phospholipids	Perfluoropropane

### **1.9.2 Basic principle in photochemical internalization**

Photochemical internalization (PCI) was first presented in 1999 as a novel technology to facilitate the escape of therapeutics from the endo/lysosomal membrane barrier and ability to reach their targets.<sup>64</sup> PCI has been established to enhance the intracellular delivery of a large variety of macromolecules including drugs, small molecules, peptides, protein toxins and genes either through viral or non-viral vectors.<sup>120</sup> The photochemical internalization by the ‘light after’ procedure involves macromolecular treatment before light exposure whereas, in the ‘light first’ protocol, the macromolecular treatment is followed by irradiation process.<sup>121</sup> The therapeutics cargo are normally potent drugs which are not bioavailable without an efficient delivery system. The loading dose can be reduced to extremely small (compared to its LD50 dose) using PCI technology. A photosensitizing compound, known as photosensitizer (PS), accumulates in the membranes of the endocytic vesicles followed by irradiated using light having specific wavelength. As shown in Figure 8, after the light absorption, the PS reaches an excited singlet state. After an intersystem crossing, the PS, now in a triplet excited state, can react in two ways: react with biomolecules through a hydrogen atom (electron) transfer to form radicals, which react with molecular oxygen to generate reactive oxygen species (type I reaction); or, the PS in its triplet state can react directly with oxygen through energy transfer, generating singlet oxygen (Type II reaction). Upon illumination, such photosensitizers become excited and subsequently induce the formation of reactive oxygen species. This highly reactive intermediate has short range of action and short lifetime, confine the damaging effect on the production site. This localized effect induces the disruption of the endosomal membrane<sup>64,122</sup> The light dose and photosensitizer

concentration required for PCI are much lower than that required for PDT treatment, where the ultimate goal is apoptosis and cell death.<sup>123</sup>

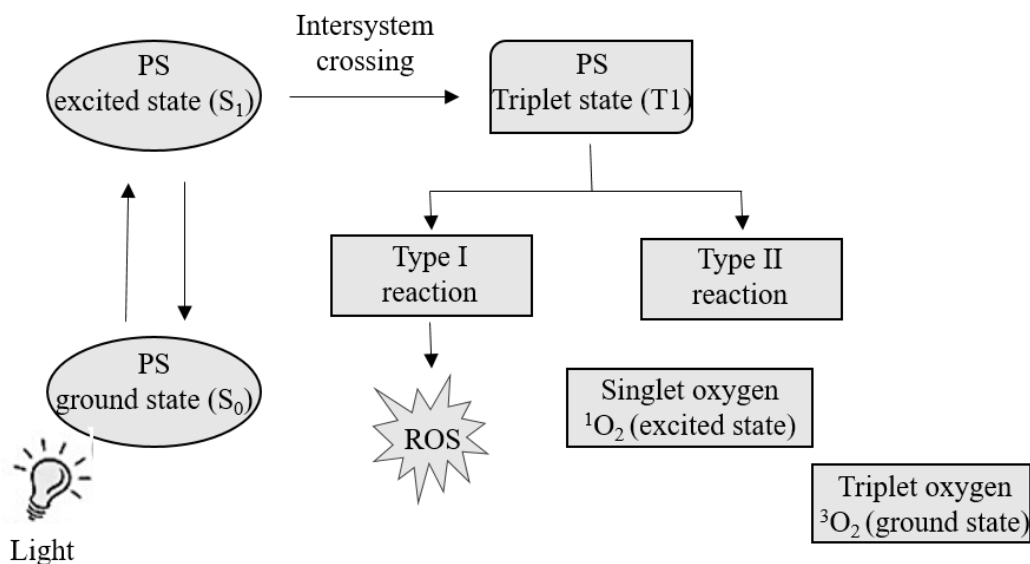


**Figure 8. Mechanism of photosensitizer-induced photochemical reactions.** The photochemical process in which a photosensitizer upon light activation transit from the ground state (S<sub>0</sub>) to an excited state (S<sub>1</sub>) and is further converted to a more stable triplet state (T<sub>1</sub>) consequently exhibits either Type I or Type II photochemical reaction.

This technique is now used for releasing nucleic acid cargo from the endocytic vesicle to the cytosol. The major considerations are transfection efficiency as well as the cytotoxicity from photosensitizer after PCI. Designing a non-viral carrier that deliver the nucleic acid along with a photothermal / photosensitizer agent promotes intracellular endosomal escape via photochemical internalization. Another way of performing PCI is to incorporate a photocleavable linker into the polymer, which will release the nucleic acid upon irradiation with a NIR laser or UV/Visible light. An “on-demand” gene release technique, requires a photosensitizer that either induces cleavage or emits heat energy upon irradiation with a light source (NIR or UV).<sup>66,124</sup> PCI technique avoids off-target gene expression and the therapeutic gene silencing effect or plasmid expression in the tumor tissue becomes more efficient. Photostimuli-responsive gene carriers are considered to be more efficient than conventional gene carriers in terms of their efficacy as therapeutics and reduction in side effects because of light-mediated gene delivery.<sup>125</sup>

### 1.10 Aim and scope

Supported by a strong literature background, there exist several physical methods which harness external triggers for gene delivery. However, these methods demonstrate limitations such as invasiveness and stochastic transfection in the in-vivo application. Owing to the development of nanotechnology, novel physical transfection platforms using a tailored nanocarriers have been surged. Lipopolyplexes, prepared using linear PEI, are well-established non-viral nanocarriers for gene delivery. This ternary formulation containing polymer and lipid delivers advantage of improved transfection efficiency and biocompatibility. The thesis contains proof of concept to employ external physical modalities to deliver lipopolyplexes in the cancer cells.

The first work presented in the thesis aimed to develop ultrasound-active lipopolyplexes. Ultrasound is a valuable tool for modifying the permeability of the cell membrane, which is also referred as sonoporation process. In presence of microbubbles, the ultrasound generates an acoustic field, which leads to the formation of transient pores on the cell membrane. However, this approach has exhibited limitations in gene delivery due to the aqueous instability of the free plasmid and the larger diameter of microbubbles. Consequently, it hinders the penetration of formulation into tumor vasculature. Moreover, the ultrasound contrast agents such as perfluorocarbons, entrapped in microbubbles, have short stability at room temperature. In this study, modified lipid vesicles were prepared wherein PEG40S was incorporated into the lipid bilayer for enhancement of sonosensitivity of the formulation. The work evaluated transfection efficiency, cytotoxicity and the potential as an image-guided gene delivery system.

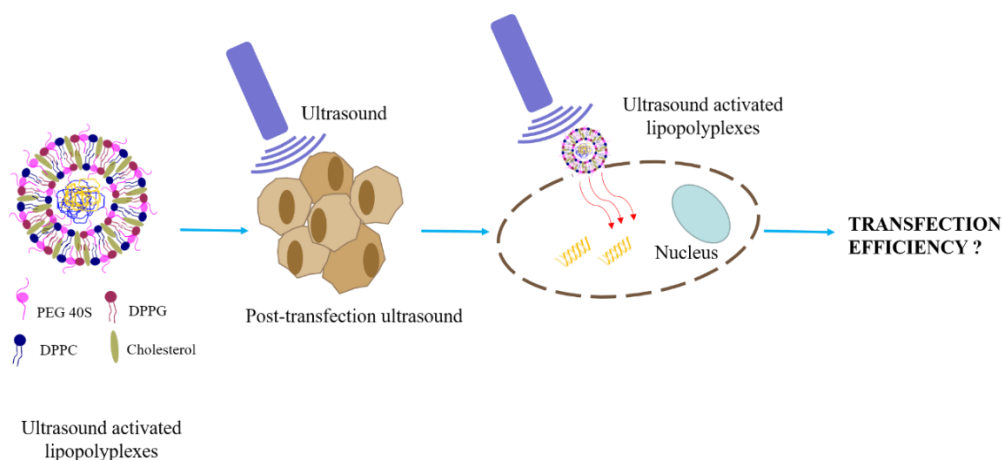


**Figure 9. Graphical abstract: Ultrasound-mediated gene delivery**

The second work presented in the thesis aimed to develop a codelivery system for photosensitizer and nucleic acid proposed for the photochemical internalization of a nucleic acid. Hypericin, widely used as photosensitizer, exhibits hydrophobicity. It stipulates a biocompatible delivery system, otherwise would involve the risk of decreased bioavailability due to aggregation in an aqueous environment. Similarly, encapsulation of nucleic acid avoid degradation by nucleases. The work focuses on dual encapsulation of the low payloads of the biomolecules in lipid-polymer based nanocarrier. The work essentially comprises preparation, physicochemical characterization, and in-vitro evaluation of hypericin lipopolyplexes. The study focuses on the elucidation of transfection efficiencies and cytotoxicities of the formulations in HepG2 cells under influence of wide range of applied photochemical dose. Additionally, the optimized formulation was modified with an anti-transferrin antibody for receptor-mediated phototransfection. The scope of the developed formulation entitles to codeliver the potent biomaterials to the target cell for photoselective transfection in the cancer cells.

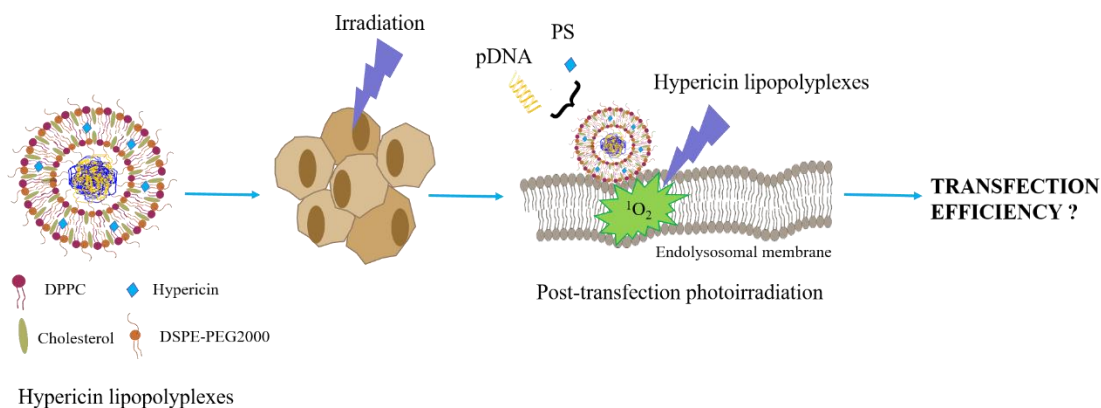


**Figure 10. Graphical abstract: Photosensitizer induced gene delivery**

## 1.11 Objectives

### **Ultrasound-mediated gene delivery in SKOV-3 cells**

1. Preparation and physicochemical characterization of ultrasound-active contrast vesicles
2. Measurement of the ultrasound contrast of formulations using tissue-mimicking agarose model
3. Optimization of N/P ratio for polyplexes (IPEI/pDNA)
4. Preparation and physicochemical characterization of ultrasound-active lipopolyplexes
5. Determination of transfection efficiency and % cell viability of polyplexes and lipopolyplexes
6. Determination of effect of ultrasound on transfection efficiency of ultrasound-active lipopolyplexes
7. Evaluation of effect of ultrasound on cellular uptake of formulation
8. Visualization of effect of ultrasound on GFP expression in monolayer and 3D- cell culture

### **Photosensitizer-induced gene delivery in HepG2 cells**

1. Preparation and physicochemical characterization of hypericin liposomes
2. Optimization of N/P ratio of polyplexes (IPEI/pDNA).
3. Preparation and physicochemical characterization of hypericin lipopolyplexes
4. Determination of photostability of encapsulated gene in hypericin lipopolyplexes
5. Determination of percentage cell viability for hypericin liposomes upon photoirradiation
6. Determination of transfection efficiency and percentage cytotoxicity for hypericin lipopolyplexes upon photoirradiation.
7. Assessment of photoirradiation on cellular uptake of hypericin lipopolyplexes
8. Assessment of intracellular reactive oxygen species generated upon photoirradiation of internalized hypericin.
9. Assessment of ligand-mediated cellular uptake of anti-transferrin conjugated hypericin lipopolyplexes
10. Visualization of GFP expression by anti-transferrin conjugated hypericin lipopolyplexes.

## 2. Materials & Methods

### 2.1 Materials

#### 2.1.1 List of materials

Materials or substances	Source
0.2 µm PES Syringe Filters	Whatman plc, Buckinghamshire, UK
12 well plates; Nunclon Delta	Nunc GmbH & Co. KG., Wiesbaden, Germany
24 well plate	Nunc GmbH & Co. KG, Wiesbaden, Germany
3,3',5,5'-Tetramethylbenzidine	Sigma Aldrich Chemie GmbH, Taufkirchen, Germany
6 well plate	Sarstedt AG & Co. KG, Nümbrecht, Germany
96 well microtiter plates; CytoOne®	Starlab International GmbH, Hamburg, Germany
Adhesive plate seals	Boehringer Mannheim GmbH, Mannheim, Germany
AFM Probe; HQ:MSC16/Al BS	µmasch, Tallinn, Estonia
Agar	Merck KGaA, Darmstadt, Germany
Agarose	Merck KGaA, Darmstadt, Germany
Ampicillin	Sigma Aldrich Chemie GmbH, Taufkirchen, Germany
Anti-transferrin antibody	Santa Cruz Biotechnology Inc., Germany
Atomic force microscope; Nanowizard®	JPK Instruments AG, Berlin, Germany
Autoclave, Tuttnauer 3850 ELC	Tuttnauer GmbH, Linden, Germany
Bath Sonicator; Transonic Digital S	Elma Schmidbauer GmbH, Singen, Germany
Bright-Glo™ Luciferase assay reagent	Promega Cooperation GmbH, Germany
Cell Culture Lysis Reagent	Promega GmbH, Mannheim, Germany
Centrifuge; Beckman J2-21	Beckman Coulter GmbH, Krefeld, Germany
Chlorpromazine	Alfa Aesar GmbH & Co. KG., Karlsruhe, Germany
Cholesterol	Sigma Aldrich Chemie GmbH, Taufkirchen, Germany
CO <sub>2</sub> Incubator, HeraCell	Heraus GmbH & Co. KG., Hanau, Germany
Confocal laser scanning microscope; LSM 510/Axiovert 100M	Carl Zeiss Microscopy GmbH, Jena, Germany

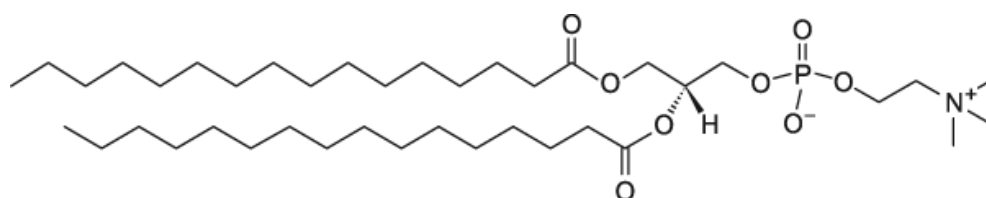


Constant Power Supply; LKB 2197	LKB Produkter AB, Bromma, Sweden
DAPI	Sigma Aldrich Chemie GmbH, Taufkirchen, Germany
DMEM-HG	Biochrom GmbH, Berlin, Germany
DMEM-LG	Biochrom GmbH, Berlin, Germany
DMSO; $\geq 99\%$	Acros Organics B.V.B.A., Geel, Belgium
DNA ladder; GeneRuler 1 kb	Fermentas Life Sciences, Vilnius, Lithuania
DPPC	Lipoid GmbH, Ludwigshafen, Germany
Ethanol	Carl Roth GmbH + Co. KG., Karlsruhe, Germany
Ethidium Bromide	Sigma Aldrich Chemie GmbH, Taufkirchen, Germany
Filipin III	Sigma Aldrich Chemie GmbH, Taufkirchen, Germany
Foetal bovine serum	PAA Laboratories GmbH, Cölbe, Germany
Formaldehyde	Alfa Aesar GmbH & Co. KG., Karlsruhe, Germany
Glutaraldehyde	Alfa Aesar GmbH & Co. KG., Karlsruhe, Germany
Hypericin	Thermo Fisher Scientific (Karlsruhe, Germany)
Laminar Flow Hood; Labgard Class II	NuAire Inc., Plymouth, USA
LDH assay Kit	Roche Diagnostics AG, Basel, Switzerland
LED irradiator	Lumundus GmbH, Eisenach, Germany
Linear PEI 22 kDa	Polysciences Europe GmbH, Hirschberg, Germany
Luminometer; FLUOstar® Optima	BMG Labtech, Ortenberg, Germany
Magnetic stirrer; MCS 66	CAT Scientific, Paso Robles, USA
Medical ultrasound device; eZono® 3000	eZono AG, Jena, Germany
Micro reagent tubes	Sarstedt AG & Co., Nümbrecht, Germany
Microscopy slides	Gerhard Menzel B.V. & Co. KG., Braunschweig, Germany
MilliQ® Water	Millipore Corporation, Billerica, USA
Mounting Medium; FluorSave™	Calbiochem Corporation, San Diego, USA
MTT Dye	Sigma Aldrich Chemie GmbH, Taufkirchen, Germany
n-2-Hydroxyethylpiperazine-n'-2-ethanesulfonic acid; HEPES $\geq 99\%$	VWR International GmbH, Darmstadt, Germany

Optima FLUOStar	BMG LABTECH, GmbH Germany
pCMV-luc	Plasmid Factory GmbH & Co. KG., Bielefeld, Germany
Pierce BCA assay kit	Thermo Fisher Scientific GmbH, Dreieich, Germany
Polycarbonate membranes	Whatman plc, Buckinghamshire, UK
RNase free water	GE Healthcare Europe GmbH, Freiburg, Germany
Rotary Evaporator; Laborota 4000	Heidolph Instruments GmbH & Co. KG., Schwabach, Germany
RPMI-1640	Capricorn Scientific, Germany
Sephadex G-50	GE Healthcare, Germany
Shaking Incubator; IKA KS4000 IC	IKA Werke & Co. KG., Staufen, Germany
SK-OV-3 cell clone	ATCC®, Manassas, USA
Sodium citrate	Eifelfango Werk GmbH & Co. KG., Bad Neuenahr-Ahrweiler, Germany
SYBR Safe DNA Gel Stain	Invitrogen™ ThermoFisher Scientific, Germany
TEM 300 mesh grids	PLANO GmbH, Wetzlar, Germany
TrackIt™ Cyan/Orange Loading Buffer	Invitrogen™ ThermoFisher Scientific, Germany
Trans-Illuminator; BioDoc Analyse	Whatman Biometra GmbH, Göttingen, Germany
Transmission electron microscope; JEM-3010	JEOL Ltd., Tokyo, Japan
Tris	Merck KGaA, Darmstadt, Germany
Triton™ X-100	Sigma Aldrich Chemie GmbH, Taufkirchen, Germany
Uranyl acetate	Sigma Aldrich Chemie GmbH, Taufkirchen, Germany
UV mini 1240	Shimadzu, Suzhou, China
Water Bath	Kottermann GmbH & Co. KG., Hänigsen, Germany
White opaque 96 well plates	Brand GmbH + Co. KG., Wertheim, Germany
Zetasizer Nano ZS	Malvern Instruments Ltd, Malvern, UK
Ø 15 mm cover slips	Gerhard Menzel B.V. & Co. KG., Braunschweig, Germany

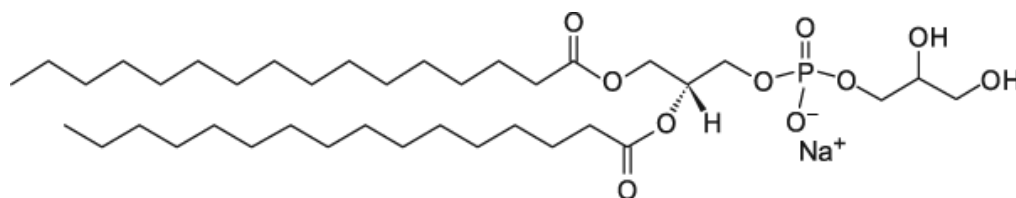
### 2.1.2 DPPC

1,2-dipalmitoyl-*sn*-glycero-3-phosphocholine (DPPC) is a phospholipid, that contains a head group (polar phosphate) and a nonpolar fatty acid chain. DPPC is an amphipathic lipid with a molecular weight of 734.039 g/mol. It is the most reasonable lipid that is used in thermosensitive liposomes since it has a phase transition temperature of  $T_m = 41^\circ\text{C}$ . DPPC can arrange itself in polar and non-polar interactions to form spherical vesicles. Usually, it is used with cholesterol which plays a role as a membrane stabilizer. DPPC used for this work had a purity of  $\geq 99\%$ . It was dissolved in 2:1 (v/v) chloroform: methanol mixture at a concentration of 10 mg/ml and stored in glass vials at  $-20^\circ\text{C}$  until use.



### 2.1.3 DPPG

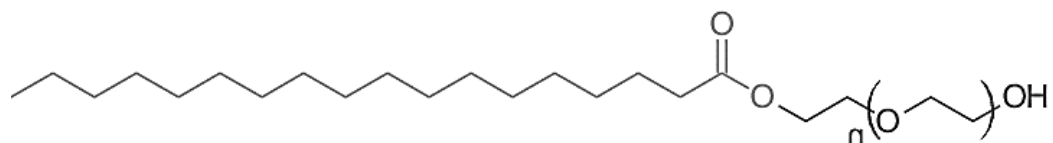
1,2-dipalmitoyl-*sn*-glycero-3-phosphoglycerol (DPPG) is a saturated lipid consisting of a phosphorylglycerol acylated chain with palmitic acids. It has a molecular weight of 744.952 g/mol with a transition temperature of  $41^\circ\text{C}$ . DPPG lipid (obtained as a gift sample from Lipoid AG, Steinhausen, Switzerland) was stored in a stock solution of 10 mg/mL in chloroform: methanol solution (2: 1, v/v) and stored at  $-20^\circ\text{C}$  till further use.



### 2.1.4 PEG40S

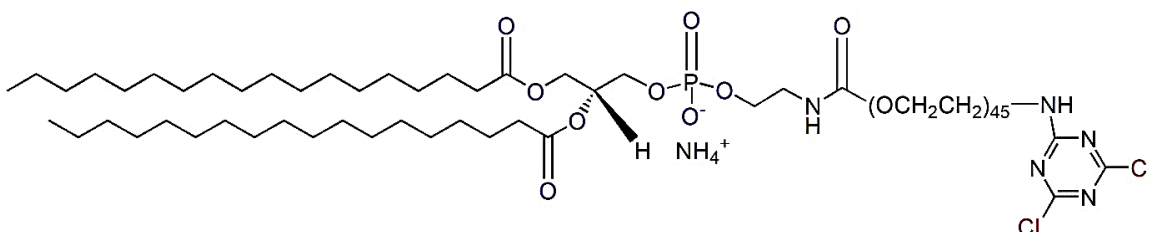
Polyoxyethylene glycol (40) stearate (PEG40S) is a single chained, also known as Myrj 52. It is an emulsifier and miscible with phospholipids. It has been utilized to produce drug-loaded nanostructured lipid carriers. Incorporation of PEG40S in bilayer makes the

shell of liposomes less ordered and easier to disrupt and reform which improves the formation of bubbles. It has a role in influencing membrane fluidity in the lipidic shells.



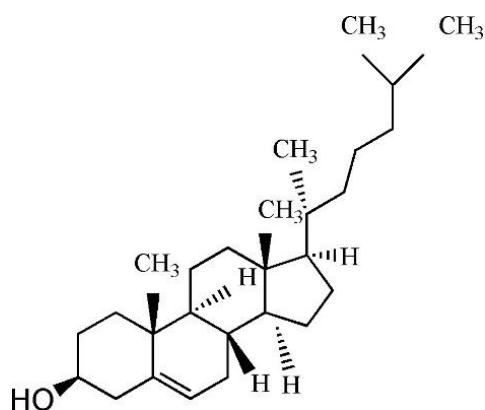
### 2.1.5 DSPE-PEG2000-cyanur

1,2-distearoyl-sn-glycero-3-phosphoethanolamine-N-[cyanur(polyethyleneglycol)-2000] (Cyanuric PEG-PE) is an end group functionalized PEG-lipid conjugate used for attachment of peptides, antibodies, etc., under mild basic conditions. Cyanuric chloride is one heterocyclic, nitrogen-containing compound with three chlorine atoms, which links the antibodies to the PEG terminus via a nucleophilic substitution at a basic pH (8.8) with either primary or secondary amine. A big advantage of using cyanuric PEG-PE is that the proteins can be coupled to this membrane anchor without the need for any previous derivatization. DSPE-PEG2000 cyanur was dissolved in 2: 1 (v/v) chloroform: methanol mixture at a concentration of 1 mg/mL and stored in glass vials at  $-20^{\circ}\text{C}$ .



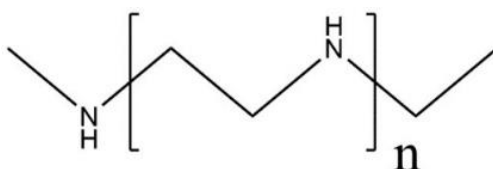
### 2.1.6 Cholesterol

Cholesterol is a hydrophobic steroid molecule that exists in the serum, it is a lipophilic molecule with a single polar hydroxyl group. Its molecular weight is 386.65 g/mol. Cholesterol is incorporated into the liposomal lipid bilayer to stabilize the membrane. It prevents vesicle aggregation and affects the phase transition temperature of the liposomes. Cholesterol was dissolved in 2:1 (v/v) chloroform: methanol mixture at a concentration of 10 mg/ml and stored in glass vials at  $-20^{\circ}\text{C}$ .



### 2.1.7 IPEI

Linear polyethylenimine (IPEI) is a linear variant of PEI containing only secondary amines. The IPEI used in this work is a commercially available fully deacylated variant. Deacylation of PEI is reported to increase the transfection efficiency. IPEI contains larger neighbouring ethylenimine segments resulting in an 11% increase in the amount of protonable nitrogen. A hydrochloride salt form of IPEI, 22 kDa was used for this work. 50 mg of the powder was dissolved in a beaker containing 40 mL of MilliQ® water. The solution was stirred on a magnetic stirrer and was neutralized to a pH of 7.0 with 6 M NaOH to obtain a 22 kDa linear polyethylenimine. The solution was made up to 50 mL with MilliQ® water and was sterilized using a 0.2 µm syringe filter (Whatman). Aliquots of 1 mg/mL were stored at -20°C.



### 2.1.8 pCMV-Luc

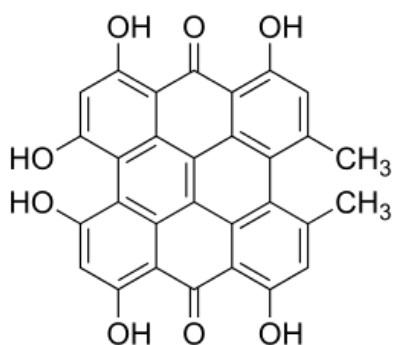
Luciferase encoding pCMV-luc (6233 base pairs) was obtained from Plasmid Factory (Bielefeld, Germany). pCMV-luc was amplified in *Escherichia coli* (DH5α strain) using an ampicillin-resistant antibiotic and purified using a Gene JET Plasmid Miniprep kit, according to the manufacturer's protocol. The concentration and purity of nucleic acids were determined by A260/280 using Nano-100 (Allsheng, China). The Integrity of plasmids was confirmed by 0.9% agarose gel electrophoresis and was stored at -20 °C for further experiments.

### 2.1.9 pCMV-GFP

Green fluorescence protein encoding pCMV-GFP plasmids (3487 base pairs) was obtained from Plasmid Factory (Bielefeld, Germany). Isolation and amplification of pCMV-GFP were similar to pCMV-luc, except for the difference in antibiotic used i.e. kanamycin.

### 2.1.10 Hypericin

4,5,7,4',5',7'-hexahydroxy-2,2'-dimethylnaphthodianthrone, hypericin, is a naturally occurring pigment. The most common of these is *Hypericum perforatum*, the St. John's Wort, which is used in folk medicine more than 2000 years ago has been described. The naphthodianthrone shows fluorescence with emission maxima around 590 nm to 640 nm and main absorption bands around 540 and 590 nm. It is soluble in solvents such as DMSO, which have potentially damaging effects on tissue. Therefore, a suitable aqueous formulation of hypericin is required. If there is sufficient oxygen, hypericin leads mainly to the formation of singlet oxygen through the photochemical type II reaction and to a lesser extent to the formation of superoxide anions by the type I reaction. The phototoxic effect of hypericin is very dependent on light and oxygen.



### 2.1.11 Anti-transferrin antibody

Anti-transferrin antibody, a high-quality monoclonal transferrin antibody was obtained as a gift sample from Santa Cruz Biotechnology. Anti-transferrin antibody (76.5 kDa) is iron (Fe) transport glycoprotein antibody, which is also designated as granulocyte pollen binding protein (GPBP) antibody.

## 2.2 Preparation method

### 2.2.1 Preparation of ultrasound-active lipopolyplexes

#### 2.2.1.1 Preparation of liposomes

The liposomes were prepared by the thin-film hydration method using a rotary evaporator (Heidolph, Schwabach, Germany) as described.<sup>97</sup> The appropriate amounts of lipids (see Table 6) from a 10 mg/mL stock solution were dissolved in 2:1 (v/v) chloroform: methanol mixture in a 5 mL round bottom flask and homogeneously mixed. Using a rotary evaporator (Laborota 4000) equipped with a vacuum pump, the lipids were evaporated at  $40 \pm 2^\circ\text{C}$  to obtain a thin film. The lipid film was rehydrated using 20 mM HEPES buffer (pH 7.4) and sonicated in a bath sonicator to obtain a uniform suspension of liposomes (Figure 11). The final concentration of the lipid mixture was 5 mg/mL in 20 mM HEPES buffer (pH 7.6).

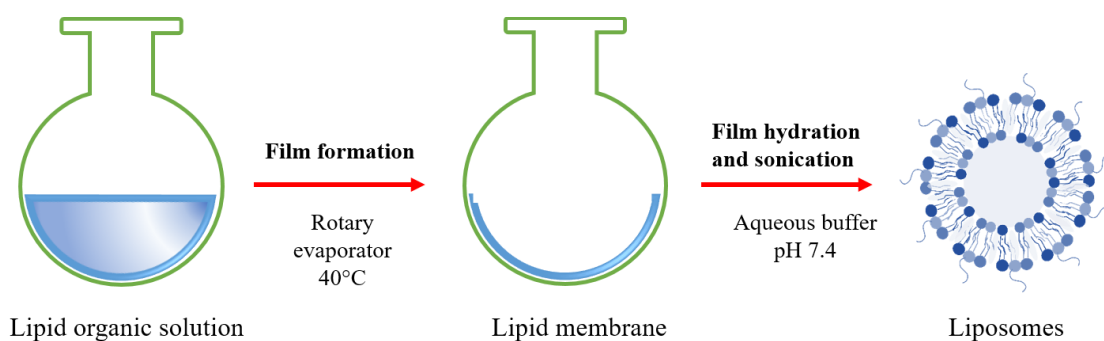


**Figure 11. Thin-film hydration method for preparation of liposome**

#### 2.2.1.2 Preparation of ultrasound-active contrast vesicles

The ultrasound-active contrast vesicles were prepared from these liposomes by an optimized agitation method. Briefly, 900  $\mu\text{L}$  liposome dispersion at  $40 \pm 2^\circ\text{C}$  was purged with air at 30 psi pressure for 120 s in a 5 mL closed vial and immediately agitated for 45 s at 3000 rpm by vial mixer (LLG-uniTEXER, Germany) to form ultrasound-active contrast vesicles. The formulations were stored at  $20 \pm 2^\circ\text{C}$ .

#### 2.2.1.3 Preparation of ultrasound-active lipopolyplexes

The polyplexes were formed by the addition of linear PEI (IPEI) to nucleic acid pDNA at a different N/P ratio. The mixture was incubated for 20 mins. The polyplexes were formed

by virtue of electrostatic interaction. For the N/P ratio, the weight of IPEI per 0.5  $\mu\text{g}$  pDNA was calculated using equation 1.

$$\frac{N}{P} \text{ ratio} = \frac{\mu\text{g IPEI}}{MW_{\text{repeated units of IPEI}} (473)} \times \frac{MW_{\text{pDNA}} (330)}{\mu\text{g of pDNA}}$$

### Equation 1. Formula for calculation of N/P ratio

Further, polyplexes were evaluated for average particle size and zeta potential and the optimized N/P ratio was selected for further study. The lipopolyplexes were formed by swiftly addition of an equal volume of liposome solution to polyplexes at different lipid: PEI mass ratios.<sup>126</sup>

## 2.2.2 Preparation of hypericin lipopolyplexes

### 2.2.2.1 Preparation of hypericin liposomes

The hypericin liposomes (Hy-Liposomes) were prepared by the ethanol injection method (Fig.12). Briefly, the homogenous mixture of lipids (in chloroform/methanol 2:1) and hypericin (in methanol), was evaporated at  $40 \pm 2^\circ\text{C}$  under vacuum by a rotary evaporator (Laborota 4000, Heidolph Instruments, Schwabach, Germany). The lipid film loaded with hypericin was dissolved in 200  $\mu\text{L}$  ethanol: water mixture (9:1) and the lipid mixture was instilled into HEPES buffer (20 mM, pH 7.4).

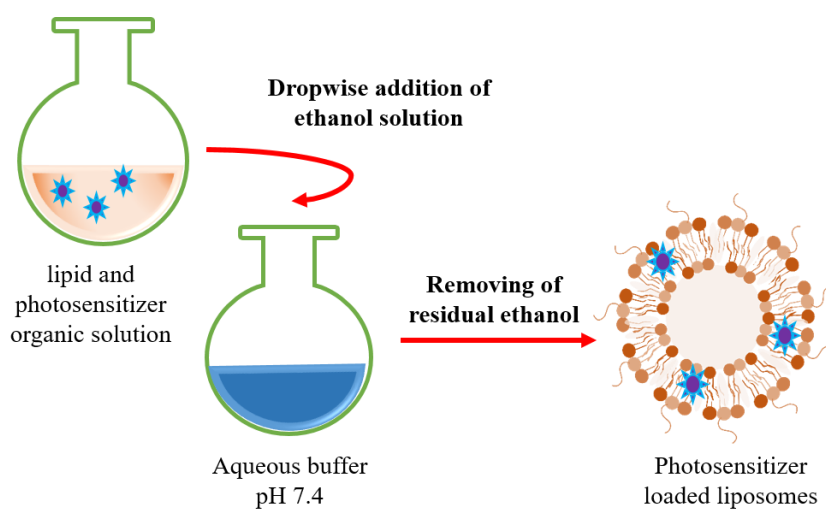


**Figure 12. Ethanol injection method for preparation of photosensitizer loaded liposome**



#### *2.2.2.2 Preparation of hypericin lipopolyplexes*

The hypericin lipopolyplexes (Hy-LPP) containing 0.5 µg pDNA were prepared at different lipid: PEI mass ratios using hypericin liposome and polyplexes.<sup>126</sup> Briefly, linear polyethylenimine (IPEI) was added into pDNA at N/P ratio 10. The mixture was incubated at room temperature for 20 mins to form polyplexes. Further, hypericin lipopolyplexes were formed by swiftly addition of an equal volume of hypericin liposomes to polyplexes at different lipid: PEI mass ratios.

### **2.2.3 Preparation of antibody conjugated formulation**

#### *2.2.3.1 Preparation of antibody-conjugated liposomes*

Briefly, the antibody- conjugated hypericin liposome was prepared by coupling an anti-transferrin antibody (sc-365871, Santa Cruz Biotechnology, Inc). The hypericin liposomes (50 nM hypericin) were prepared containing 1 mol % DSPE-PEG200 Cyanur. 10 µg/mL antibody was added into liposomes at the molar ratio of cyanur lipid: antibody was 1000: 1 and incubated in dark at pH 8.8 for 16 h.<sup>61</sup> With the cyanur present at the distal end of PEG the antibody forms -CONH- bond with lipid at basic pH of the formulation. Any unconjugated antibody is removed using the Sephadex G-50 column.

#### *2.2.3.2 Preparation of antibody conjugated hypericin lipopolyplexes*

The antibody-conjugated hypericin liposomes (50 nM hypericin) were prepared as described in Section 2.2.3.1 with anti-transferrin antibody at 1000: 1 molar ratio of cyanur: antibody. Further, the polyplexes (IPEI/pDNA) containing 0.5 µg pDNA were prepared as described in Section 2.2.2.2. The antibody conjugated hypericin liposomes were swiftly added to an equal volume of polyplexes at lipid: PEI mass ratio to form anti-transferrin conjugated hypericin lipopolyplexes. The formulation was evaluated for average particle size, zeta potential and in-vitro cellular studies.

#### *2.2.3.3 Preparation of FITC-labelled transferrin conjugate*

FITC labelled transferrin was prepared using the following protocol described by Sigma. Briefly, add appropriate amounts of FITC and transferrin into 5 mL round bottom flask. The mixture was stirred gently in a reaction medium of carbonate bicarbonate buffer (pH 9.0) at room temperature for 72 h. Further, the free transferrin was separated from FITC

conjugated transferrin using G25 Sephadex column. The eluents were collected and analyzed by UV spectrophotometer (UV Mini 1240, Shimadzu) at 287 nm and 494 nm for transferrin and FITC concentration, respectively. The F/P ratio of formed was calculated using equation 2.

$$\frac{F}{P} \text{ ratio} = \frac{A_{495} \times C}{A_{280} - [(0.35 \times A_{495})]}$$

$$\text{where } C = \frac{MW_p \times E_{280}^{0.1\%}}{389 \times 195}$$

**Equation 2. Formula for calculation of F/P ratio in FITC labelled transferrin**

A is measured absorbance at a specified wavelength,  $MW_p$  is the molecular weight of the protein,  $MW_f$  is the molecular weight of FITC, C is a constant value for a given protein

## **2.3 Characterization methods**

### **2.3.1 Dynamic light scattering**

The hydrodynamic diameter and polydispersity index of the formulations were determined by photon correlation spectroscopy (NanoZS, Malvern Instruments, Herrenberg, Germany). The measurements were performed at 25°C and at a scattering angle of 173° on dispersion that was diluted with purified water at a volume ratio of 1:9. The average size was calculated with the data of three independent formulations (mean ± standard deviation). The results were expressed as size distribution by intensity.

### **2.3.2 Laser Doppler anemometry**

The zeta potential was determined at a scattering angle 17° by measuring electrophoretic mobility with Laser Doppler Velocimetry on (NanoZS, Malvern Instruments, Herrenberg, Germany). The measurements were made in triplicate and average results were considered.

### **2.3.3 Atomic force microscopy**

The atomic force microscopy is a highly sensitive imaging technique based on molecular interaction between the moving cantilever tip and stationary sample surface and measures interatomic potential developed between these atoms.<sup>78</sup> Atomic force microscopy was performed with a NanoWizard 3 NanoScience (JPK Instruments, Berlin, Germany). 20 µL sample dispersion was fixed on a silicon wafer. The tip was oscillated at a scan rate between 0.5 and 1.5 Hz, in intermittent contact mode. Cantilever tip (NSC 14 AIBS, Micromash, Tallinn, Estonia) that had a length of 125 mm with a resonance frequency of about 130 kHz and a nominal force constant of 5 N m<sup>-1</sup> were used for the experiment. The AFM micrographs were scanned in the amplitude view at about 1 × 1 µm<sup>2</sup> (512 × 512 pixels) dimension.

### **2.3.4 Gel retardation assay**

DNA retardation assay was performed to evaluate encapsulation of the pDNA in the respective formulation using agarose gel electrophoresis.<sup>127</sup> Briefly, 1% agarose gel containing SYBR DNA stain dye was prepared in 1X TAE buffer. The wells were cast on the gel using the 8 well comb. After the gel was formed, the formulation containing

0.5 µg pDNA was added to each 5 mm lane along with a loading buffer containing cyan/orange dye (Invitrogen, Thermo Fischer Scientific). The gel was electrophoresed at 80 V for 1 h. The DNA migration was observed under UV transilluminator (BioDoc Analyze, Biometra) and compared with controls which were free pDNA or DNA ladder (TrackIt DNA ladder, Invitrogen Thermo Fischer scientific).

### **2.3.5 Characterization of ultrasound contrast**

The ultrasound contrast of formulation was determined by a method utilizing agar phantom, a tissue-mimicking material, in a self-developed closed-loop flow system as described elsewhere<sup>128</sup> (Figure 13). The circulation adjusted to the mean pressure of the artery. It contains 50 mL volume of buffer, and the reservoir contains another 50 mL of the same buffer. The transducer which had a mechanical index of 1.5 and emitted ultrasound of 1.4 MHz frequency was mounted above the agar chamber and the penetration depth was set to 9 cm, where exactly the silicon tube runs through the agar chamber. 100 µL of ultrasound-active contrast vesicles were pipetted into a reservoir near the input end of the silicon tube. After 30 s, images were sampled every 0.5 s for 1 min. The images were converted to 8-bit grey-scale and the first image was used as a background reference image. The same region of interest was evaluated in each picture. ImageJ software (National institution Health, MD) was used to count mean grey values of atleast 15 images for each formulation. The mean grey value of SonoVue<sup>®</sup> was considered a positive standard and results were represented as mean grey values of the formulations.

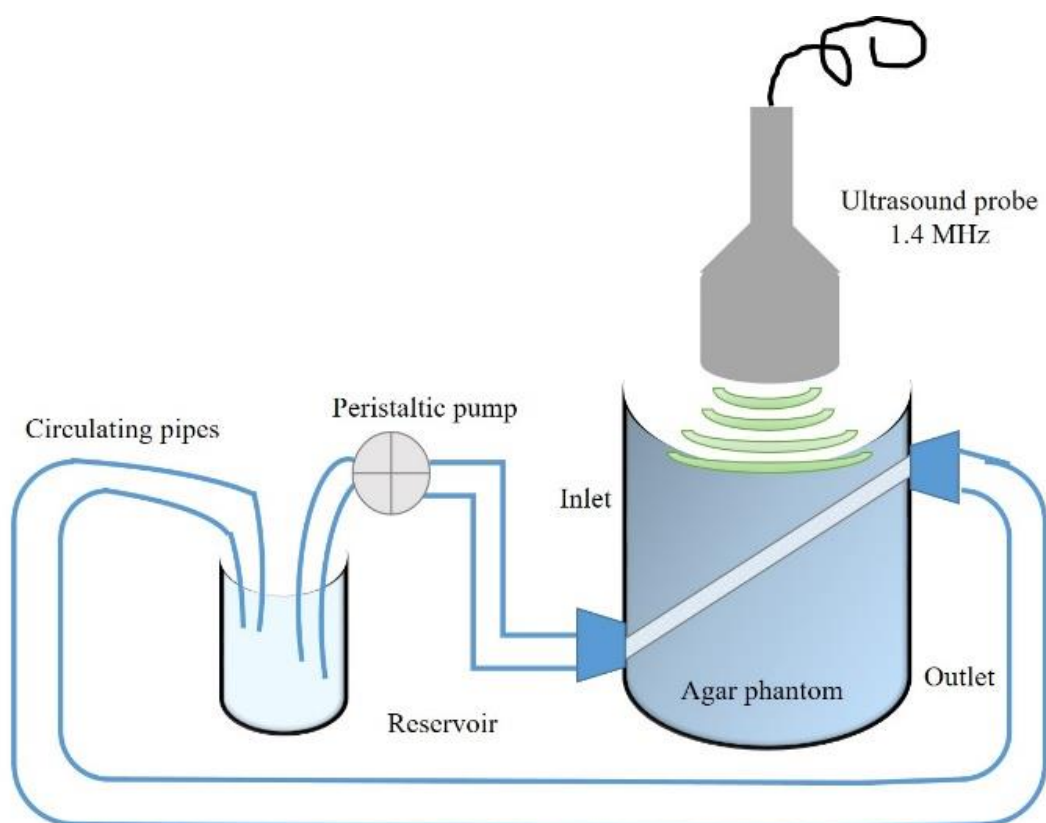


**Figure 13. Schematic presentation of flow model used for determining the ultrasound contrast.** The formulation, injected into the reservoir near the inlet pipe, is conveyed via a peristaltic pump and pushed into the flow system across the agar phantom. The agar bed was viewed by an ultrasound transducer having 1.4 MHz frequency on the eZono display unit.

### 2.3.6 Characterization of photosensitizer loaded formulation

#### 2.3.6.1 Entrapment efficiency

The free hypericin was removed from hypericin liposomes dispersion (containing 1  $\mu\text{M}$  and 5 $\mu\text{M}$  hypericin) using a PD-10 column (GE Healthcare Lifesciences).<sup>129</sup> The column was pre-equilibrated with HEPES (20 mM, pH 7.4). The eluent was monitored by measuring hypericin absorbance at  $\lambda_{\text{max}}$  587 nm using UV-spectrophotometer (UV-Multiscan Shimadzu). The fraction containing liposomes was collected and the hypericin concentration was quantified using the standard calibration curve of hypericin (range: 2-20  $\mu\text{g}/\text{mL}$ ). The percentage entrapment efficiency was calculated using equation 3 and their hence lipid: hypericin mass ratio were determined.

$$\% EE = \frac{[\text{Amount of hypericin in seperated liposomes}]}{[\text{Total amount of hypericin added into liposomes}]} \times 100$$

**Equation 3. Formula for calculation of hypericin entrapment efficiency**

*2.3.6.2 TEM*

A negative staining transmission electron microscopy was performed for empty liposomes and hypericin liposomes. Briefly, 20  $\mu\text{L}$  of liposomes (50  $\mu\text{g/mL}$ ) was placed on a carbon grid, and the excess of the formulation was removed by filter paper. A drop of 2% (w/v) aqueous solution of uranyl acetate was added and left in contact with the sample for 5 mins. The sample was dried at room temperature and imaged with a TEM operating at an accelerating voltage of 300 kV (TEM JEOL 3010, 500 kV) and 110  $\mu\text{A}$  emission current with current densities between 50-60  $\text{pA/cm}^2$ .

*2.3.6.3 Fluorescence quenching assay*

The intercalation of pDNA complexed with lPEI and hypericin liposome was assessed and compared with free pDNA by using SYBR quenching assay.<sup>98</sup> The formulations were prepared and incubated with 15  $\mu\text{L}$  1X SYBR solution (in 1X TAE buffer ) in a white 96 well plate. The mixture was incubated in dark for 10 mins followed by observation of emitted fluorescence at excitation/emission wavelength 485/520 nm by a multiplate reader (FLUOstar, Optima BMG). The relative quenching of fluorescence was calculated in percentage to control the sample using equation 4.

$$F_r = \frac{F_{obs} - F_d}{F_o - F_d} \times 100$$

**Equation 4. Formula for calculation of % fluorescence quenching**

$F_r$  depicts relative fluorescence measurements  $F_{obs}$  is the observed fluorescence of the given sample,  $F_d$  is the fluorescence of SYBR DNA dye and  $F_o$  is the initial fluorescence of free nucleic acid

*2.3.6.4 Photostability of encapsulated plasmid*

25  $\mu\text{L}$  hypericin lipopolyplexes containing 0.5  $\mu\text{g}$  pDNA and different hypericin concentration (50 nM – 500 nM) were prepared. Each formulation was photoirradiated at

600 mJ/cm<sup>2</sup> light dose using an LED device at 587 nm (Lumundus, Eisenach, Germany). As control group, each formulation was photoirradiated and lysed using the lysis buffer. The formulations were further electrophoresed using agarose gel (Section 2.3.4). For the lysis of formulation, 10 µL of 0.1% SDS added to hypericin lipopolyplexes and vortexed for 2 mins followed by incubation for 15 mins before loading into the gel.

## **2.4 In-vitro cell culture experiments**

### **2.4.1 Maintenance and harvesting of cell lines**

SKOV-3 Luc cells line was cultivated at 37 °C and 7 % CO<sub>2</sub> under humid conditions in DMEM medium (Biochrom) supplemented with 10 % foetal bovine serum (FCS) (PAA Laboratories). HepG2 cell line was cultivated at 37 °C and 5 % CO<sub>2</sub> under humid conditions in RPMI medium (Biochrom) supplemented with 10 % FCS (PAA Laboratories). All cells were maintained under humid conditions. Cells were grown as monolayers in diameter 100 mm tissue culture grade petri dishes and passaged upon reaching 80 % confluency.

### **2.4.2 Ultrasound mediated gene delivery**

#### *2.4.2.1 Determination of transfection efficiency*

The polyplexes and lipopolyplexes, containing 0.2 µg pCMV-Luc, were prepared and evaluated for transfection efficiency. Briefly, the cells were seeded in 96 well plate at a confluence cell density of 10<sup>4</sup> cells / 0.35 cm<sup>2</sup>. The cells were washed and incubated with 100 µL cell culture medium containing 25 µL formulation and incubated for 4 h. Further, additional 100 µL of cell culture medium was added and cells were incubated for 48 h. Following the incubation period, the cells were washed with sterile PBS buffer (pH 7.4; without Ca<sup>+2</sup> and Mg<sup>+2</sup>). The cells were suspended in 100 µL lysis buffer and rotated for 30 min at 300 rpm on a shaking Incubator: IKA KS4000 IC (IKA Werke & Co. KG, Staufen, Germany). On complete cell lysis, 20 µL lysate was transferred to a white-opaque 96 well microtiter plate (Brand GmbH & Co. KG, Wertheim, Germany). Luciferase assay buffer and D-luciferin were freshly thawed and mixed just before analysis. The luminescence was recorded with 10 s of total interval time per well and 50

$\mu$ L reagent mixture was automatically pumped by FLUOstar (Optima microplate reader) in each well.

#### 2.4.2.2 *Protein quantification assay*

The ng of Luciferase protein produced after transfection was quantified using a Pierce Protein BCA assay kit (Fisher Scientific Schwerte, Germany), according to manufacture protocol. Briefly, on the addition of a working reagent to cell lysate in a ratio of 1: 8 v/v, a purple-coloured complex was formed which was quantified against the standard protein concentration range by measuring absorbance at 562 nm using a plate reader (Optima microplate reader).

#### 2.4.2.3 *Cell viability*

Cell viability was assayed using MTT assay to evaluate the biocompatibility of the formulation. SKOV-3 cells were seeded at cell density  $10^4$  cells /  $0.35 \text{ cm}^2$  in a 96 well microtiter plate and incubated for 24 h. Briefly, the cells were transfected with different polyplexes and lipopolyplexes containing  $0.2 \mu\text{g}$  pCMV-Luc and followed by 24 h incubation period. The culture medium was aspirated completely.  $100 \mu\text{L}$  MTT (1:10 in DMEM) was added to each well and the cells were incubated at  $37 \text{ }^\circ\text{C}$  for 4 h. The formazan product produced in each well was dissolved in  $100 \mu\text{L}$  of DMSO solution. The absorbance was measured by FLUOstar (Optima microplate reader) at 485 nm. Each experiment was repeated thrice. The average absorbance was calculated based on the absorbance of 0.1% Triton-X treated cells.

#### 2.4.2.4 *Ultrasound mediated transfection efficiency*

SKOV-3 cells were seeded at a confluence cell density of  $3 \times 10^5$  cells /  $10 \text{ cm}^2$  in a 6 well plate. After 24 h of incubation, the cells were washed thrice with sterile 1X PBS buffer (pH 7.4; without  $\text{Ca}^{+2}$  and  $\text{Mg}^{+2}$ ). The cells were treated with ultrasound-active lipopolyplexes containing  $1 \mu\text{g}$  pCMV-Luc. Subsequently, a sufficient cell culture medium was added in the well and rotated for 30 s. The ultrasound waves having 3 MHz frequency with 1 cm penetration depth and 1.5 mechanical index were applied by using a transducer eZONO 3000 (Ultrasound medical device, eZono AG, Jena, Germany). The experimental group were pre-defined by post-transfection incubation of 5, 60, and 240 min, respectively before ultrasound treatment was applied. The duration of ultrasound



treatment was 60 s for all groups, except the control group. After 4 h incubation, the cell culture medium was added to make up 4 mL and further incubated for 48 h. The transfection efficiency was analyzed by the luciferase assay method as described in Section 2.4.2.1.

#### 2.4.2.5 LDH assay

LDH release was performed to analyse cell damage done by ultrasound-mediated transfection with the LDH-cytotoxicity assay kit.<sup>130</sup> The cell membrane integrity was measured in terms of relative LDH release from transfected cells.  $3 \times 10^5$  cells /  $10 \text{ cm}^2$  SKOV-3 cells were seeded in a 6 well plate and were incubated for 24 h. The ultrasound-active lipopolyplexes containing 1  $\mu\text{g}$  pCMV-Luc were transfected as described in Section 2.4.2.4 and the cells were further incubated for 48 h. After incubation period 100  $\mu\text{L}$  of the medium from the assay plate was carefully transferred to another 96 well  $\mu\text{L}$  plate. To this 100  $\mu\text{L}$  freshly prepared reaction mixture containing WST-1, a substrate to lactate dehydrogenase was added. The mixture was incubated for 30 min at room temperature. The absorbance was determined at 485 nm using a FLUOstar Optima plate reader. The absorbance was indicative of the relative LDH release from the transfected cells. The mean value of LDH-release of the positive control group (0.1% Triton X-100 treated cells) was considered as 100%.

#### 2.4.2.6 GFP Visualization

SKOV-3 cells were seeded in a 6 well plate at a cell density of  $3 \times 10^5$  cells /  $10 \text{ cm}^2$ . The ultrasound-active lipopolyplexes containing 1  $\mu\text{g}$  pCMV-GFP were transfected as described in ultrasound-mediated transfection. The cells were exposed to post-transfection ultrasound for 60 s after 240 min incubation. The cells transfected with complexes without ultrasound were considered as control groups to compare the effect of ultrasound. After 48 h of incubation, the cells were observed under the microscope (CKX-53 Olympus, USA microscope) at excitation/emission wavelength 505/530 nm.

#### 2.4.2.7 Sub-toxic concentration of chlorpromazine

SKOV-3 cells were seeded at cell density  $10^4$  cells /  $0.35 \text{ cm}^2$  in a 96 well microtiter plate and incubated for 24 h. Briefly, the cells were with the different concentrations of chlorpromazine and followed by 24 h incubation period. The culture medium was

aspirated completely. The cell viability was evaluated using MTT assay, described in Section 2.4.2.3.

#### *2.4.2.8 Ultrasound-mediated cellular uptake*

The cells were seeded in a 6 well plate at a cell density of  $3 \times 10^5$  cells /  $10 \text{ cm}^2$ . The cells were treated with  $5 \times 10^{-6}$  M chlorpromazine, a clathrin-dependent endocytosis inhibitor and the cells were incubated for 30 min. The cell culture medium containing inhibitor was aspirated, and cells were washed with PBS (pH 7.4) followed by ultrasound-mediated transfection of DPPC/CH/DPPG/PEG40S ultrasound active lipopolyplexes as described in section 2.4.2.4. The transfection efficiency for cells pretreated with chlorpromazine treated and non-treated cells was measured with different combination of ‘ultrasound’ and no ultrasound’ treatment. The results were evaluated statistically by performing a two-way ANOVA test for multiple comparisons.

#### *2.4.2.9 Harvesting SKOV-3 cells as 3D cell culture*

3D cell culture was cultivated using an ultralow attachment method using agar coated 24 - well plate.<sup>131</sup> Briefly, 200  $\mu\text{L}$  of sterile 1% agar was added per well and equilibrated with a culture medium. After the agar congeals, 5000 cells were harvested in each well and incubated for until spheroid diameter reached around  $\geq 800 \mu\text{m}$ . The culture medium was aspirated, and spheroids were washed with PBS (pH 7.4) before further evaluation.

#### *2.4.2.10 Ultrasound mediated transfection in 3D cell culture*

The viable spheroids were first carefully transferred to a 2 mL sterile reaction tube, followed by the addition of polyplexes, lipopolyplexes and ultrasound-active lipopolyplexes containing 1  $\mu\text{g}$  pCMV-GFP in each spheroid and the fresh medium was added up to the brim of the vial. The ultrasound probe was exposed to the spheroid in a water bath for 60 s after 240 min incubation time interval. The spheroids were transferred to an agar coated well plate along with the rest of the medium. The transfected spheroids were incubated for 72 h for complete GFP expression. After incubation, the spheroids were observed under the microscope (CKX-53 Olympus, USA microscope) at excitation/emission wavelength 505/530 nm.

### 2.4.3 Photosensitizer induced gene delivery

#### 2.4.3.1 Cell viability

Briefly, HepG2 cells were seeded at a cell density of  $10^4$  cells /  $0.3 \text{ cm}^2$  in a 96 well microtiter plate and incubated for 24 h. Further, the cells were incubated with hypericin liposomes with different hypericin concentrations followed by photoirradiation.<sup>66</sup> For irradiation experiments, a prototype low power light-emitting diode (Lumundus, Eisenach, Germany) was adopted for 96 - well plates, providing irradiance fluence of  $27 \text{ W/cm}^2$  at 589 nm was used. The cells were exposed to irradiation for  $200 \text{ mJ/cm}^2$ ,  $400 \text{ mJ/cm}^2$ ,  $600 \text{ mJ/cm}^2$ ,  $1000 \text{ mJ/cm}^2$  and  $2000 \text{ mJ/cm}^2$  respectively and incubated. The duration of irradiation was calculated using equation 5.

$$\text{Light dose } \left( \frac{J}{\text{cm}^2} \right) = \text{Irradaiton fluence } \left( \frac{W}{\text{cm}^2} \right) \times \text{exposure (sec)}$$

#### Equation 5. Formula for calculation of irradiation duration

After 24 h incubation period, the culture medium was aspirated completely.  $100 \mu\text{L}$  MTT (1:10 in DMEM) was added to each well and the cells were incubated at  $37^\circ\text{C}$  for 4 h. The formazan product produced in each well was dissolved in  $100 \mu\text{L}$  of DMSO solution. The absorbance was measured by FLUOstar (Optima microplate reader) at 485 nm. Each experiment was repeated thrice. The average absorbance was calculated based on the absorbance of 0.1% Triton-X treated cells.

#### 2.4.3.2 Photosensitizer induced gene delivery

Briefly, HepG2 cells were seeded at a cell density of  $10^4$  cells /  $0.35 \text{ cm}^2$  in the sterile white 96 well microtiter plate. The cells were transfected with  $25 \mu\text{L}$  hypericin lipopolyplexes containing  $0.25 \mu\text{g}$  pCMV-Luc and hypericin (50 nM to 500 nM). The group of cells transfected with free pDNA, polyplexes and lipopolyplexes respectively were considered as control. All formulations were prepared at optimized concentrations (N/P 10 and lipid: PEI 0.45). The cells were incubated for 2 h with the formulations in  $75 \mu\text{L}$  of fresh cell culture medium. After 2 h, the well plates were either irradiated at specific energies  $200 \text{ mJ/cm}^2$ ,  $600 \text{ mJ/cm}^2$  and  $1000 \text{ mJ/cm}^2$  or kept dark as the control as described in section 2.4.3.1. After additional 2 h incubation, the wells were then filled with the remaining  $25 \mu\text{L}$  medium and incubated for 48 h before further assay.

Following the incubation period, 100  $\mu\text{L}$  of Bright-glow Luciferase assay reagent (Promega) was added to the culture medium. The well plate was rotated for 2 min at 200 rpm for complete lysis followed by immediate measurement of luminescence on a multiplate reader (FLUOstar, Optima BMG). The cells were transfected in triplicates in each group and the protein quantification was performed as described in section 2.4.2.2. The results were represented as RLU/mg of protein  $\pm$  S.D.

#### 2.4.3.3 Photocytotoxicity

The cytotoxicity was studied upstream to the evaluation of transfection efficiency in the same transfected cells by hypericin lipopolyplexes using LDH Assay. The cells were transfected and irradiated as described in section 2.4.3.2. After 48 h of incubation, 100  $\mu\text{L}$  of cell culture medium was carefully transferred to another optical transparent bottom white 96 well microtiter plate. To this 100  $\mu\text{L}$  of freshly prepared LDH assay buffer having WST-1, a substrate to lactate dehydrogenase was added and incubated for 30 mins at room temperature. The absorbance of the orange complex formed by the reaction was determined at 485 nm using a multiplate reader (FLUOstar, Optima BMG). The cells treated with 10  $\mu\text{L}$  of cell lysis solution were considered as a positive control. The experiment was carried out in triplicate and the mean absorbance  $\pm$  S.D. was considered. As per the manufacturer's protocol percentage cytotoxicity was calculated by using the following equation 6.

$$\% \text{ Cytotoxicity} = \frac{[\text{OD}_{485} \text{ transfected cells} - \text{OD}_{485} \text{ non transfected cells}]}{[\text{OD}_{485} \text{ lysed cells} - \text{OD}_{485} \text{ non transfected cells}]} \times 100$$

#### **Equation 6. Formula for calculation of % cytotoxicity**

#### 2.4.3.4 Cellular uptake of hypericin lipopolyplexes

Briefly,  $9 \times 10^4$  cells /  $3.5 \text{ cm}^2$  were seeded onto a sterile coverslip in a 12 well plate and incubated overnight. Further, hypericin lipopolyplexes (50 nM hypericin) were incubated with cells for a 2 h time interval. The old medium was washed and replaced with a fresh medium and incubated further for 5 mins. For assessment of the effect of photoirradiation, the group of cells were exposed to light at  $200 \text{ mJ/cm}^2$ ,  $600 \text{ mJ/cm}^2$ ,  $1000 \text{ mJ/cm}^2$  light doses and kept in dark respectively. The cells were washed with PBS followed by fixing with 4% paraformaldehyde for 15 min at room temperature. The cells were counterstained with DAPI (0.6  $\mu\text{g/mL}$ ) for 20 min in dark at room temperature. The cells were washed,

and the coverslips were mounted on the slide using FluroSave™ as a mounting agent. The cells were observed at excitation/emission wavelength 590/620 nm for hypericin and 358/461 nm for DAPI visualization using a confocal laser scanning microscope (Zeiss LSM 700, Carl Zeiss Microscopy GmbH, Jena, Germany)

#### *2.4.3.5 Quantification of intracellular reactive oxygen species*

The intracellular reactive oxygen species (ROS) generated upon photoirradiation of hypericin were evaluated using 2',7'-dichlorofluorescein diacetate (DCFDA) (Merck Millipore).<sup>132</sup> Briefly,  $2 \times 10^4$  cells /  $0.35 \text{ cm}^2$  were seeded and incubated overnight at 37 °C. After incubation, the cells were treated with 25  $\mu\text{L}$  hypericin lipopolyplexes containing 0.25  $\mu\text{g}$  pCMV-Luc and 50 nM hypericin per well along with the addition of 75  $\mu\text{L}$  RPMI medium and incubated for 2 h. The medium was replaced with 10  $\mu\text{M}$  DCFDA (a non-fluorescent dye) in 75  $\mu\text{L}$  phenol red-free culture medium in each well. The well plates were incubated for 45 mins at 37 °C. After incubation, the cells were washed three times with 1X PBS and were irradiated at 200  $\text{mJ}/\text{cm}^2$ , 600  $\text{mJ}/\text{cm}^2$  and 1000  $\text{mJ}/\text{cm}^2$  energies or kept dark as the control. Immediately 125  $\mu\text{L}$  cell lysis reagent was added and the cells were vortexed for 10 mins. The cell lysates of all well plates were transferred to a single black bottom opaque 96 well plate and the green fluorescence of DCFH at excitation/emission wavelength 485/535 nm was measured. The cells with 'no treatment' and treatment with 50  $\mu\text{M}$  TBHP were considered as negative and positive control respectively for each group. The experiment was carried out in triplicate and the mean fluorescence  $\pm$  S.D. was considered.

For visualization of green fluorescence of DCFH, the above procedure was repeated till photoirradiation procedure as described above. The cells were washed and fixed using 4% paraformaldehyde. The cells were observed under the microscope (CKX-53 Olympus, USA microscope) at excitation/emission wavelength 505/530 nm.

### **2.4.4 Selective phototransfection**

#### *2.4.4.1 Transferrin receptor (TfR) expression in HepG2 cells*

To visualize cellular uptake of Tf-Fitc conjugate via TfR receptor,  $9 \times 10^4$  cells /  $3.5 \text{ cm}^2$  were seeded onto sterile coverslip in a 12 well plate.<sup>133</sup> The cells were incubated in FCS free cell culture medium for 30 mins at 37°C. The cells were washed thrice with PBS

with  $\text{Ca}^{+2}/\text{Mg}^{+2}$  followed by addition of 50  $\mu\text{g}/\text{mL}$  FITC labelled transferrin. The cells were incubated under different conditions. The cells were incubated for 25 min at  $4^{\circ}\text{C}$  and washed with PBS buffer followed by incubation for 5 min at  $37^{\circ}\text{C}$  (phase-chase period). The cells incubated at  $37^{\circ}\text{C}$  for 30 min were considered as control. The cells were fixed, counterstained and mounted as described in Section 2.4.3.4. The cells were observed under a confocal laser scanning microscope at excitation/emission wavelength 485/535 nm for FITC and 358/461 nm for DAPI. The mean fluorescence intensity was calculated by ImageJ software (n=3).

#### 2.4.4.2 *Ligand mediated cellular uptake*

To visualize binding of formulation with surface receptor, the cellular uptake of antibody conjugated formulation Tf-Hy-LPP was evaluated. Briefly,  $9 \times 10^4$  cells /  $3.5 \text{ cm}^2$  were seeded onto sterile coverslip in a 12 well plate and incubated for 24 h to obtain confluency. The cells were pre-treated with receptor blocking buffer containing 10  $\mu\text{M}$  chlorpromazine in 3% BSA in PBS for 1 h at  $37^{\circ}\text{C}$ . The cells without pretreatment were considered as control group. Further, the cells were washed and treated with Tf-Hy-LPP and Hy-LPP formulation containing 1  $\mu\text{g}$  pCMV-Luc and 50 nM hypericin and were incubated with cells for 4 h at  $37^{\circ}\text{C}$ . The sample slides were prepared as described in Section 2.4.3.4. The cells were observed under a confocal laser scanning microscope at excitation/emission wavelength 590/620 nm for hypericin and 358/461 nm for DAPI.

#### 2.4.4.3 *GFP Visualization*

For the determination of the GFP expression  $5 \times 10^4$  cells /  $1.9 \text{ cm}^2$  were seeded onto 24 well plate and transfected. The cells were transfected with PP, Hy-LPP and Tf-Hy-LPP formulations containing 1  $\mu\text{g}$  pCMV-GFP and 50 nM hypericin. After 2 h incubation, the cells were exposed to irradiation at 600  $\text{mJ}/\text{cm}^2$  light dose or kept in dark as a control. Further, the cells were incubated for 48 h for expression of the green fluorescent protein and observed under the microscope (CKX-53 Olympus, USA microscope) at excitation/emission wavelength 505/530 nm for GFP.

### **3. Results & Discussion - Ultrasound - mediated gene delivery**

#### **3.1 Characterization of ultrasound-active contrast vesicles**

##### **3.1.1 Ultrasound contrast measurements**

In this study, the lipid vesicles were prepared using the mixture of lipids and polyethylene glycol (40) stearate. The ultrasound-active contrast vesicles were prepared by the mechanical agitation of preformed lipid vesicles. The visualization of DPPC/CH/PEG40S and DPPC/CH/DPPG/PEG40S using ultrasound transducer at 1.4 MHz frequency exhibited ultrasound contrast in the tissue-mimicking flow model. (Figure 14). DPPC/CH/DPPG/PEG40S displayed stronger ultrasound contrast. The inclusion of PEG40S facilitates the non-lamellar orientation in phospholipid bilayer of lipid vesicles. The non-bilayer structure of lipid shell has been influential role in destabilization of the membrane upon exposure to external stimuli such as ultrasound. The lipid-emulsifier composition affects the sonosensitivity of the vesicles by virtue of the packing parameter of the phospholipid.<sup>128,134</sup> These vesicles were stored at +4 °C and were found to retain their contrast property for as long as 72 h. The albumin nanobubbles filled with perfluorocarbon remain stable for 2 h. Similarly, marketed ultrasound contrast agents have been recommended to use within 6 h, once reconstituted.<sup>116</sup>

##### **3.1.2 Average particle size and zeta potential**

The systemized air purging and agitation at optimized speed and duration affect the particle size of the prepared formulations. The average particle size and the polydispersity index of the formulations were found to increase after agitation process (Table 6). It was observed that the presence of cholesterol retards the influence of agitation on size distribution of vesicles. Moreover, inclusion of DPPG lipid preserve the lower particle size distribution of the formulation, with PDI ~ 0.19 after agitation process. It was attributed that the double chained lipid with small anionic head group facilitate the formation of non-lamellar bilayer phospholipid membrane of formulation.

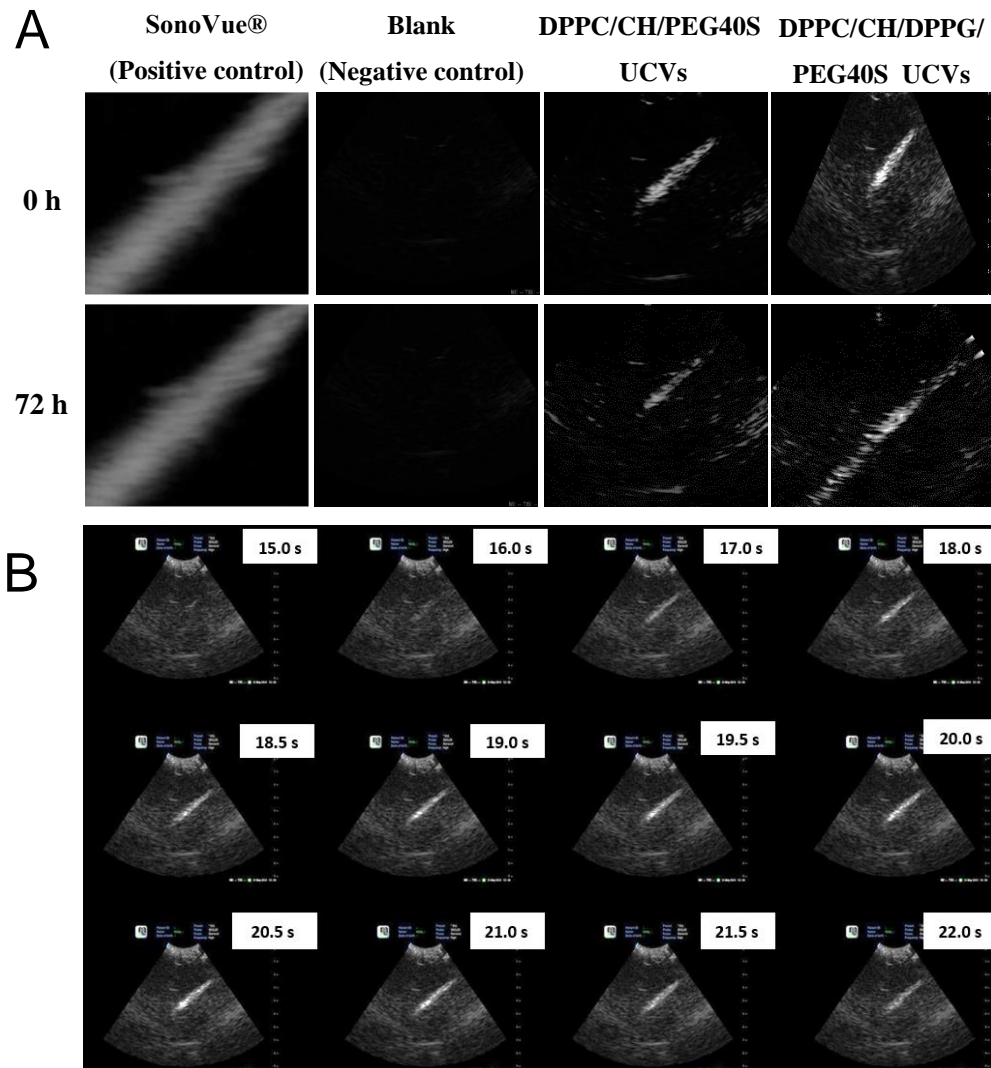


**Figure 14. Ultrasound contrast measurements of ultrasound-active contrast vesicles.** (A) The ultrasound contrast images in a tissue-mimicking agarose model using an ultrasound transducer at 1.4 MHz frequency after 0 h and 72 h storage (a) SonoVue® (positive control) (b) blank (negative control) (c) DPPC/CH/PEG40S UCVs (d) DPPC/CH/DPPG/PEG40S UCVs. (B) A visual comparison of the ultrasound contrast exhibited by DPPC/CH/DPPG/PEG40S UCVs at different time intervals during the flow.

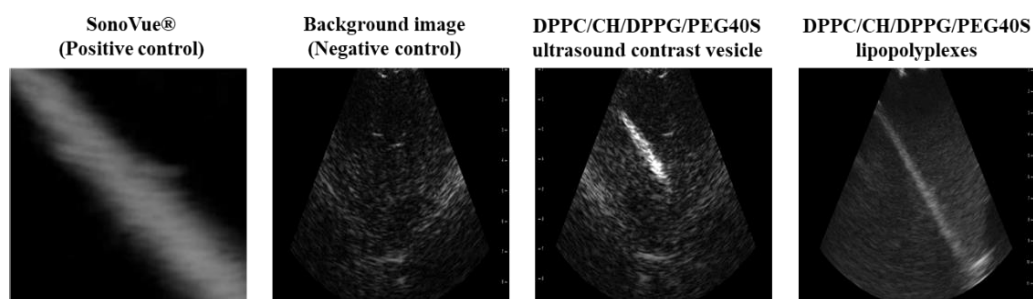


**Figure 15. Ultrasound contrast measurements of ultrasound-active lipopolyplexes.** The ultrasound contrast images in a tissue-mimicking agarose model using an ultrasound transducer at 1.4 MHz frequency: (a) SonoVue® (positive control) (b) blank (negative control) (c) DPPC/CH/DPPG/PEG40S UCVs (d) DPPC/CH/DPPG/PEG40S ultrasound-active lipopolyplexes



The single chained PEG40S lipid has a small portion of the hydrophobic part. Therefore, PEG40S arranges at the interface of the aqueous/lipid phases of the phospholipid bilayer of ultrasound-active contrast vesicles.<sup>135,136</sup> The mechanical agitation improves the interface between the phospholipid bilayer of prepared ultrasound-contrast vesicles. It has been interpreted that the presence of PEG40S facilitate the gas phase, that has been entrapped by the pressurized air-purging process, in the core or between bilayers of ultrasound-active contrast vesicles. The observed increment in average particle size and polydispersity index of ultrasound-active contrast vesicles was ascribed to the agitation process. It was observed that the surface potential of the liposomes remained unchanged due to the agitation process. DPPC/CH/PEG40S UCVs and DPPC/CH/DPPG/PEG40S UCVs exhibited nearly about  $-5.0 \pm 0.02$  mV and  $-8.0 \pm 0.01$  mV, respectively. UCVs maintains its vascular retention for a longer period due to anionic surface charge.<sup>137,127</sup>

**Table 6. Physicochemical properties of the formulations**

Lipid composition (Molar ratio)	Liposomes			Ultrasound-active contrast vesicles		
	Average particle size (nm $\pm$ S.D)	Zeta potential (mV $\pm$ S.D)	PDI	Average particle size (nm $\pm$ S.D)	Zeta potential (mV $\pm$ S.D)	PDI
DPPC/ PEG40S (95: 5)	70.74 $\pm$ 1.59	-3.7 $\pm$ 0.04	0.15 $\pm$ 0.02	157.2 $\pm$ 65.28	-3.0 $\pm$ 0.06	0.96 $\pm$ 0.06
DPPC/CH/ PEG40S (80: 15: 5)	115.0 $\pm$ 0.56	-4.0 $\pm$ 0.05	0.16 $\pm$ 0.01	125.6 $\pm$ 2.77	-5.0 $\pm$ 0.02	0.27 $\pm$ 0.05
DPPC/ CH/ DPPG/ PEG40S (80: 10: 5:5)	118.0 $\pm$ 3.36	-8.0 $\pm$ 0.03	0.19 $\pm$ 0.01	126.0 $\pm$ 3.59	-8.8 $\pm$ 0.01	0.19 $\pm$ 0.02

### 3.1.3 AFM

Atomic force microscopy (AFM) was performed to visualize the surface morphology and diameter of the ultrasound-active contrast vesicles. DPPC/CH/PEG40S UCVs and DPPC/CH/DPPG/PEG40S UCVs were distinctly spherical shaped, and their diameters were  $150.3 \pm 16.8$  nm and  $119 \pm 5.7$  nm, respectively (Figure 16). DPPC/CH/PEG40S ultrasound-active vesicles displayed evident polydispersity. It was attributed to the effect

of lower magnitude of negative surface potential that could lead to aggregation after agitation process. On contrary, presence of DPPG lipid increased the surface charge of DPPC/CH/DPPG/PEG40S UCVs which prevented aggregation upon the agitation process.

The mean diameters ranges from 1.5 – 2.5  $\mu\text{m}$  and 2.0 – 4.5  $\mu\text{m}$  for SonoVue<sup>®</sup> and Optison, respectively.<sup>115</sup> The average particle size and ultrasound contrast of formulations were compared with the standard formulation, SonoVue<sup>®</sup> (a marketed ultrasound contrast agent). Moreover, the ultrasound contrast results were represented in terms of a grey-scale as shown in Figure 17. It was measured that DPPC/CH/DPPG/PEG40S UCVs showed 70% equivalent ultrasound contrast as compared to SonoVue<sup>®</sup>. The prepared UCVs were superior to the marketed preparation as both UCVs exhibited lower average particle size and comparable ultrasound contrast. These characteristics of ultrasound-active contrast vesicles were suitable for image-guided passive tumor targeting in the tumor vasculature region that ranges from 200 nm to 1.2  $\mu\text{m}$ .<sup>116</sup>

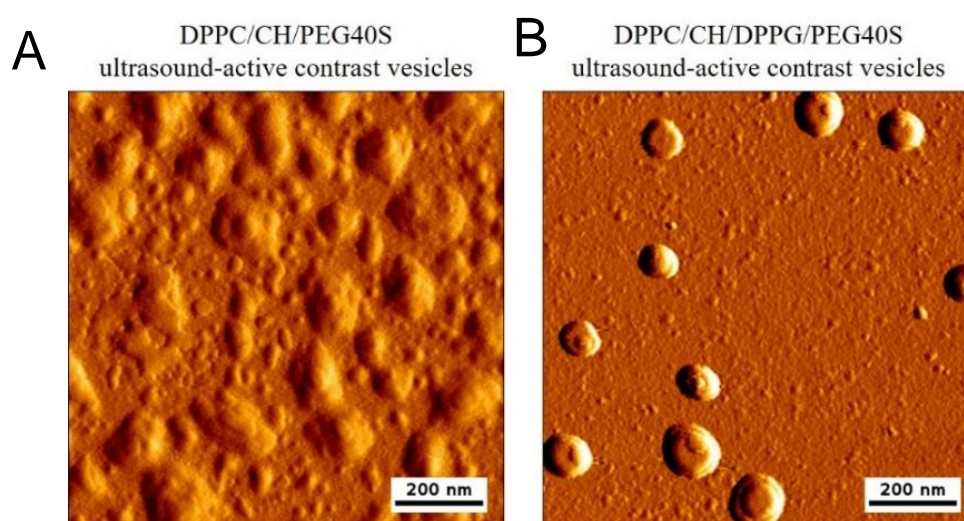


**Figure 16. AFM micrograph of ultrasound-active contrast vesicles.** AFM micrograph of (A) DPPC/CH/PEG40S UCV and (B) AFM DPPC/CH/DPPG/PEG40S UCV using intermittent contact mode of Cantilever tip and scanned in the amplitude view at about  $1 \times 1 \mu\text{m}^2$  ( $512 \times 512$  pixels) dimension. (Scale bar 200 nm)

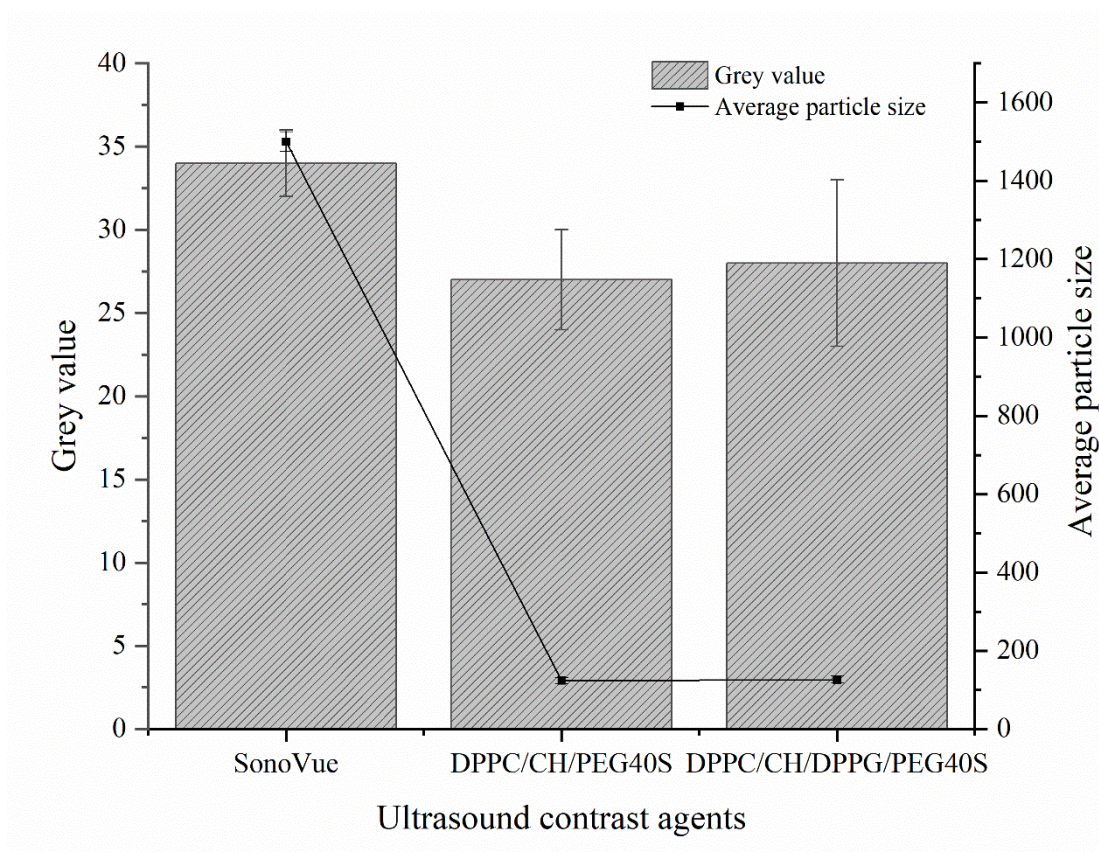


**Figure 17. Comparison of ultrasound-active contrast vesicles with standard UCA.** Relative comparison of the size represented as ‘average particle size’ and ultrasound contrast represented as ‘grey value’ of UCVs with SonoVue®. The data are expressed as the mean ± SD (n = 3)

## 3.2 Characterization of polyplexes and lipopolyplexes

### 3.2.1 N/P ratio optimization

The addition of IPEI at a different concentration to pDNA forms a series of complexes which were assessed by photon correlation spectroscopy (PCS). Depending upon the N/P ratio, the average particle size of the polyplexes ranges between 250 to 500 nm, while the zeta potential drifted towards positive potential with increase in N/P ratio (Figure 18). The minimum average particle size of polyplexes prepared at N/P ratio 12 was reported to be  $170.5 \pm 17.7$  nm (n=3) and zeta potential was  $+14.7 \pm 2.4$  mV. The primary amines and secondary amines present in the backbone of IPEI condense with DNA to form positively charged polyplexes (IPEI/pDNA complexes).<sup>98,138</sup> The increase in the particle size at a low N/P ratio was attributed to the formation of loose aggregates. Further, lipopolyplexes were prepared using polyplexes at N/P ratio 12.

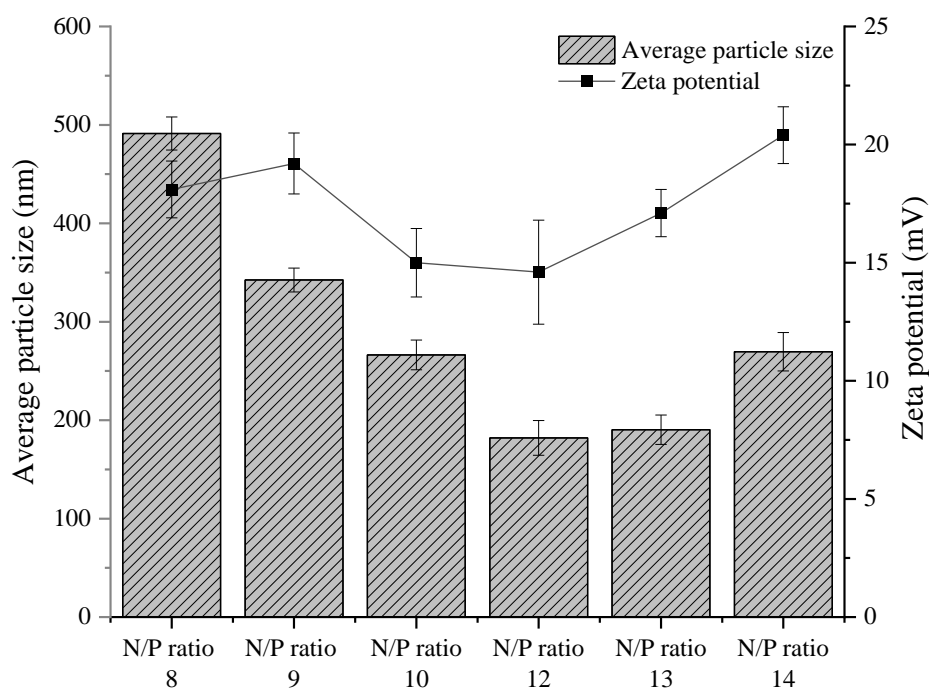


**Figure 18. Optimization of N/P ratio.** Average particle size and zeta potential of polyplexes (IPEI/pDNA complexes) at different N/P ratios. The data are expressed as the mean  $\pm$  SD (n = 3)

### 3.2.2 Average particle size and zeta potential

The lipopolyplexes were formed with electrostatic interaction between positively charged polyplex and negatively charged ultrasound-active contrast vesicles. The dynamic light scattering technique measured average particle size and zeta potential of DPPC/CH/PEG40S lipopolyplexes (LPP 1) and DPPC/CH/DPPG/PEG40S lipopolyplexes (LPP 2) at lipid: PEI mass ratio 0.4 to 0.7 as shown in Table 7.

The lipid: PEI mass ratio 0.5 was optimized for further studies. DPPC/CH/PEG40S LPPx (LPP 1) showed minimum average size  $338.9 \pm 4.5$  nm and zeta potential  $4.85 \pm 1.5$  mV. DPPC/CH/DPPG/PEG40S LPPx (LPP 2) showed minimum average particle size  $238.7 \pm 4.7$  nm and zeta potential  $+5.68 \pm 1.6$  mV. At higher lipid: PEI mass ratio the average particle size increased which was attributed to the aggregation of lipopolyplexes.<sup>98</sup> The zeta potential of lipopolyplexes at lipid:PEI mass ratio 0.7 exhibited  $2.18 \pm 1.3$  mV and  $1.83 \pm 0.5$  mV for LPP 1 and LPP 2, respectively. It was attributed to increasing

concentration of anionic lipid vesicles (Table 7). Notably, the particle size of both lipopolyplexes formulations was larger than the particle sizes of initial ultrasound-active contrast vesicles. The results pointed out that the ultrasound-active contrast vesicles may form a lipid coat on polyplexes, which was in agreement with previous findings.<sup>97</sup>

**Table 7. Physicochemical properties of ultrasound-active lipopolyplexes**

Lipid: PEI mass ratios	DPPC/CH/PEG40S LPP <sub>x</sub>			DPPC/CH/DPPG/PEG40S LPP <sub>x</sub>		
	Average particle size (nm ± S.D)	Zeta potential (mV ± S.D)	PDI	Average particle size (nm ± S.D)	Zeta potential (mV ± S.D)	PDI
LPP (0.4)	478.2 ± 18.9	8.18 ± 2.4	0.54 ± 0.01	471.4 ± 12.2	6.95 ± 1.5	0.37 ± 0.04
LPP (0.5)	338.9 ± 4.5	4.85 ± 1.5	0.29 ± 0.03	238.7 ± 4.7	5.68 ± 1.6	0.22 ± 0.09
LPP (0.6)	751.5 ± 9.9	1.20 ± 0.5	0.44 ± 0.03	349.6 ± 6.4	4.00 ± 0.1	0.29 ± 0.06
LPP (0.7)	735.0 ± 5.6	2.18 ± 1.3	0.70 ± 0.07	523.6 ± 4.2	1.83 ± 0.5	0.45 ± 0.02

### 3.2.3 AFM

The atomic force microscopy was performed to visualize surface morphology and measure the diameter of the DPPC/CH/PEG40S (LPP 1) and DPPC/CH/DPPG/PEG40S (LPP 2) ultrasound-active lipopolyplexes. It was found that the diameter of LPP 1 was  $243.4 \pm 24.3$  nm while LPP 2 were  $168.84 \pm 5.4$  nm (Figure 19). The results were in agreement with PCS analysis. It was observed that LPP 2 showed the integration of uncoiled PEG40S tail oriented on the consequent lipid. It was observed elsewhere that echogenicity is based on the polyethyleneglycol chain regime on the surface of the vesicle.<sup>128,139</sup> Further, it was observed that LPP 2 exhibited ultrasound contrast comparable to the controls in a tissue mimicking agarose model as shown in Figure 15.

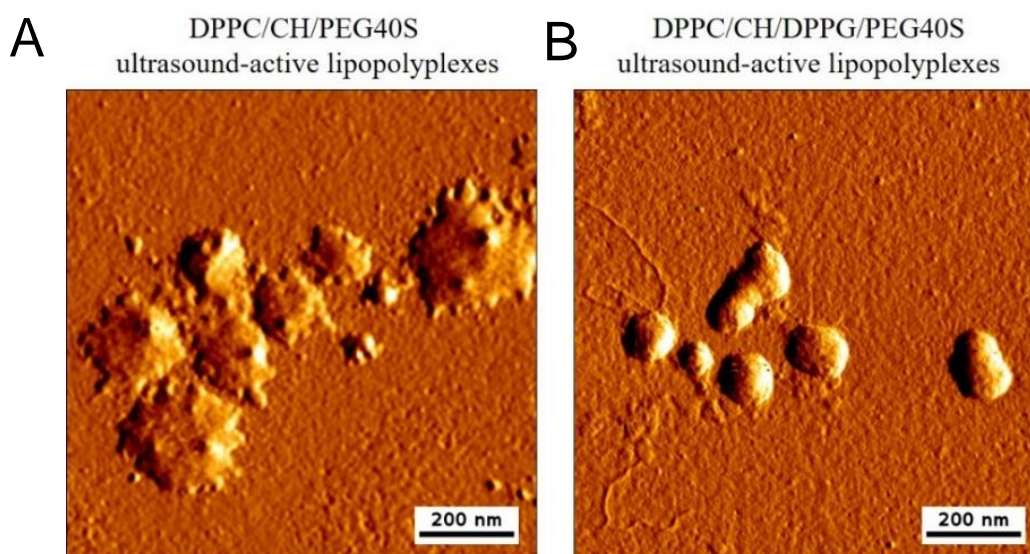


**Figure 19. AFM micrographs of ultrasound-active lipopolyplexes.** AFM micrograph of (A) DPPC/CH/PEG40S and (B) DPPC/CH/DPPG/PEG40S ultrasound active lipopolyplexes using intermittent contact mode of Cantilever tip and scanned in the amplitude view at about  $1 \times 1 \mu\text{m}^2$  ( $512 \times 512$  pixels) dimension. (Scale bar 200 nm)

### 3.3 In-vitro cell culture evaluation

#### 3.3.1 Transfection efficiency

The in-vitro optimization of the formulations was based on evaluation of their transfection efficiency and cell viability. The transfection efficiencies of polyplexes (IPEI/pDNA) were evaluated in SKOV-3 cells. The transfection efficiency of polyplexes at different N/P ratio was significantly raised as compared to the free plasmid.<sup>45</sup> A higher transfection efficiency was observed at N/P ratio 12 (Figure 20). However, lipopolyplexes at different lipid: PEI mass ratios transfected more SKOV-3 cells than polyplexes (N/P ratio 12) (Figure 20). DPPC/CH/PEG40S lipopolyplexes (LPP 1) showed 10-fold higher transfection than polyplexes ( $p < 0.001$ ). No significant difference in luciferase activity between lipopolyplexes at different lipid: PEI mass ratio. The similarity in luciferase expression was attributed to non-uniform particle size distribution of DPPC/CH/PEG40S ultrasound-active contrast vesicles (Section 3.1.3). The transfection efficiency of DPPC/CH/DPPG/PEG40S lipopolyplexes (LPP 2) at lipid:PEI mass ratio 0.5 increased 20-fold than polyplexes ( $p < 0.001$ ). The lower transfection efficiency at lipid: PEI mass ratio  $> 0.5$  was attributed to aggregation of the particles at lower zeta potential of ultrasound-active lipopolyplexes.<sup>140</sup>

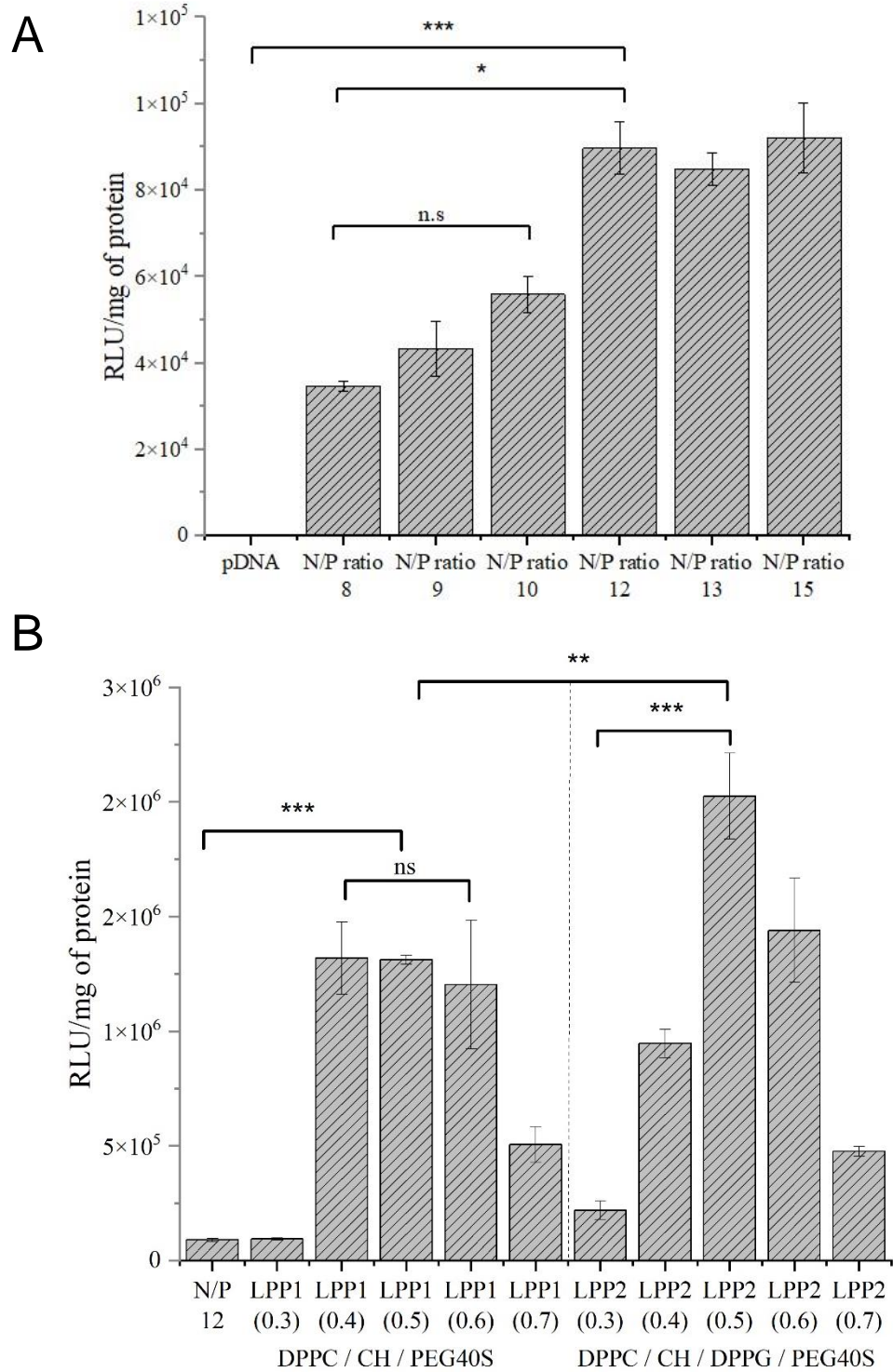


**Figure 20. Transfection efficiency of polyplexes (IPEI/pDNA complexes) and lipopolyplexes.** (A) Luciferase expression by polyplexes at different N/P ratios in SKOV-3 cells. (B) Luciferase expression by lipopolyplexes (LPP 1 and LPP2) in SKOV-3 cells, prepared by complex formation between polyplexes (N/P ratio 12) and ultrasound-active contrast vesicles at different lipid: PEI mass ratio. The data are expressed as the mean  $\pm$  SD (n = 3) and the statistical significance, evaluated using two-tailed Student t-test, is indicated as \*\*p<0.01 and \*\*\*p<0.001.

The result confirmed the initial hypothesis that ultrasound-active contrast vesicles encapsulate polyplexes and form ultrasound-active lipopolyplexes. The transfection efficiency of lipopolyplexes is affected by cell uptake of formulation, which is based on the architecture, size, and zeta potential of the formulation.<sup>141</sup> It was observed that DPPC/CH/DPPG/PEG40S lipopolyplexes (LPP 2) showed fivefold higher transfection than DPPC/CH/PEG40S lipopolyplexes (LPP 1) ( $p < 0.01$ ). The reduced size of the carrier improved the transfection efficiency of the non-viral carrier.<sup>117</sup>

### **3.3.2 Cell viability**

The cell viability of different polyplexes and ultrasound-active lipopolyplexes formulations were evaluated and compared with cell viability of blank cells (positive control group; ~ 100 %). The cell viability of SKOV-3 cells treated with pDNA showed no effect as the free plasmid easily degrades in aqueous medium. Further, the cell viability was reduced when the cells were treated polyplexes (IPEI/pDNA complexes). The cell viability decreased with increase in N/P ratio (Figure 21). The polyplexes with N/P ratio 12 was considered for further evaluation based on its transfection efficiency and cell viability.

On the contrary, the cell viability improved when cells were treated with DPPC/CH/PEG40S lipopolyplexes and DPPC/CH/DPPG/PEG40S lipopolyplexes as compared to polyplexes (N/P ratio 12). (Figure 21). This increase in cell viability of SKOV-3 cells was manifested by the encapsulation of PEI/pDNA complexes by lipid vesicles. It was observed that lipopolyplexes exhibited nearly 20 % higher cell viability than polyplexes ( $p < 0.01$ ). The higher lipid: PEI mass ratios of lipopolyplexes did not further improve cell viability. The results proved that ultrasound-active lipopolyplexes were biocompatible formulations.



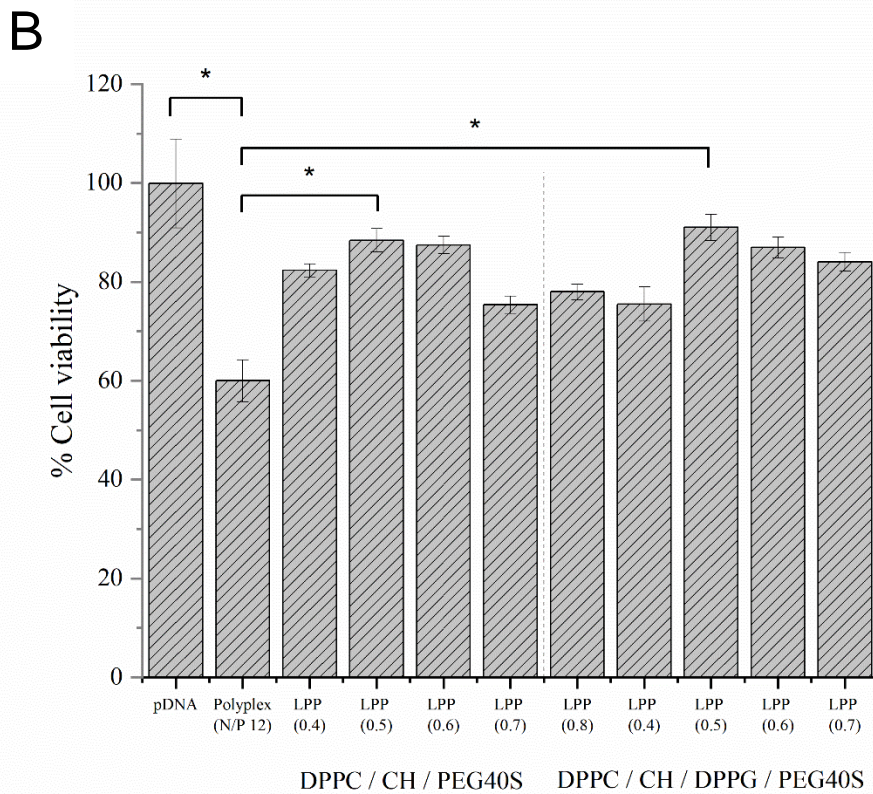
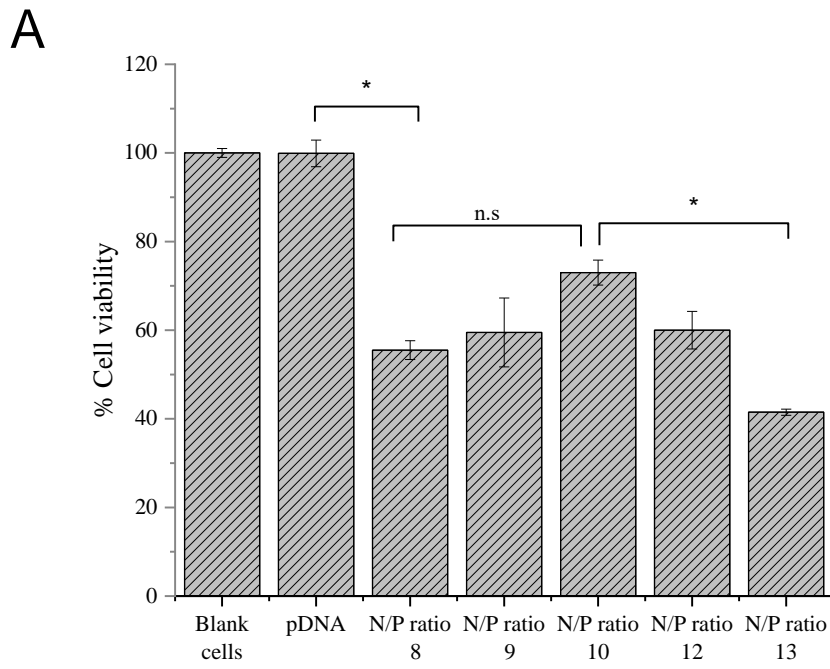


**Figure 21. Cell viability of cells incubated with polyplexes (IPEI/pDNA complexes) and lipopolyplexes.** (A) SKOV-3 cells transfected with polyplexes at different N/P ratios in SKOV-3 cells. (B) SKOV-3 cells transfected by lipopolyplexes, prepared by complex formation between polyplexes (N/P ratio 12) and ultrasound-active contrast vesicles at different lipid: PEI mass ratios. The data are expressed as the mean  $\pm$  SD (n = 3) and the statistical significance is indicated as \* $p < 0.01$ .

### 3.3.3 Ultrasound-mediated transfection

The ultrasound-active lipopolyplexes were prepared using polyplex (N/P ratio 12) complexed with DPPC/CH/PEG40S and DPPC/CH/DPPG/PEG40S ultrasound-active contrast vesicles, respectively. To determine the effect of ultrasound on transfection of ultrasound-active lipopolyplexes, the cells were exposed to the low-frequency ultrasound (3 MHz) at a different post-transfection time interval. The transfection efficiency was evaluated using pCMV-Luc as a reporter gene and the optical readouts represented firefly luciferase expression in the SKOV-3 cell line. A medical ultrasound probe having a low mechanical index (1.0) was utilized for the experiments.

In this experiment, the cells without US treatment were considered as control and the cells with post-transfection US treatment were compared with the control group (Figure 22). The post-transfection ultrasound after 60 mins and 240 mins of cell incubation exhibited significant gene transfer ( $p < 0.0001$ ). It was observed that the longer incubation time intervals showed 50-fold rise in luciferase expression as compared to control group. Conversely, the post-transfection ultrasound treatment after 5 mins of cell incubation facilitates gene transfer however to a lesser extent. The shorter incubation time interval showed 4-fold higher in the transfection efficiency of the ultrasound-active lipopolyplexes as compared to control ( $p < 0.001$ ). Thus, it was interpreted that the ultrasound significantly facilitates the transfection efficiency of ultrasound-active lipopolyplexes.<sup>142</sup> However, the immediate exposure to ultrasound treatment after transfection did not yield substantial improvement in the transfection efficiency of the carrier.<sup>136</sup>

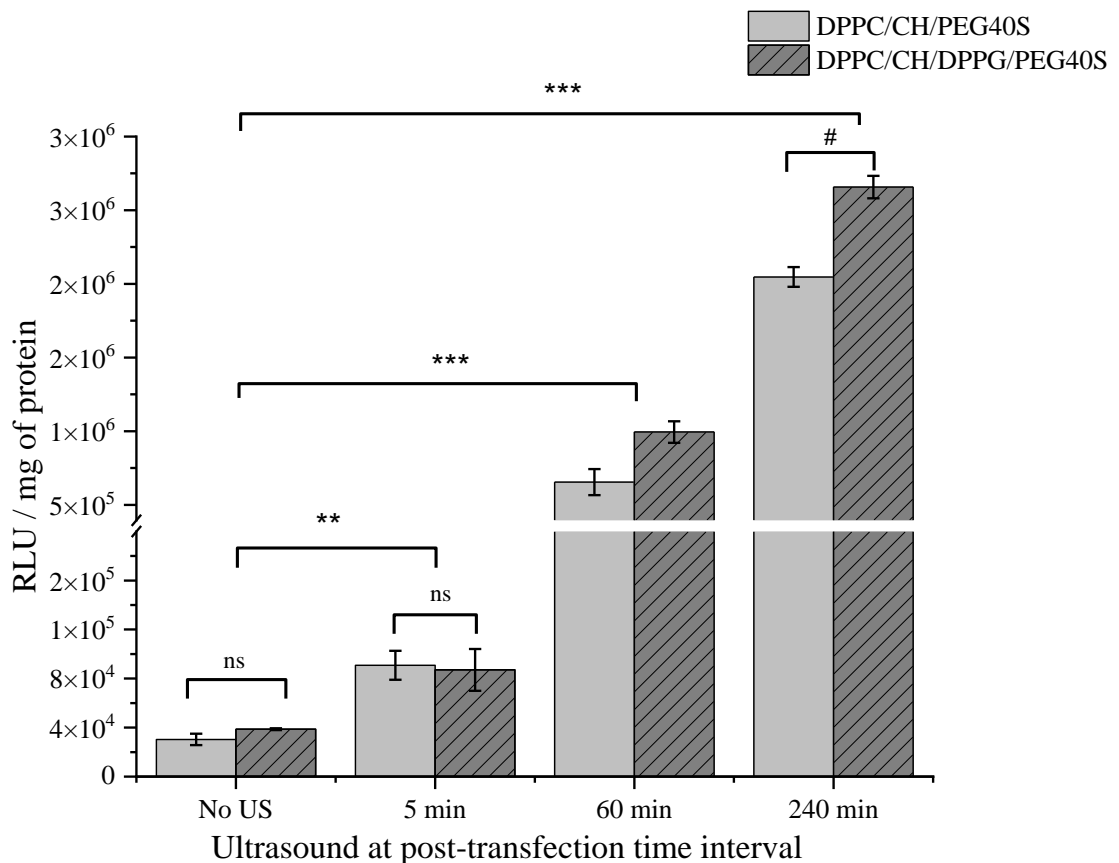


**Figure 22. Ultrasound-mediated transfection efficiency of ultrasound-active lipopolyplexes.** SKOV-3 cells were incubated with the ultrasound-active lipopolyplexes and exposed to ultrasound at 1.4 MHz for 60s at different time intervals. Luciferase expression by formulations were compared with the control cells i.e., no ultrasound exposure. The data are expressed as the mean  $\pm$  SD (n = 3) and the statistical significance is indicated as \*\*p<0.001 and \*\*\*p<0.0001 by Dunnett's multiple comparison test, #p<0.01 by the two-tailed Student t-test between two formulations.

The post-transfection ultrasound effect on transfection efficiency for LPP 1, having average particle size  $238.7 \pm 4.7$  nm, was nearly 25% higher as compared to LPP 2, having average particle size  $338.0 \pm 9.1$  nm. A significant difference in luciferase expression was observed (p < 0.01). This could be indicative that the size of the carrier established as an influencing parameter for the transfection of the nanocarrier. Taken together, the enhanced cell transfection of the carrier was noticeable only when the time interval between transfection and ultrasound treatment was  $\geq 1$  h. The result indicated that the time interval before ultrasound treatment as well as the size of nanocarriers are the significant factors.<sup>143,144</sup>

### 3.3.4 LDH release

To investigate cell damage due to the exposure of ultrasound, lactate dehydrogenase release by LDH assay was determined. It indicates the cell membrane integrity and thus the cytotoxicity of the carrier can be measured.<sup>126</sup> The transfected cells were subjected to post-transfection ultrasound at time intervals and subsequently LDH, which was released from the cells, was quantified (Figure 23). It was found that exposure to the ultrasound treatment slightly increased LDH release. It was observed that all formulations exhibited LDH levels, which were significantly lower as compared to the positive control. The formulations exhibited < 10 % cytotoxicity. Thus, ultrasound-active lipopolyplexes were considered non-toxic to the cells.<sup>130</sup> The results also demonstrated that the influence of ultrasound at low frequency for a short duration (60 s) does not alter the cell membrane integrity. The low-frequency ultrasound enhances the transfection efficiency of these non-viral carriers without significant cytotoxicity. It was established that ultrasound was non-invasive external stimuli for gene delivery.<sup>119,145</sup>

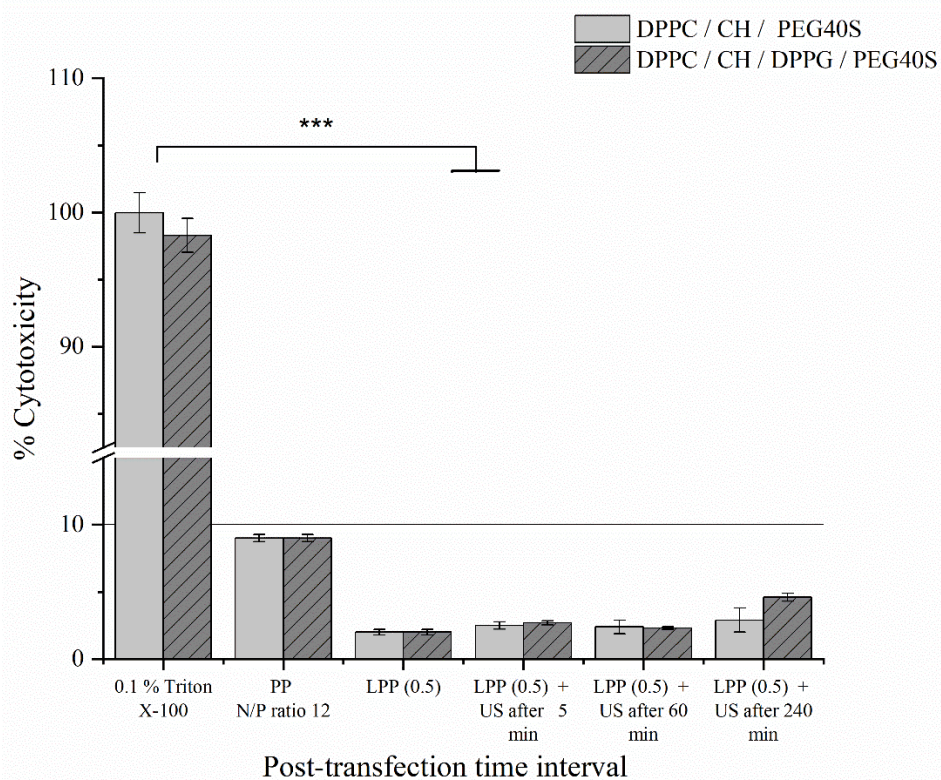


**Figure 23. LDH release upon ultrasound-mediated transfection.** The cells were incubated with the ultrasound-active lipopolyplexes and exposed to ultrasound at 1.4 MHz at different time intervals. The mean LDH-release in 0.1% Triton X-100 treated cells was considered as positive control. The data are expressed as the mean  $\pm$  SD (n = 3) and the statistical significance is indicated as \*\*\*p<0.001

### 3.3.5 GFP expression

SKOV-3 cells were transfected with pCMV-GFP, a reporter gene, encapsulated in DPPC/CH/DPPG/PEG40S ultrasound-active lipopolyplexes. The cells were transfected and were exposed to ultrasound after 240 mins incubation followed by visualization using fluorescence microscopy for. A substantial amount of translation of pCMV-GFP to green fluorescent protein in the cells with ultrasound treatment was observed (Figure 24). A significant difference was observed between the “no ultrasound” treatment group and the ultrasound treatment group.

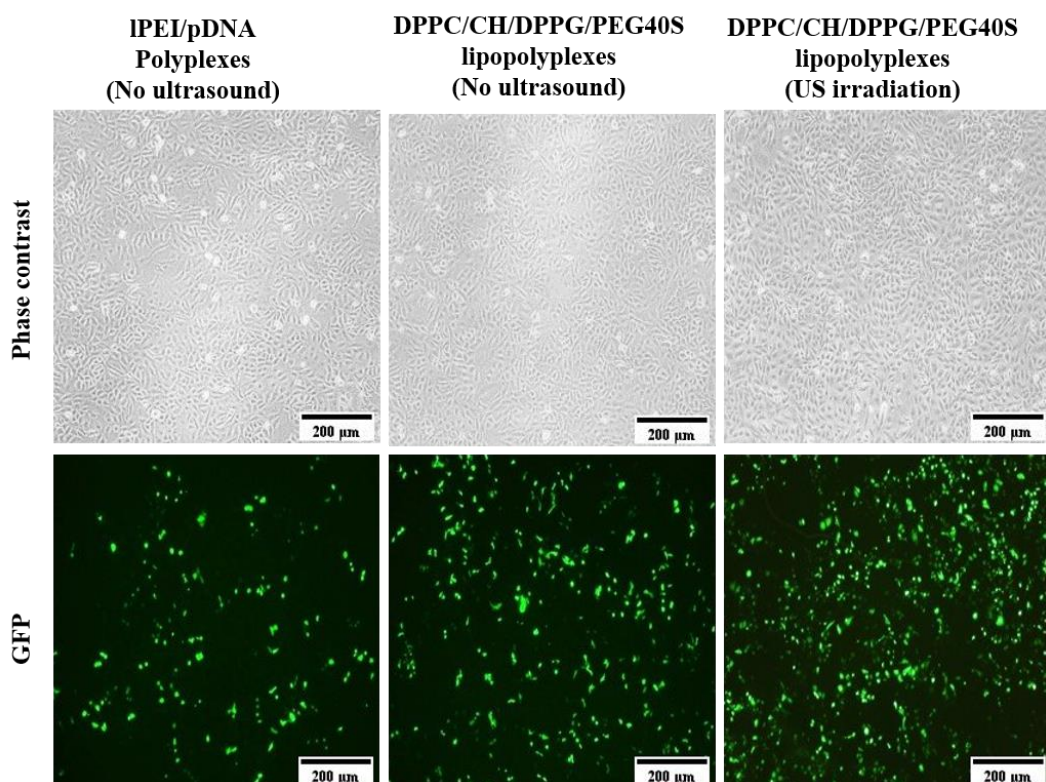


**Figure 24. Visualization of GFP expression.** SKOV-3 cells were transfected with DPPC/CH/DPPG/PEG40S ultrasound-active lipopolyplexes containing 1  $\mu\text{g}$  pCMV-GFP and exposed to ultrasound at 1.4 MHz after 240 min post-transfection time interval. The cells transfected with polyplexes and lipopolyplexes without ultrasound treatment were considered as control. (Scale bar 200  $\mu\text{m}$ )

### 3.3.6 Effect of ultrasound on cellular uptake

The gene transfer mechanism is a dynamic process and depends on various factors such as cellular internalization. The effect of low-frequency ultrasound on transfection of DPPC/CH/DPPG/PEG40S ultrasound-active lipopolyplexes in the presence of cellular

uptake pathway inhibitor was studied. Lipopolyplexes have been reported to primarily utilize clathrin-mediated endocytosis for cellular internalization.<sup>97,126</sup>

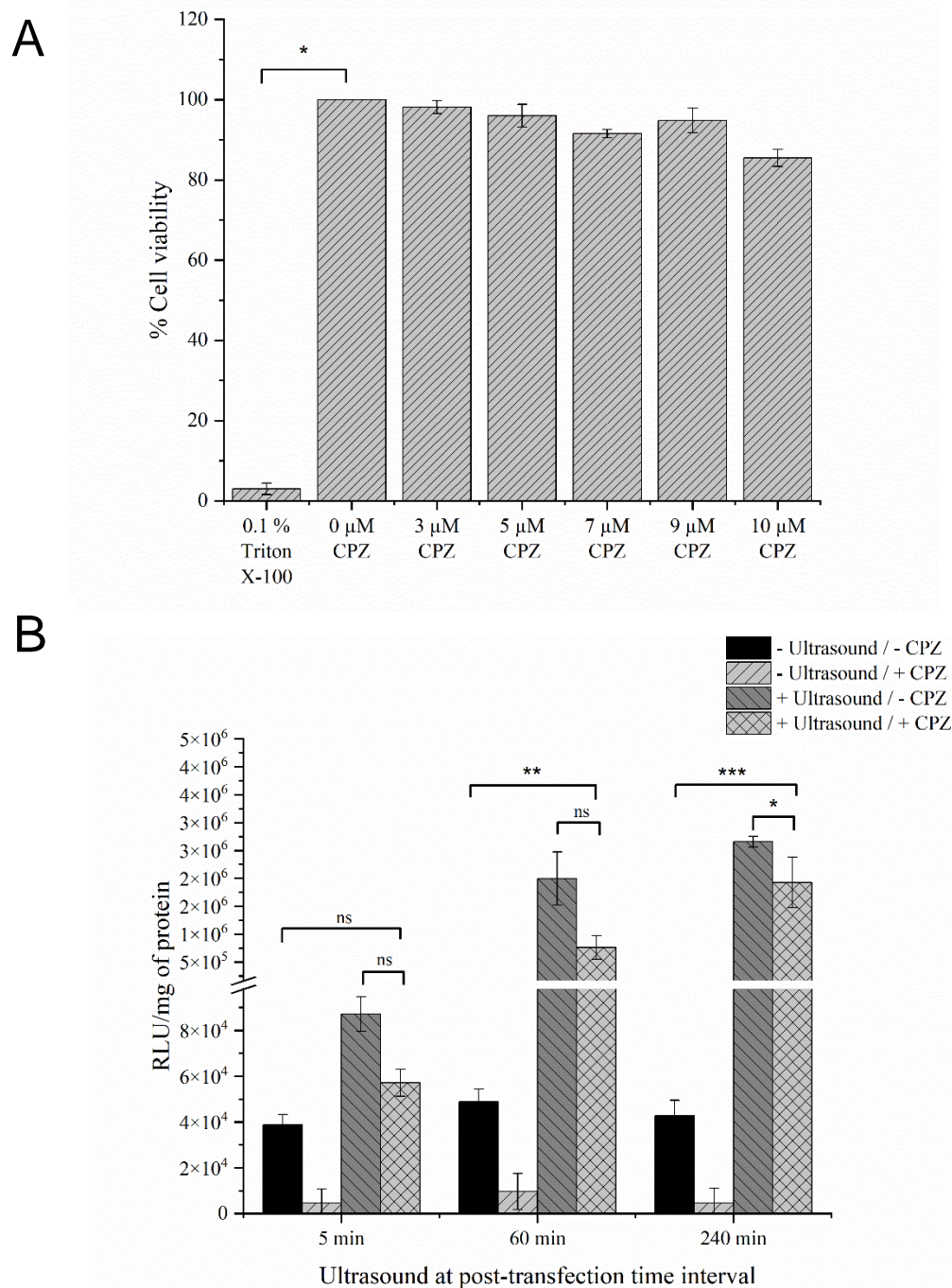


**Figure 25. Effect of post-transfection ultrasound treatment on the cellular uptake.** (A) SKOV-3 cells were treated with Chlorpromazine (CPZ) at 0 - 10  $\mu$ M concentration for selection of concentration for inhibition of the pathway. (B) The cells, pre-treated with 5  $\mu$ M chlorpromazine, were transfected with DPPC/CH/DPPG/PEG40S ultrasound-active lipopolyplexes and exposed to ultrasound after incubation. The cells without pretreatment of inhibitor and/or exposure to ultrasound were considered as control. The data are expressed as the mean  $\pm$  SD (n=3) and the statistical significance is indicated as \*p<0.01, \*\*p<0.001 and \*\*\*p<0.0001 by the two-way ANOVA multiple comparison test.

The sub-toxic concentration of chlorpromazine (5  $\mu\text{M}$ ) was determined (Figure 25). The transfection efficiency of lipopolyplexes in SKOV-3 cells, pre-treated with chlorpromazine, was determined in presence and absence of post-transfection ultrasound treatment. It was interpreted that when the predominant endocytosis pathway for the formulation was blocked with chlorpromazine, it resulted in declined cellular uptake of the formulation (Figure 25). However, the cells pretreated with chlorpromazine showed that the post-transfection ultrasound treatment boosted the transfection of lipopolyplexes even in the presence of an endocytosis inhibitor ( $p < 0.001$ ). In presence of post-transfection ultrasound treatment, the lipid nanocarrier may not undergo endocytosis. In presence of ultrasound, the ultrasound-active formulation, in the vicinity of the cell membrane, cause vulnerability of the cell membrane.<sup>146,118</sup> The exposure to the ultrasound probably created pores to a greater extent and thus increased the semi-permeability of the cell membrane.<sup>44,147</sup> The result pointed out that ultrasound-active lipopolyplexes when exposed to ultrasound at the time of endocytosis, exhibit higher transfection which was inferred to endosomal escape in presence of chlorpromazine.<sup>148</sup>

### **3.3.7 Ultrasound mediated transfection in 3D cell culture**

The effectiveness of ultrasound on transfection efficiency in the 3D cell- culture, also known as spheroids or organoids which mimics in-vivo tumor physiology, was examined. Generally, the cells are harvested by different methods to develop 3D-cell culture namely hanging drop, gel embedding, magnetic levitation, or spinner culture. Its shape, size, and compactness depend mainly on cell-cell interactions, incubation time, initial cell seeding densities and cell-extracellular matrix interaction.<sup>149</sup> To facilitate the spheroid formation, SKOV-3 cells were cultivated in a low attachment agarose coated plate with the modified harvesting medium that exhibited desired extracellular matrix properties. The agarose surface prevents the proliferation of cells in a monolayer fashion.<sup>150,151</sup> The size of the harvested spheroid cultures were measured and the results were expressed in terms of an “equivalent sphere diameter”. The spheroids equivalent sphere diameter ranged from 600–800  $\mu\text{m}$  diameter (Figure 26 A). It was observed that the diameter of the spheroid depends on the initial cell seeding number. Initially, loose aggregates are formed on the 2<sup>nd</sup> day of seeding which develops eventually into compact spheroid after continuous 10 days incubation and maintenance of the cells. Under the phase-contrast microscope, the spheroids distinctly showed two characteristic regions namely the quiescent zone, which

was the innermost area and the proliferating zone, which was the outermost layers of cells.<sup>152</sup> The viable spheroids were selected for further transfection experiments.

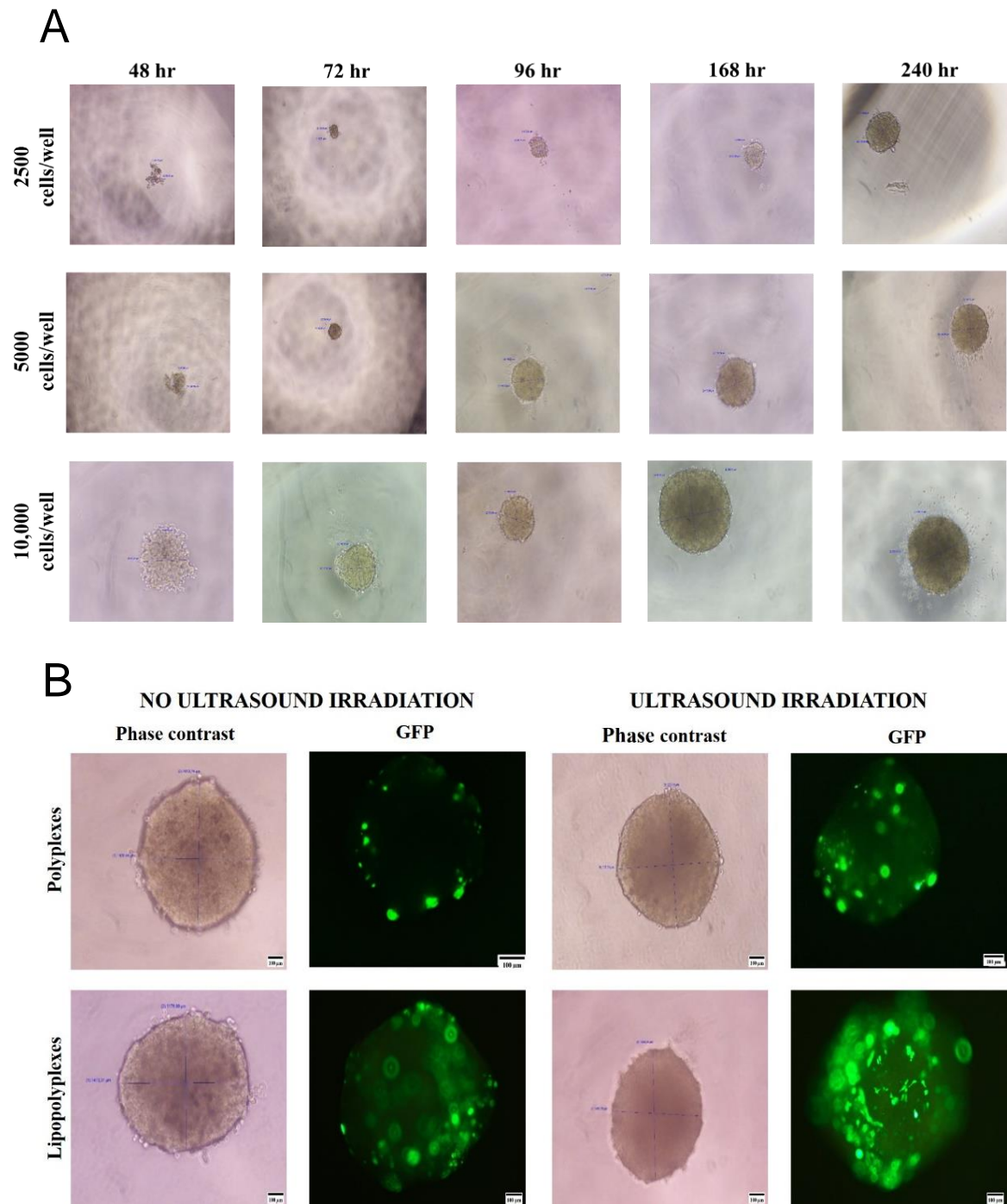


**Figure 26. Transfection efficiency of ultrasound-active lipopolyplexes in 3D - cell culture.** A) Harvesting of spheroid SKOV-3 cells by ultra-low attachment method and obtaining microscopic images of cell cultures at different cell-seeding densities on agar coated well-plate. (B) Visualization of GFP expression in SKOV-3 spheroid culture transfected with DPPC/CH/DPPG/PEG40S ultrasound-active lipopolyplexes under the exposure of low-frequency ultrasound. The spheroids transfected with polyplexes were considered as control. (Scale bar=100 $\mu$ m)



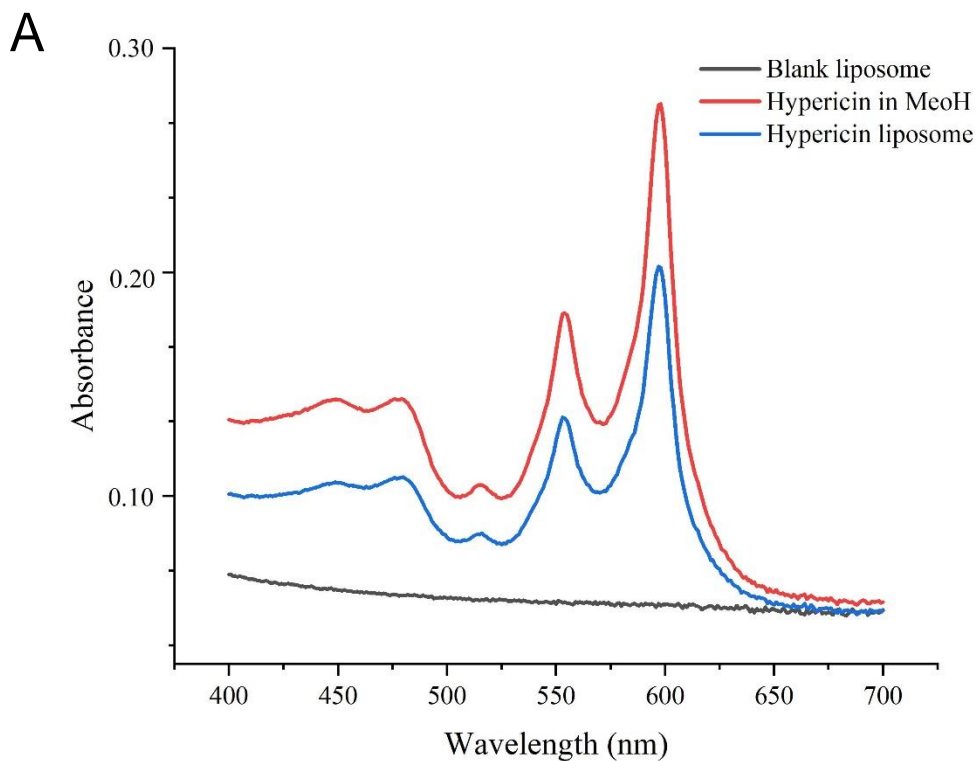
SKOV-3 spheroids were transfected with DPPC/CH/DPPG/PEG40S ultrasound-active lipopolyplexes in presence and absence of post-transfection ultrasound (Figure 26 B). It was observed that the spheroids, which were transfected using ultrasound-active lipopolyplexes, showed higher green fluorescent protein on the surface cell layers than polyplexes. The transfection efficiency of lipopolyplexes in the spheroid culture was confined to outer regions of the spheroid and suggested limited access of carrier towards inner core regions of a spheroid. Nevertheless, post-transfection ultrasound treatment after 240 min incubation showed increased GFP expression in peripheral regions than in the spheroid which were transfected without ultrasound treatment. The results obtained with multicellular 3D-cell culture coincide with that observed with monolayer culture of SKOV-3 cells. The result suggested that the ultrasound-active lipopolyplexes were an effective and safe carrier to transfect the proliferating cell layers of a spheroid.

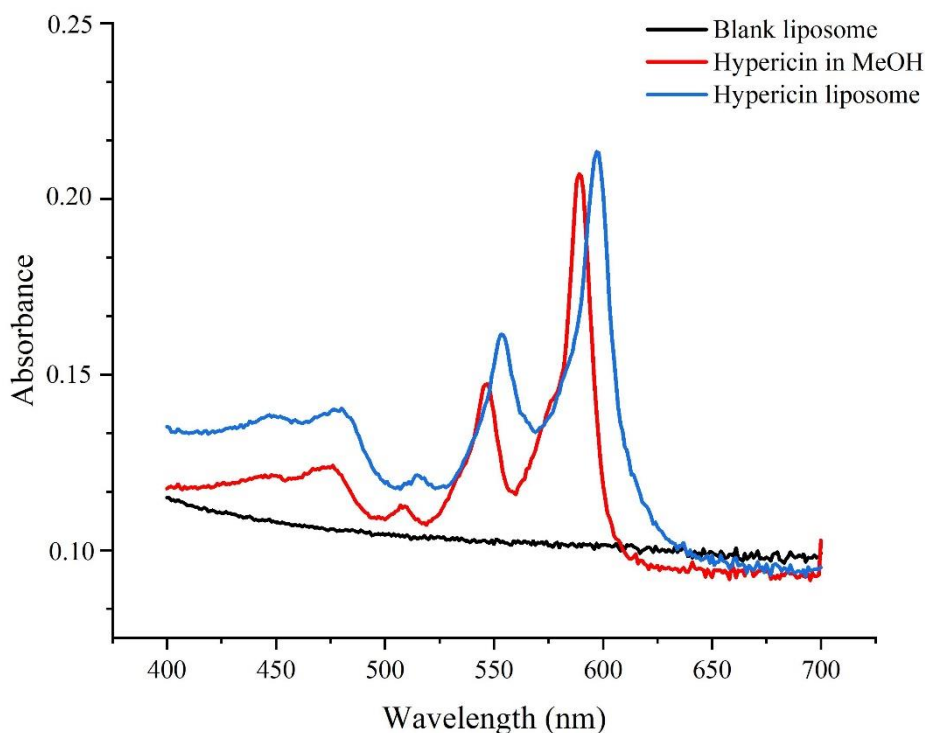
## 4. Result & Discussion - Photosensitizer induced gene delivery

### 4.1 Characterization of liposomes

#### 4.1.1 Entrapment efficiency of hypericin

In this method, hypericin was passively loaded into liposomes by concurrent entrapment during the liposome formation process. 5  $\mu$ M hypericin loading concentration showed  $66.1 \pm 2.5\%$  encapsulation efficiency using DPPC/CH/DSPE-PEG2000 liposome (50: 1 lipid: hypericin mass ratio). When the hypericin concentration was reduced fivefold i.e., 1  $\mu$ M hypericin (200: 1: lipid: hypericin mass ratio), the entrapment efficiency increased to  $80.24 \pm 5.6\%$ . The results coincide with other similar findings where a bathochromic shift to the free drug was observed for an encapsulated drug (Figure 27). As compared to free PS, the entrapped PS was reported to exhibit improved absorbance.<sup>153</sup>



**B**

**Figure 27. Absorbance spectra of hypericin liposomes.** UV-spectra in the range of 400 – 700 nm for HyL is represented by a blue line, hypericin in methanol is represented by a red line and EL is represented by a black line (A) hypericin liposomes (5  $\mu$ M hypericin) (B) hypericin liposomes (1  $\mu$ M hypericin).

#### 4.1.2 Average particle size and zeta potential

Initially, empty liposomes (ELs) with lipid composition DPPC/CH/DSPE-PEG2000 (84:15:1) were prepared by the ethanol injection method. The small unilamellar vesicles (SUVs) with  $115.5 \pm 9.22$  nm average particle size and  $-14.3 \pm 2.60$  mV zeta potential were formed. It was observed that the factors such as lipid concentration, solvent ratio and injection speed affected liposome size, therefore these parameters were kept constant. It was observed that the dilution of ethanol with aqueous buffer and subsequent ethanol evaporation favours the formation of liposomes.<sup>74,154</sup> The solvent ratio of ethanol: aqueous during mixing was kept 25% (v/v). The lower polydispersity index ( $p = 0.19$ ) confirmed that prepared liposomes clearly had the advantage of narrow size distribution. It was interpreted that the slipping plane over ELs moved further away from the liposome surface due to the PEG shield which favors negative zeta potential.<sup>155</sup>

**Table 8. Physicochemical properties of hypericin liposomes.**

Lipid composition (Molar ratio)	Hypericin concentration (nM)	Average particle size (nm $\pm$ S.D)	Zeta potential (mV $\pm$ S.D)	PDI
DPPC/CH/DSPE-PEG-2000 (84: 15:1)	-	115.5 $\pm$ 9.22	-14.3 $\pm$ 2.60	0.19 $\pm$ 0.01
	50 nM	187.8 $\pm$ 14.01	-19.4 $\pm$ 2.17	0.17 $\pm$ 0.01
	100 nM	177.4 $\pm$ 12.30	-18.7 $\pm$ 1.18	0.25 $\pm$ 0.02
	200 nM	196.5 $\pm$ 10.21	-18.9 $\pm$ 3.32	0.26 $\pm$ 0.04
	500 nM	229.0 $\pm$ 8.20	-25.6 $\pm$ 2.74	0.21 $\pm$ 0.02
	1 $\mu$ M	198.5 $\pm$ 6.26	-31.2 $\pm$ 5.60	0.23 $\pm$ 0.02

Further, the hypericin liposomes (HyL) containing different hypericin concentrations were prepared. HyL showed a unimodal size distribution, measured by PCS technique. The hypericin entrapment was evident by the increased average particle size of HyL (Table 8). However, reduced average particle size was noted for HyL containing 1  $\mu$ M hypericin. It was also observed that zeta potential of HyL increases with increase in hypericin concentration. The zeta potential of hypericin suspension was reported around  $-10 \pm 0.5$  mV.<sup>153</sup> The polydispersity indices (PDI) for all HyL were  $\sim 0.2$  indicating a homogenous distribution of liposomes favouring their stability. The structural stability was attributed to the rigidity of lipid bilayer due to the presence of cholesterol whereas prevention of aggregation was attributed to incorporation of PEG lipid.<sup>156,157</sup> The storage stability of hypericin liposomes determined no dramatic changes in average particle size and zeta potential (Figure 28). Further, HyL containing different hypericin concentrations (50 nM, 100 nM, 200 nM, and 500 nM) were used to prepare hypericin lipopolyplexes.

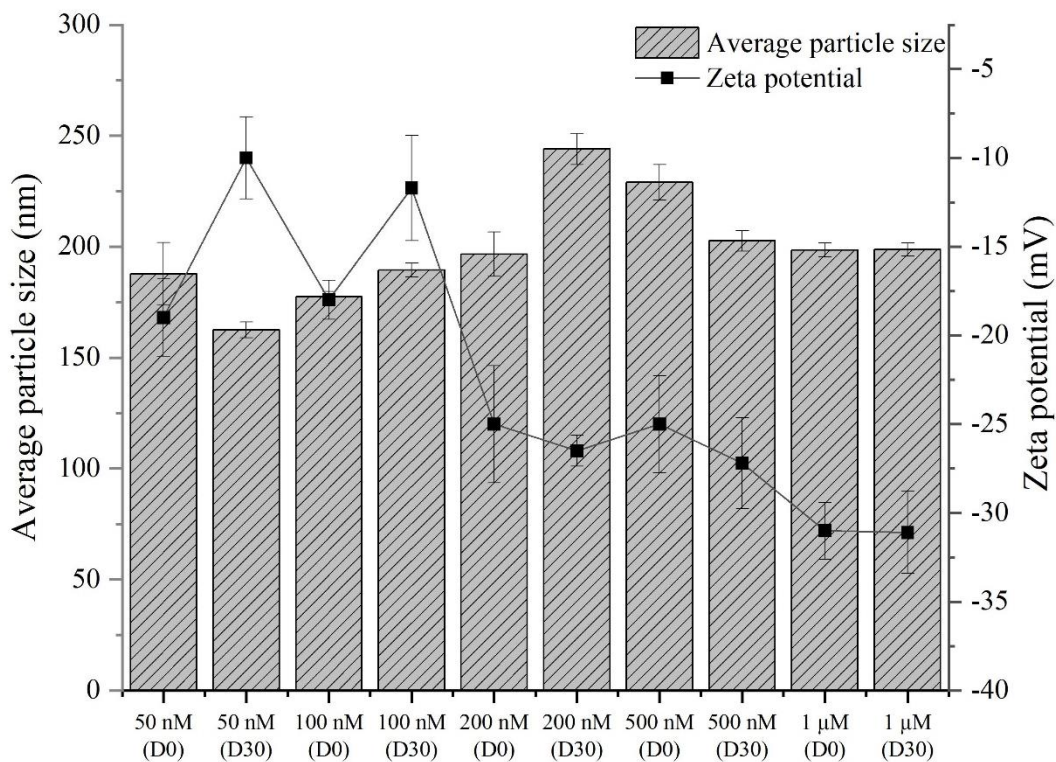


**Figure 28. Colloidal stability of hypericin liposomes.** The average particle size and zeta potential of HyL (50 nM to 1000 nM hypericin) were freshly prepared (D0) and after 1-month storage (D30). The data are expressed as the mean  $\pm$  SD (n=3).

#### 4.1.3 TEM

TEM images showed spherical structures of ELs and HyL (200 nM hypericin) with homogeneous diameters  $114.68 \pm 18.7$  nm and  $177.92 \pm 22.2$  nm respectively (Figure 29). The particle size obtained from TEM were slightly smaller than their hydrodynamic diameters, measured by the PCS technique. This may be due to difference between the working principles of particle size measurement technique.

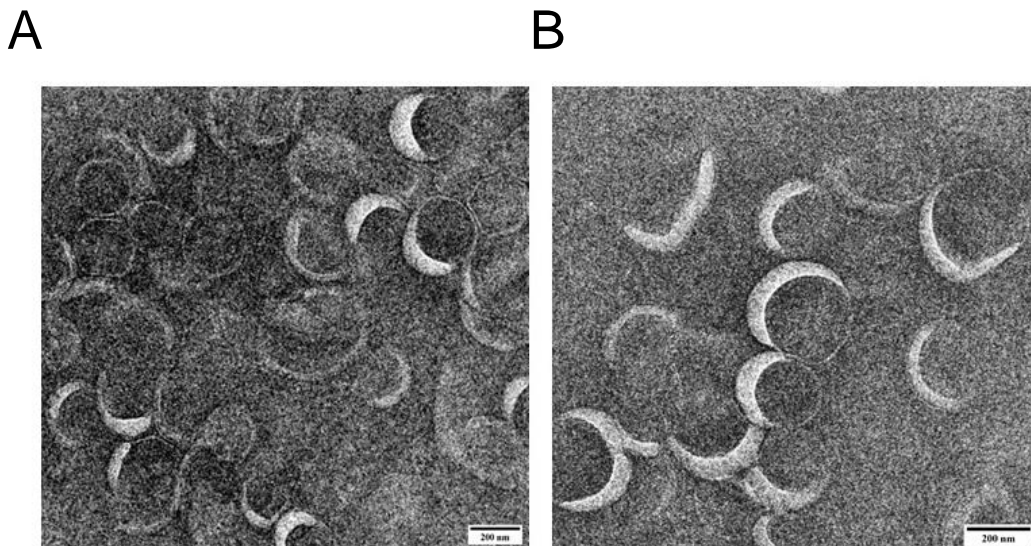


**Figure 29. Visualization of hypericin liposomes using TEM.** The size and shape of formulations were obtained by the negative staining TEM method. (A) EL and (B) HyL (200 nM hypericin) (Scale bar=200 nm)

## 4.2 Characterization of polyplexes, lipopolyplexes and hypericin lipopolyplexes

### 4.2.1 N/P ratio optimization

The N/P ratio of cationic polymer (IPEI) to nucleic acid was determined by DNA migration assay using agarose gel electrophoresis. The polyplexes (IPEI/pDNA) were prepared at different N/P ratios 2, 4, 6, 8, 10. As the N/P ratio increases, the polymer concentration increases, while amount of nucleic acid remains constant. Reduced DNA migration in an agarose bed was observed for polyplexes with higher N/P ratio (Figure 30). This emphasized the formation of the complex.<sup>127</sup> For further experiments, the N/P ratio 10 was considered as optimized.

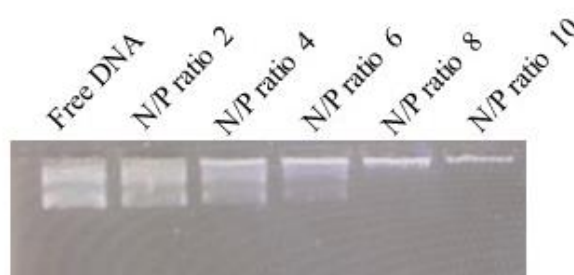
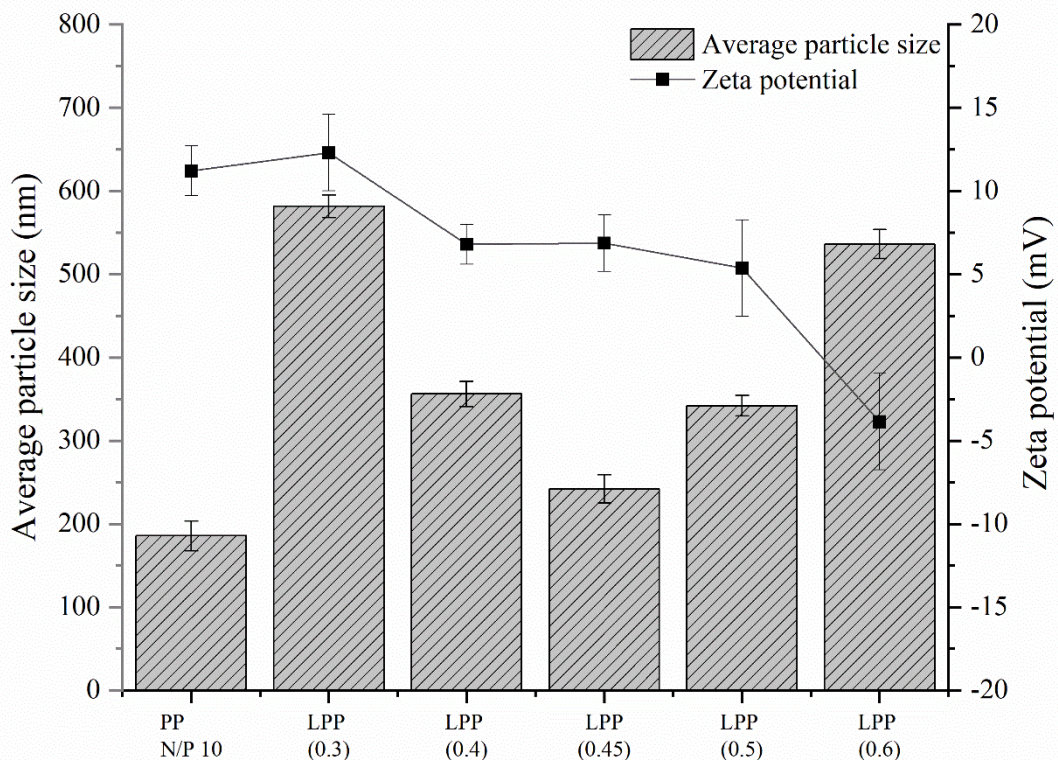


**Figure 30. Entrapment of pDNA in polyplexes by gel electrophoresis.** The IPEI complexes with pDNA at N/P ratio forms polyplexes (IPEI/pDNA). Optimization of the ratio between the nitrogen of IPEI and the phosphate group of pDNA by DNA retardation assay.

#### 4.2.2 Average particle size and zeta potential

The polyplexes at N/P ratio 10 showed an average particle size  $185.6 \pm 7.74$  nm and zeta potential  $+11.2 \pm 1.49$  mV. Further, the lipopolyplexes (LPP) prepared using ELs were characterized by the PCS technique (Figure 31). The minimum average particle size and zeta potential of LPP at lipid: PEI mass ratio 0.45 were  $242.1 \pm 10.4$  nm and  $+6.8 \pm 5.70$  mV respectively. The results were in accordance with the reported study that for lipopolyplexes condensation of nucleic acid occurs at a lower C/P ratio (carrier/pDNA ratio).<sup>158</sup> The lipopolyplexes showed an increase in average particle size as compared to liposomes and polyplexes. Similarly, hypericin lipopolyplexes (Hy-LPP) prepared using HyL showed increase in average particle size (Figure 31). It was found that the average particle size of Hy-LPP was independent of hypericin concentration. The zeta potential of Hy-LPP remains positive. Hy-LPP, containing nucleic acid and hypericin, were observed to overall reduce the positive charge partially as compared to polyplexes.<sup>159</sup>

A



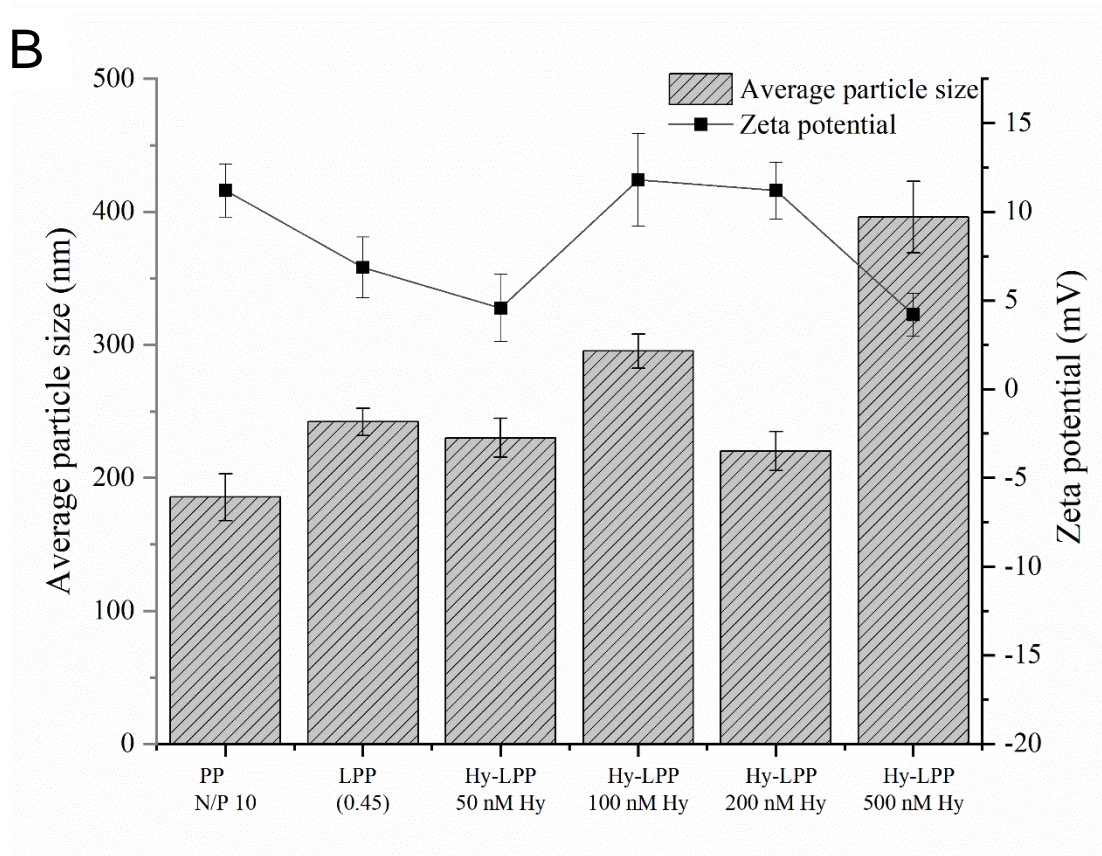


**Figure 31. Physicochemical characterization of hypericin lipopolyplexes.** A) The average particle size and zeta potential of PP at N/P ratio 10 and LPP at different lipid: PEI mass ratios and polyplexes at N/P ratio 10. (B) The average particle size and zeta potential of PP at N/P ratio 10 and Hy-LPP using different HyL at optimized lipid: PEI mass ratio 0.45 and polyplexes at N/P ratio 10. The data are expressed as the mean  $\pm$  SD (n=3).

#### 4.2.3 AFM

The liposomes were visualized for their structure and surface morphology using an atomic force microscope. It was observed that the prepared formulations were spherical and well-shaped (Figure 32). The diameters of EL and HyL formulation were measured by AFM. The size of the formulation was measured by the plot of height measured (nm) v/s offset (nm). ELs exhibited  $102.7 \pm 2.98$  nm diameter while HyL (200 nM hypericin) exhibited  $214.8 \pm 10.32$  nm diameter. The results coincide with the hydrodynamic diameter of the respective formulation as shown in Table 8. The diameter of hypericin lipopolyplexes (50 nM hypericin) was found  $226.8 \pm 9.78$  nm (Figure 32). Hy-LPP exhibited a non-spherical shape which could be attributed to the encapsulation of polyplexes in Hy-liposomes.<sup>160</sup>



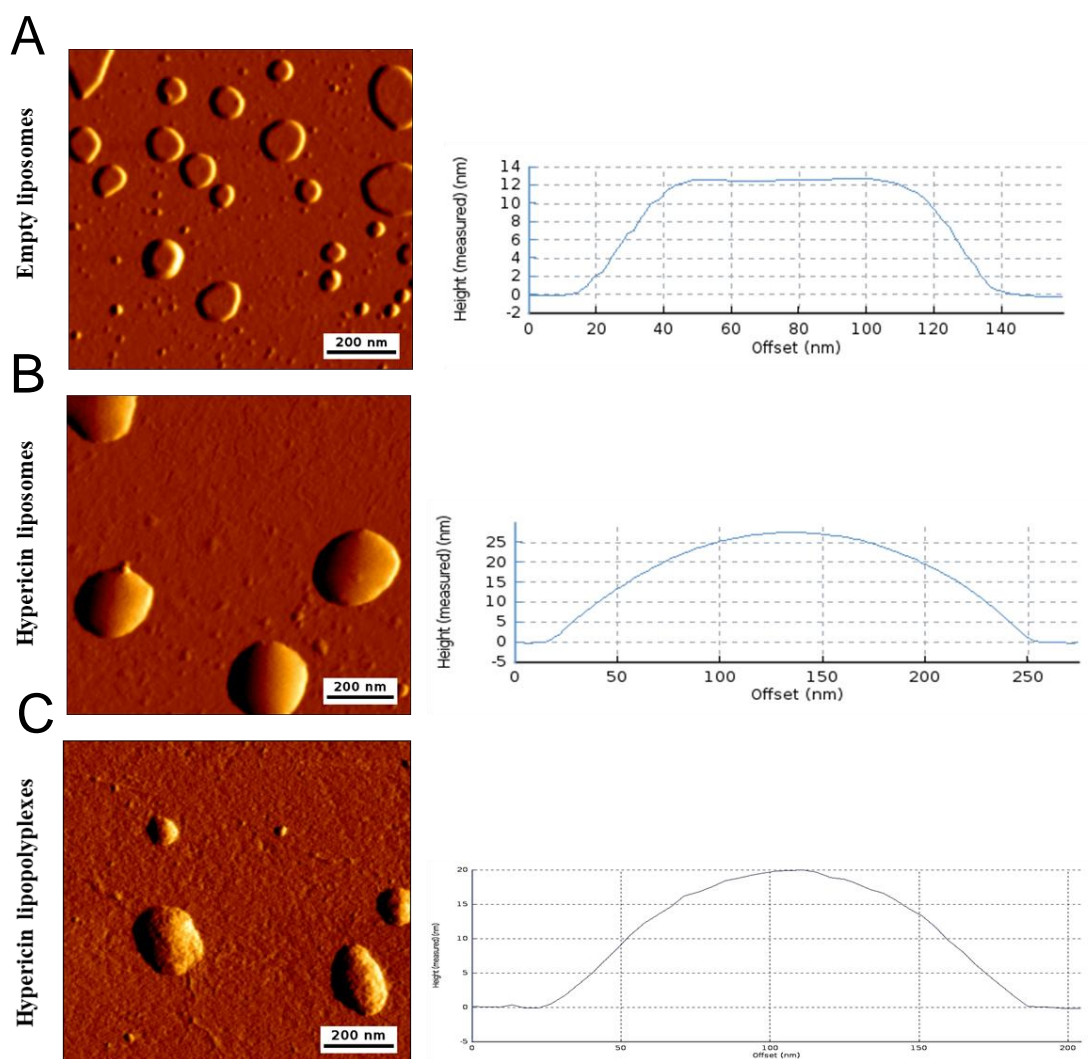


**Figure 32. AFM micrograph of hypericin formulation.** (A) EL, (B) HyL (200 nM hypericin) (C) Hy-LPP (50 nM hypericin) using intermittent contact mode of Cantilever tip and scanned in the amplitude view at about  $1 \times 1 \mu\text{m}^2$  ( $512 \times 512$  pixels) dimension. (Scale bar 200 nm)

#### 4.2.4 Fluorescence quenching

The fluorescence quenching assay was used to determine the complex integrity of lipopolyplexes (liposome-polyethylenimine complex). When free nucleic acid was encapsulated, it becomes inaccessible to SYBR gold, a nucleic acid-intercalating fluorescent dye, and consequently a decrease in fluorescence was observed.<sup>18</sup> A significantly reduced fluorescence of the intercalating dye was observed for polyplexes at N/P ratio 10 and above (Figure 33 A). IPEI condenses and protects the pDNA at N/P 10 which was consistent with previous reports.<sup>126</sup>

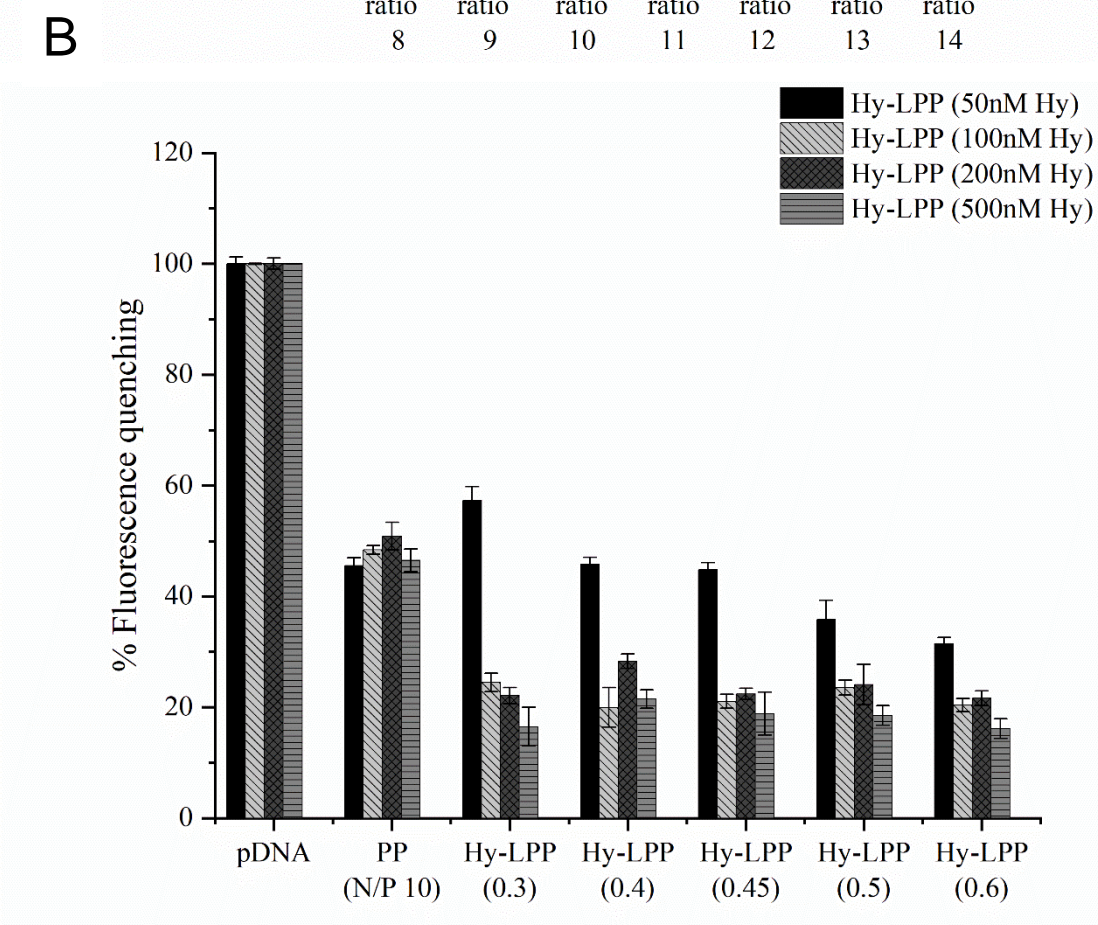
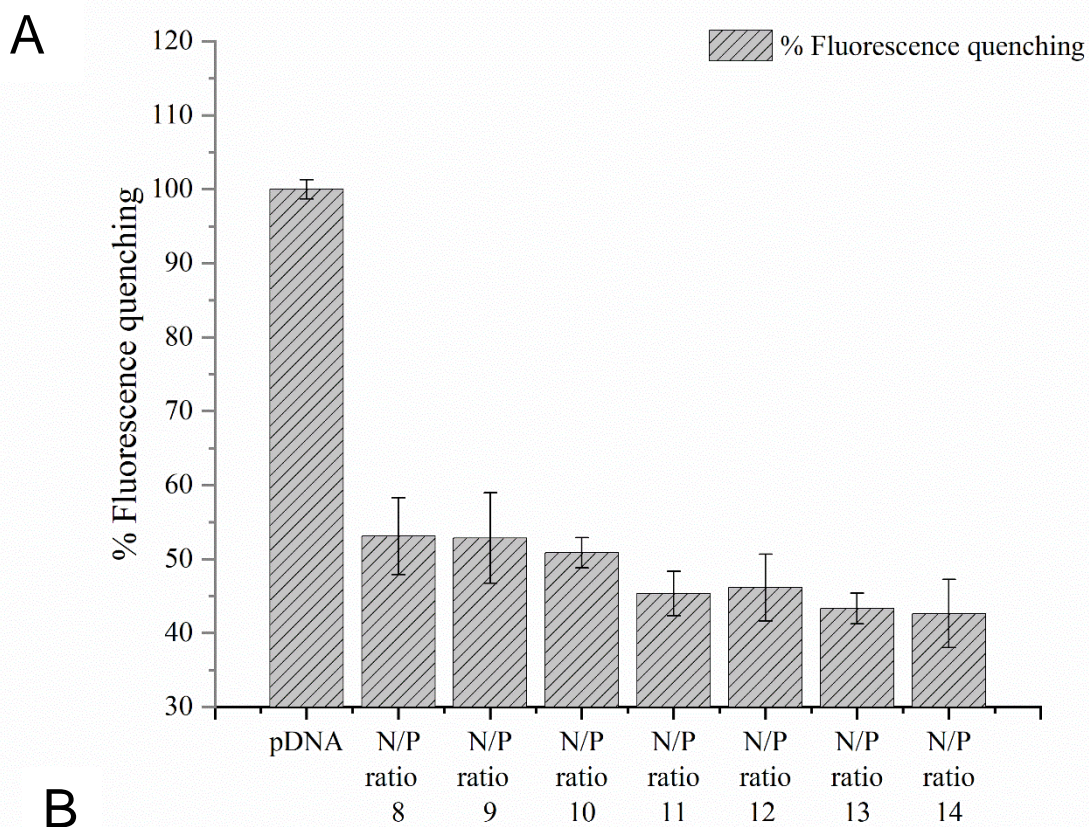


**Figure 33. Determination of complex integrity by % fluorescence quenching assay** (A) polyplexes at different N/P ratio (B) hypericin lipopolyplexes at different lipid: PEI mass ratio. The data are expressed as the mean  $\pm$  SD (n=3).

To determine the condensation efficiency of Hy-LPPs, the liposome formulations were incubated with polyplexes and HyLPP were formed by electrostatic interaction. The fluorescence quenching was determined and compared with polyplex, containing unmodified IPEI, as a control group. It was observed that Hy-LPP formations exhibited nearly 80% and 30% higher fluorescence quenching as compared to free pDNA and polyplexes, respectively. (Figure 33 B). The results confirmed that free pDNA was efficiently shielded by the liposome-polyethylenimine complex formation as compared to polyplexes.<sup>18</sup>

#### 4.2.5 Photostability of encapsulated plasmid

The stability of encapsulated pDNA in presence of hypericin was evaluated at different irradiation energies. A prerequisite for the nanocarrier is to protect the encapsulated plasmid from intracellular reactive oxygen species, which are generated from photoexcitation of photosensitizers.<sup>161</sup> Figure 34 demonstrates different Hy-LPP formulations containing 50 nM, 100 nM, 200 nM and 500 nM hypericin), which were irradiated at 600mJ/cm<sup>2</sup> light dose and electrophoresed. It showed no release of pDNA (left panel). However, the Hy-LPP formulations, which were irradiated and lysis before electrophoresis, exhibited distinct DNA bands which were similar to the free DNA in the agarose bed (right panel). It was clear that there was no degradation effect on pDNA upon photoirradiation.<sup>121,150</sup>

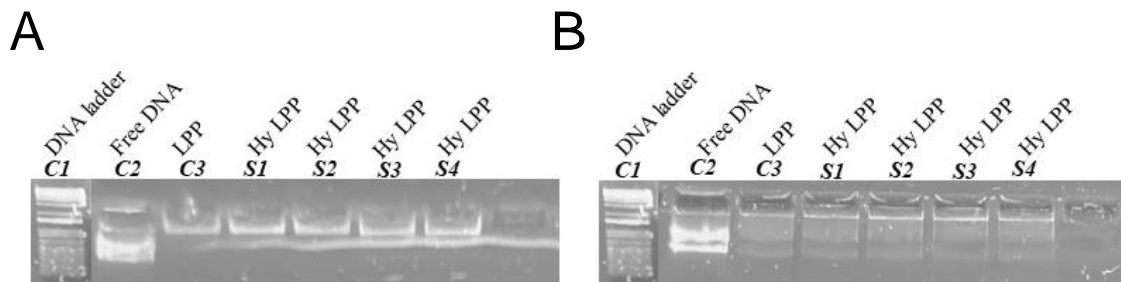


**Figure 34. Photostability of encapsulated pDNA by gel electrophoresis.** Photostability of delivered pDNA in Hy LPP after photoirradiation 600 mJ/cm<sup>2</sup>. The DNA migration bands obtained for samples (S) Hy-LPP with hypericin concentrations (1) 50 nM, (2) 100 nM, (3) 200 nM and (4) 500 nM are compared with the control (C): DNA ladder, free pDNA and LPP. (A) photoirradiated and non-lysed formulations and (B) photoirradiated and lysed formulations.

It was confirmed that the hypericin and pDNA in hypericin lipopolyplexes are efficiently segregated from each other. The irradiation causes damage to the biomaterial in the ‘light after’ protocol. Therefore, many reports cited encapsulation of genetic material as a separate entity from a photosensitizer.<sup>162</sup> As an alternative, a ‘light before’ method has also been reported as an approach to minimize the potential photodamage to delivered DNA complexes.<sup>121</sup>

### 4.3 In-vitro cell culture evaluation

#### 4.3.1 Transfection efficiency

Initially, the transfection of LPP without the influence of hypericin in HepG2 cells was evaluated. It was observed that DPPC/CH lipopolyplexes (LPP 1; control formulation) exhibited 1.5-fold higher transfection efficiency as compared to DPPC/CH/PEG2000 lipopolyplexes (LPP 2; test formulation) (Figure 35). The transfection efficiency of the test formulation decreased due to the steric hindrance offered by the terminal PEG tail. The PEG modified surface of lipopolyplexes can lead to inhibition of cellular uptake.<sup>157,163</sup> Hence, the light-induced transfection was evaluated for pegylated hypericin lipopolyplexes by the ‘light after’ PCI approach.

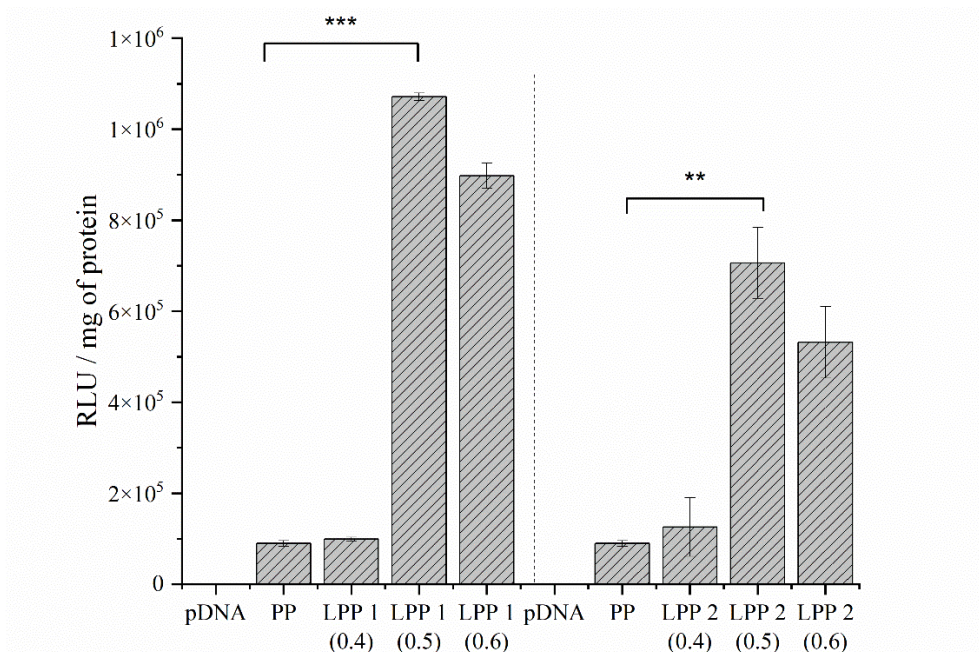


**Figure 35. Transfection efficiency of lipopolyplexes.** Luciferase expression in HepG2 cells obtained after transfection of DPPC/CH lipopolyplexes (LPP 1; control) and DPPC/CH/DSPE-PEG-2000 lipopolyplexes (LPP 2; test) at different lipid: PEI mass ratios. The data are expressed as the mean ± SD (n=3).

### 4.3.2 Cell viability

The right balance between transfection efficiency and cell viability is critical for photochemical internalization.<sup>123</sup> The cells incubated with different hypericin liposomes containing 50 nM, 100 nM, 200 nM and 500 nM hypericin, respectively showed maximum cell viability in dark conditions (non-irradiated). The cells treated with ELs were considered control group. It was observed that the cell viability remained ~ 80 % or above for the non-irradiated cells. (Figure 36).

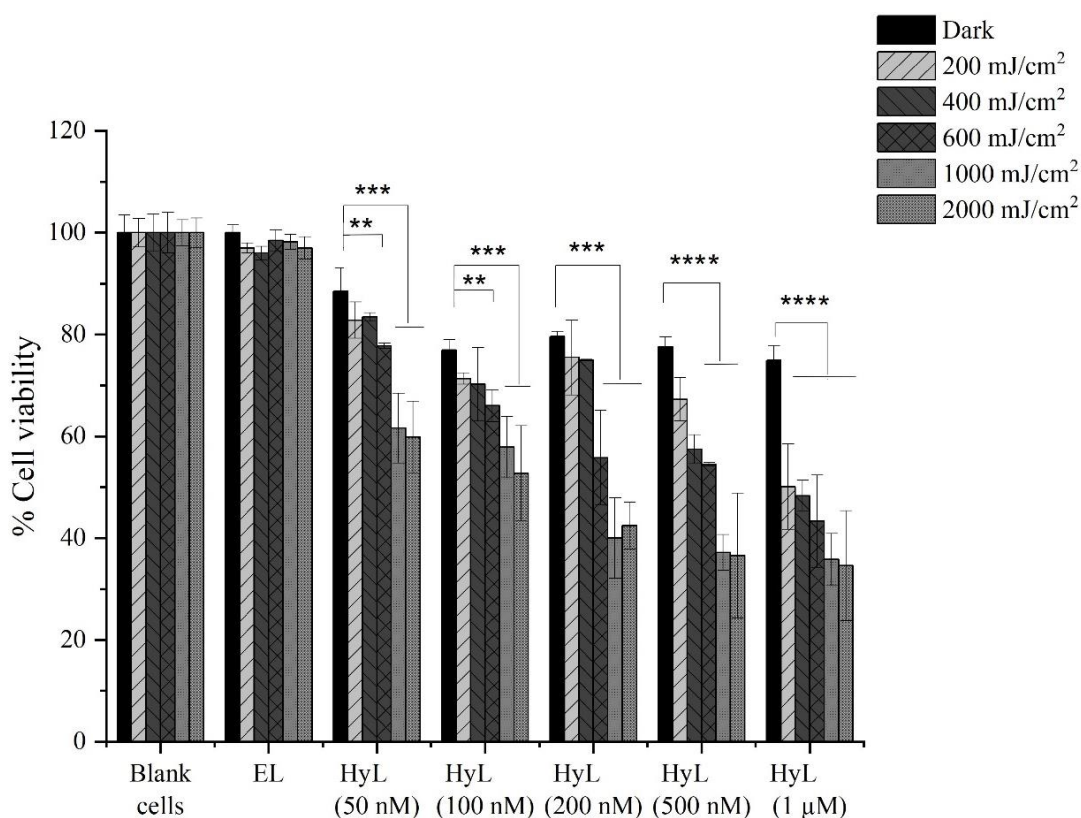


**Figure 36. Cell viability of cells incubated with hypericin liposomes and photoirradiated.** HepG2 cells were treated with HyL containing hypericin concentration between 50 nM to 1000 nM. The cells treated with 0.1 % Triton-100 were considered a positive control and untreated cells were considered a negative control. The data are expressed as the mean  $\pm$  SD (n=3). For statistical analysis, the results were compared against the results of non-irradiated cells (\*\*p<0.01, \*\*\*p<0.001, and \*\*\*\*p<0.0001).

Further, HyL treated cells were exposed to LED yellow light ( $\lambda_{589}$ ) at increasing light doses. The hypericin concentration-dependent decrease in the cell viability was evident upon irradiation. The cell viability was reduced in irradiated cells albeit less significant with HyL containing 50 nM hypericin (p < 0.01) whereas more significantly with 500 nM

hypericin ( $p < 0.0001$ ). It was reported that HyL was non-toxic in dark conditions until it reached its effective dose  $IC_{50} 2.50 \pm 1.0 \mu M$  (Table 9). As irradiation fluency increases, the  $IC_{50}$  values reduces exponentially.<sup>153,164</sup>

The photoirradiation decreased the cell viability significantly at light dose  $200 \text{ mJ/cm}^2$  ( $p < 0.01$ ) and  $1000 \text{ mJ/cm}^2$  ( $p < 0.0001$ ). Moreover, the cells treated with HyL (200 nM hypericin) exhibited cell viabilities around 80% (for  $\leq 400 \text{ mJ/cm}^2$ ) and 50 % (for  $\geq 600 \text{ mJ/cm}^2$ ) at lower and higher irradiation energies, respectively. The results suggested that the degree of cytotoxicity in HepG2 cells might be associated with the extent of intracellular photochemical reactions.<sup>165</sup> It was reported that hypericin liposome formulations showed cytotoxic effect at  $IC_{50} 237 \text{ nM}$  in SKOV-3 cells at  $2.1 \text{ J/cm}^2$  light dose and  $IC_{50} 90.8 \text{ nM}$  in MDA-MB-231 cells at  $1.6 \text{ J/cm}^2$  light dose.<sup>129,66</sup>  $IC_{50}$  values of hypericin depend on intracellular trafficking of hypericin loaded nanocarrier which depends on the physicochemical characteristics of the formulation and the cell line.<sup>153</sup>

**Table 9.  $IC_{50}$  values of hypericin liposomes at different irradiation energies**

<b>Irradiation energies</b>	<b><math>IC_{50}</math> values</b>
Dark	$2.50 \pm 1.0 \mu M$
$200 \text{ mJ/cm}^2$	$643.83 \pm 106.0 \text{ nM}$
$400 \text{ mJ/cm}^2$	$530.65 \pm 109.0 \text{ nM}$
$600 \text{ mJ/cm}^2$	$202.55 \pm 35.6 \text{ nM}$
$1000 \text{ mJ/cm}^2$	$155.10 \pm 21.4 \text{ nM}$
$2000 \text{ mJ/cm}^2$	$89.40 \pm 7.9 \text{ nM}$

Further,  $200 \text{ mJ/cm}^2$ ,  $400 \text{ mJ/cm}^2$ ,  $600 \text{ mJ/cm}^2$  and  $1000 \text{ mJ/cm}^2$  irradiation light dose were selected for evaluating PS induced cell viability using hypericin lipopolyplexes (50 nM, 100 nM, 200 nM, and 500 nM hypericin) in HepG2 cells. The hypericin lipopolyplexes were incubated with HepG2 cells and exposed to irradiation light dose or kept in dark, as the control group (Figure 37). In dark conditions, the polyplexes showed  $75.0 \pm 2.5 \%$  cell viability whereas the lipopolyplexes exhibited  $88.0 \pm 6.1 \%$  cell viability. It was attributed that PEI mediated cytotoxicity was shielded by lipopolyplexes.<sup>166</sup> In comparison with non-irradiated cells, the cells exposed to  $600 \text{ mJ/cm}^2$  light dose exhibited no significant difference whereas the cells exposed at

1000 mJ/cm<sup>2</sup> light dose exhibited strongest reduction in cell viability ( $p < 0.0001$ ). It was interpreted that the cell-killing was observed when HyLPP treated cells were irradiated at higher doses. Further, it was essential to evaluate the right balance between light dose and hypericin concentration, which exerts a photochemical reaction for enhancing the transfection efficiency of the carrier. The minimum cell death was observed which was attributed to lower applied photochemical dose (light dose and hypericin concentration). The cells incubated with Hy-LPP ( $< 100$  nM hypericin) and irradiated with a light dose  $\leq 600$  mJ/cm<sup>2</sup> did not significantly retard cell viabilities. On the contrary, increased cell death at higher photochemical dose was attributed to hypericin-induced PDT. The interpretation harmonized with findings that the light energy required to induce PCI is much lower than that to induce PDT in cancer cells.<sup>167</sup>

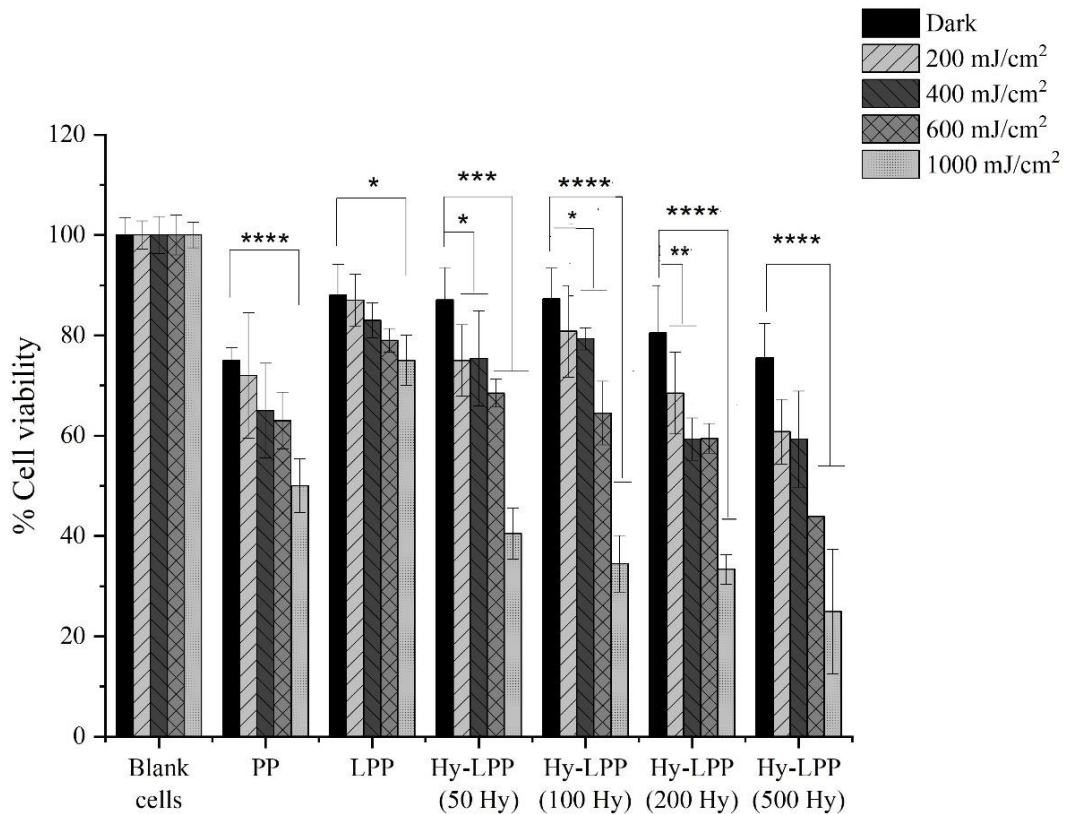


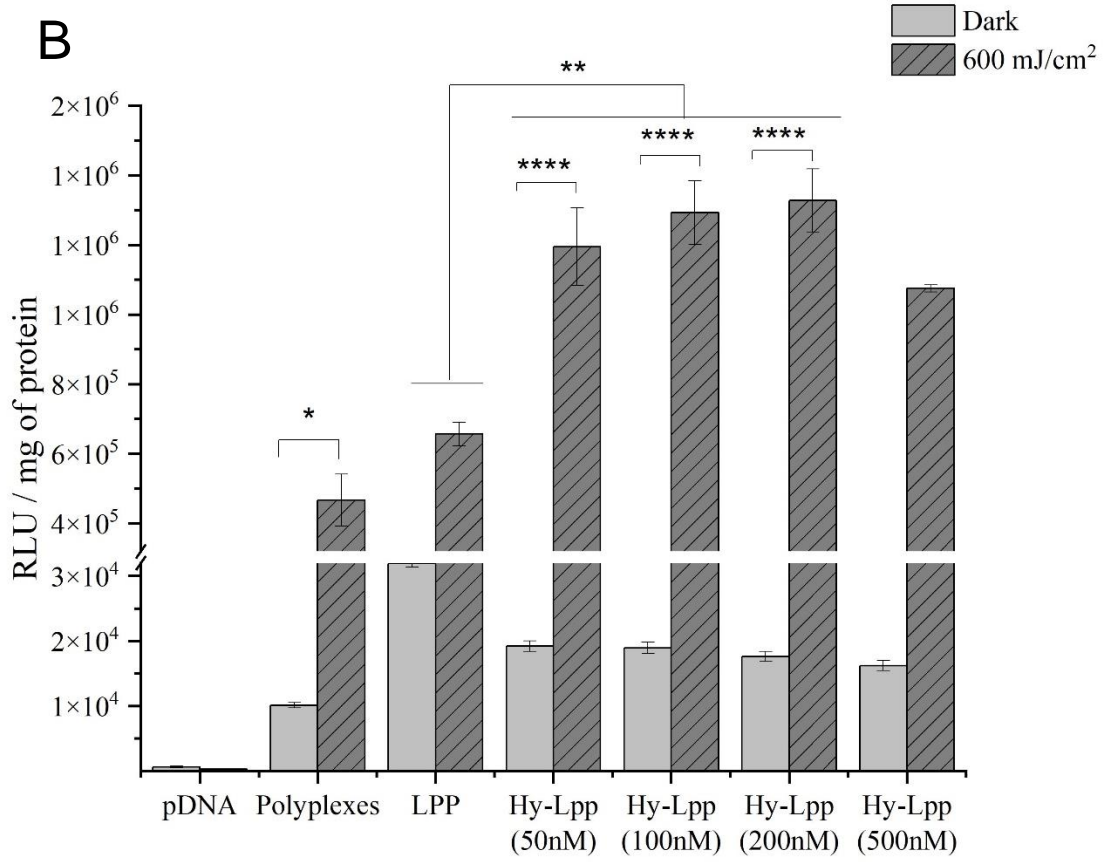
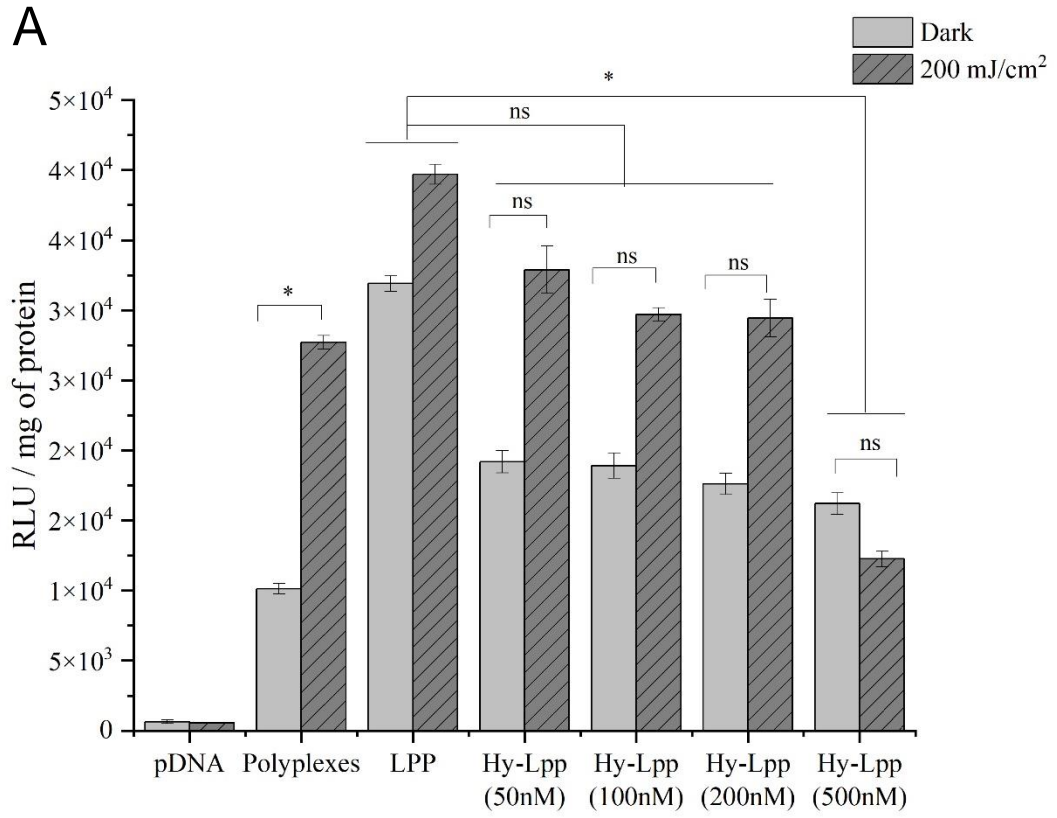
**Figure 37. Cell viability of cells treated with hypericin lipopolyplexes and photoirradiated.** HepG2 cells were treated with Hy-LPP containing hypericin concentration between 50 nM to 1000 nM and 0.25  $\mu$ g pCMV-Luc. The cells treated with 0.1 % Triton-100 were considered a positive control and untreated cells were considered a negative control. The data are expressed as the mean  $\pm$  SD ( $n=3$ ). For statistical analysis, the results were compared against the results of non-irradiated cells (\* $p < 0.05$ , \*\* $p < 0.01$ , \*\*\* $p < 0.001$ , and \*\*\*\* $p < 0.0001$ ).

### 4.3.3 Phototransfection

The cells were incubated with hypericin lipopolyplexes containing 50 nM, 100 nM, 200 nM, and 500 nM hypericin followed by post-transfection photoirradiation at 200 mJ/cm<sup>2</sup>, 600 mJ/cm<sup>2</sup> and 1000 mJ/cm<sup>2</sup> light doses. The cells transfected with free pDNA, polyplexes and lipopolyplexes were considered as control group (Figure 38 A to C). It was vigilantly observed that photoirradiation improved transfection efficiency of IPEI/pDNA complexes, irrespective of light dose. PEI demonstrates the 'proton sponge effect' due to the pK values of its amino group being closed to intracellular endosomal pH. The synergistic effect on transfection of polyplexes attributed to accelerated buffering capacity of the polycationic polymer upon exposure to light.<sup>92,157</sup> IPEI protects the encapsulated pDNA from in-vitro photodegradation. It was supported by the results obtained from SYBR quenching assay (section 4.2.4) and gel electrophoresis assay (section 4.2.5). However, lipopolyplexes exhibited no significant improvement due to exposure to irradiation at all three light doses. It was reported elsewhere that the light effect on the lipid-based non-viral carrier is more dependent on the structure of the formulation used for the transfection regimen.<sup>168</sup> Further, 0.25 µg pCMV-Luc was codelivered with variable hypericin concentration: 50 nM, 100 nM, 200 nM and 500 nM in HepG2 cells and the transfection efficiency was evaluated upon irradiation at different light doses. When HyLPP transfected cells were exposed to 200 mJ/cm<sup>2</sup> light dose the transfection efficiency was hindered for 500 nM hypericin lipopolyplexes as compared to lipopolyplexes (p<0.05). However, the irradiation at 600 mJ/cm<sup>2</sup> light dose, showed a drastic elevation in luciferase expression in the cells (Figure 38). The transfection efficiency was increased by 100-folds as compared to non-irradiated (p<0.0001).

Further, the transfection efficiency of multicomponent nanocarrier was dropped 10-fold at 1000 mJ/cm<sup>2</sup> light dose for cells transfected with Hy-LPP (≥ 200 nM hypericin) which was attributed to hypericin IC<sub>50</sub> concentration 155.10 ± 21.4 nM at 1000 mJ/cm<sup>2</sup> light dose. The results pointed out that when the light dose was increased, there was a relative increase in the photochemical reaction of internalized hypericin in the cells. The previous studies reported that irradiation fluence affects light-induced gene transfer.<sup>169, 170</sup> The results also support that the effective light dose for PCI depends on the concentration of the photosensitizer.<sup>162, 171</sup> Thus the functionality of hypericin lipopolyplexes as co-delivery of photosensitizer and gene was demonstrated.





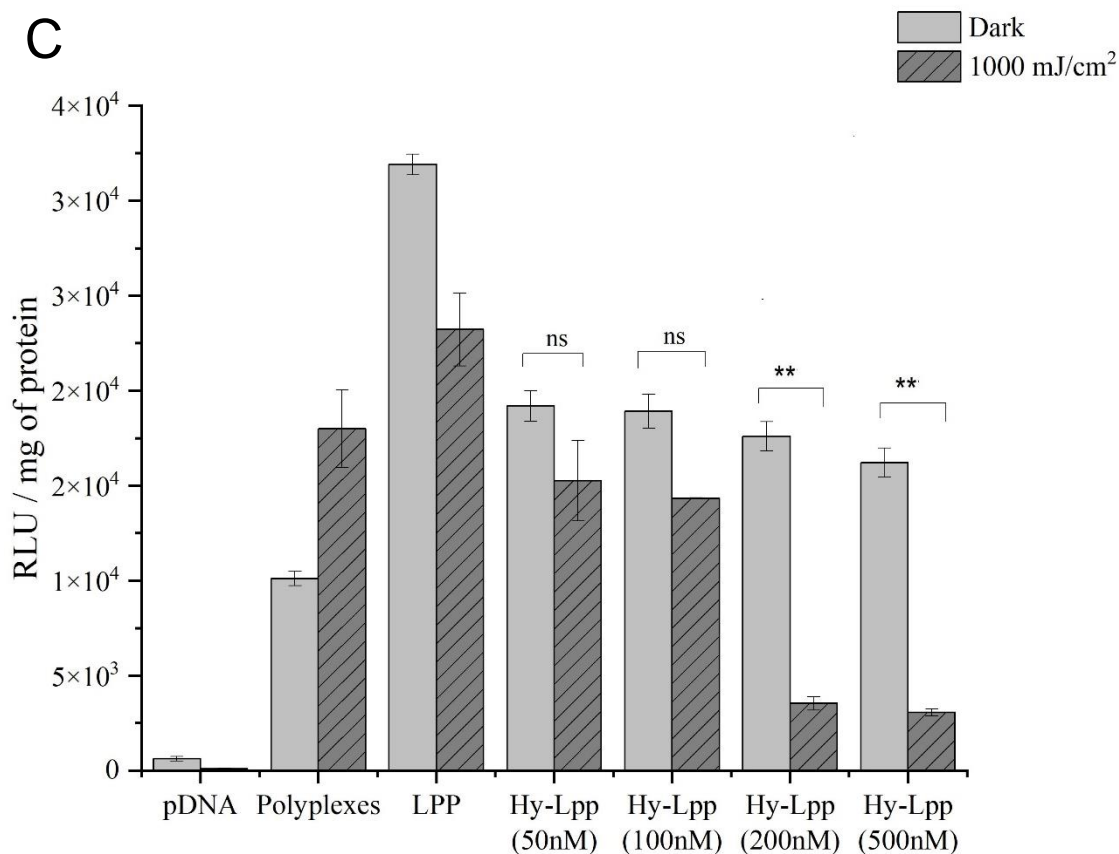


**Figure 38. Photochemical induced transfection efficiency of hypericin lipopolyplexes in HepG2 cells.** HepG2 cells were treated with Hy-LPP containing hypericin concentration between 50 nM to 1000 nM and 0.25  $\mu$ g pCMV-Luc. The cells were incubated for 2 h and photoirradiated at (A) 200 mJ/cm<sup>2</sup>, (B) 600 mJ/cm<sup>2</sup> and (C) 1000 mJ/cm<sup>2</sup> irradiation fluencies. The cells treated with free pDNA, PP and LPP were considered the control group. The data are expressed as the mean  $\pm$  SD (n=3). For statistical analysis, the results were compared against the results of non-irradiated cells (\*p<0.05, \*\*p<0.01, \*\*\*p<0.001, and \*\*\*\*p<0.0001).

#### 4.3.4 Photocytotoxicity

The photosensitizer induced cytotoxicity was anticipated along with the effective transfection by Hy-LPP (50 nM, 100 nM, 200 nM, and 500 nM hypericin). It was observed that the cytotoxicity of polyplexes doubles after irradiation treatment which could be due to higher internalization of cationic IPEI, which caused PEI-mediated cytotoxicity.<sup>166</sup> In non-irradiated cells, the cytotoxicities of hypericin lipopolyplexes were within the permissible limit. Similarly, the cytotoxicity profile of cells irradiated at 200 mJ/cm<sup>2</sup> light dose remained below 20% for the lower hypericin dose (Figure 39). It was attributed to the hypericin IC<sub>50</sub> concentration  $643.83 \pm 106.0$  nM at 200 mJ/cm<sup>2</sup> light

dose. A minimal cytotoxic effect ( $\sim 30\%$ ) was observed at  $600 \text{ mJ/cm}^2$  light dose, which were incubated with hypericin concentrations  $\leq 100 \text{ nM}$  ( $p < 0.001$ ). However, it was veiled by the substantial increase in the luciferase expression in irradiated cells (Section 4.3.3). The irradiation at  $1000 \text{ mJ/cm}^2$  light dose exhibited a significant rise in cytotoxicity was observed in the cells incubated with Hy-LPP ( $\geq 200 \text{ nM}$  hypericin) ( $p < 0.0001$ ). Relocalization of the photosensitizer during light exposure has been previously described for other amphiphilic photosensitizer and their second intracellular location sites have been proposed to play an important role in cytotoxicity.<sup>123,172</sup>

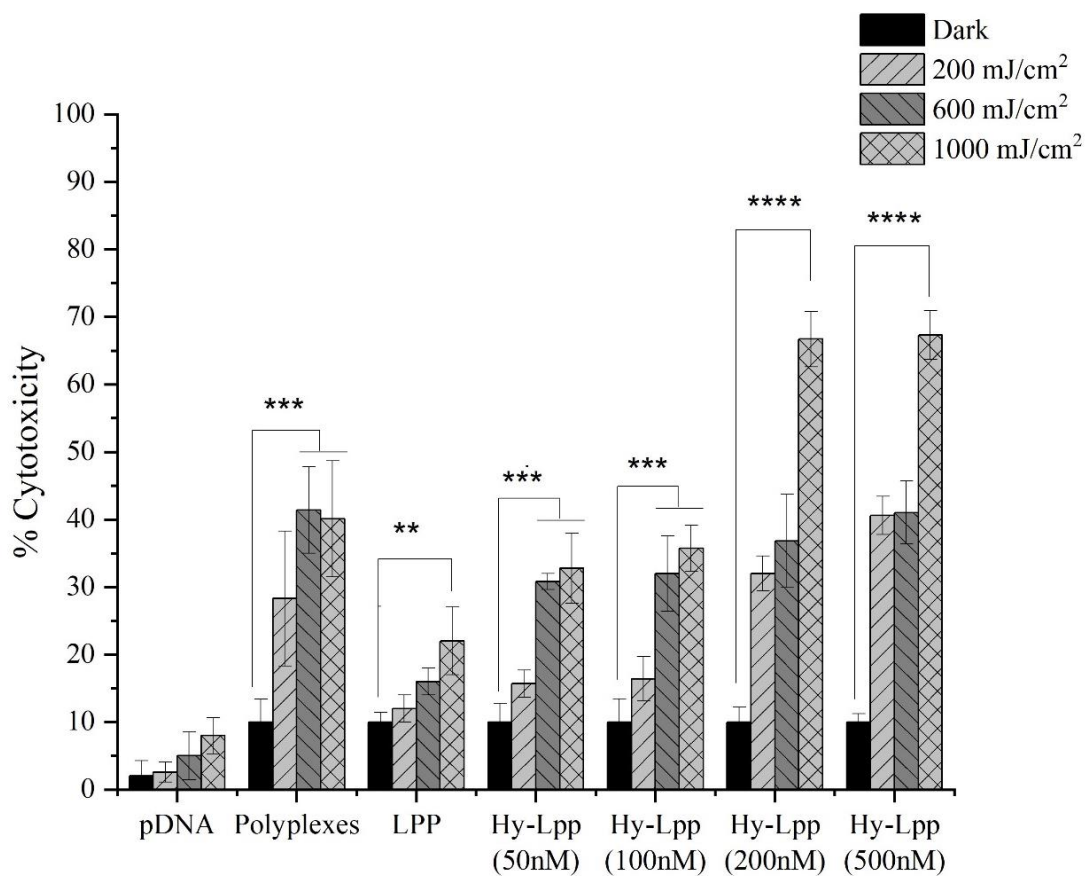


**Figure 39. Photocytotoxicity of hypericin lipopolyplexes.** HepG2 cells were treated with Hy-LPP containing hypericin concentration between 50 nM to 1000 nM and  $0.25 \mu\text{g}$  pCMV-Luc. The cells treated with free pDNA, PP and LPP were considered the control group. The data are expressed as the mean  $\pm$  SD ( $n=3$ ). For statistical analysis, the results were compared against the results of non-irradiated cells (\*\* $p < 0.01$ , \*\*\* $p < 0.001$ , and \*\*\*\* $p < 0.0001$ ).

When the statistical analysis was performed on cytotoxicity data, the results showed a significant difference between no hypericin and 500 nM hypericin containing formulation as per the ANOVA test (Tukey test,  $p < 0.0001$ ). Taken together, it can be interpreted that the Hy-LPP exhibit cytotoxicity by virtue of hypericin-induced photochemical reactions.<sup>125</sup> The cells that survived the photochemical reaction damage exhibited luciferase expression. On the other hand, when reporter gene is replaced with a therapeutic oligonucleotide such as siRNA in the formulation, it would eventually show efficient gene knockdown in the remainder viable cells and thus would exhibit synergistic anticancer effect. Hence, it was reported that the transfection efficiency was dependent on irradiation effective light dose, whereas the cytotoxicity was dependent on hypericin concentration for photoirradiation.

#### **4.3.5 Cellular uptake of hypericin lipopolyplexes**

The cells were incubated with Hy-LPP (50 nM hypericin) for 2 h followed by photoirradiation at 200 mJ/cm<sup>2</sup>, 600 mJ/cm<sup>2</sup> and 1000 mJ/cm<sup>2</sup> light doses or kept at dark conditions. The red fluorescence of intracellular hypericin after incubation was promptly viewed by confocal laser microscopy (Figure 40). The non-irradiated cells exhibited negligible fluorescence which suggested limited cellular uptake of Hy-LPP. It was attributed to stearic hinderance for cellular uptake due to the presence of PEG tail as well as lesser incubation time allotted in the experiment.<sup>173</sup> The cells irradiated at 600 mJ/cm<sup>2</sup> and 1000 mJ/cm<sup>2</sup> light doses showed distinct Hy-LPP throughout the cytoplasm. The results indicated that photoexcitation of hypericin facilitated cellular internalization of the formulation. The observation could be the effect of promoting the intracellular trafficking of nanocarrier such as the release of formulation from the intracellular vesicles into the cytoplasm.<sup>174,175</sup>

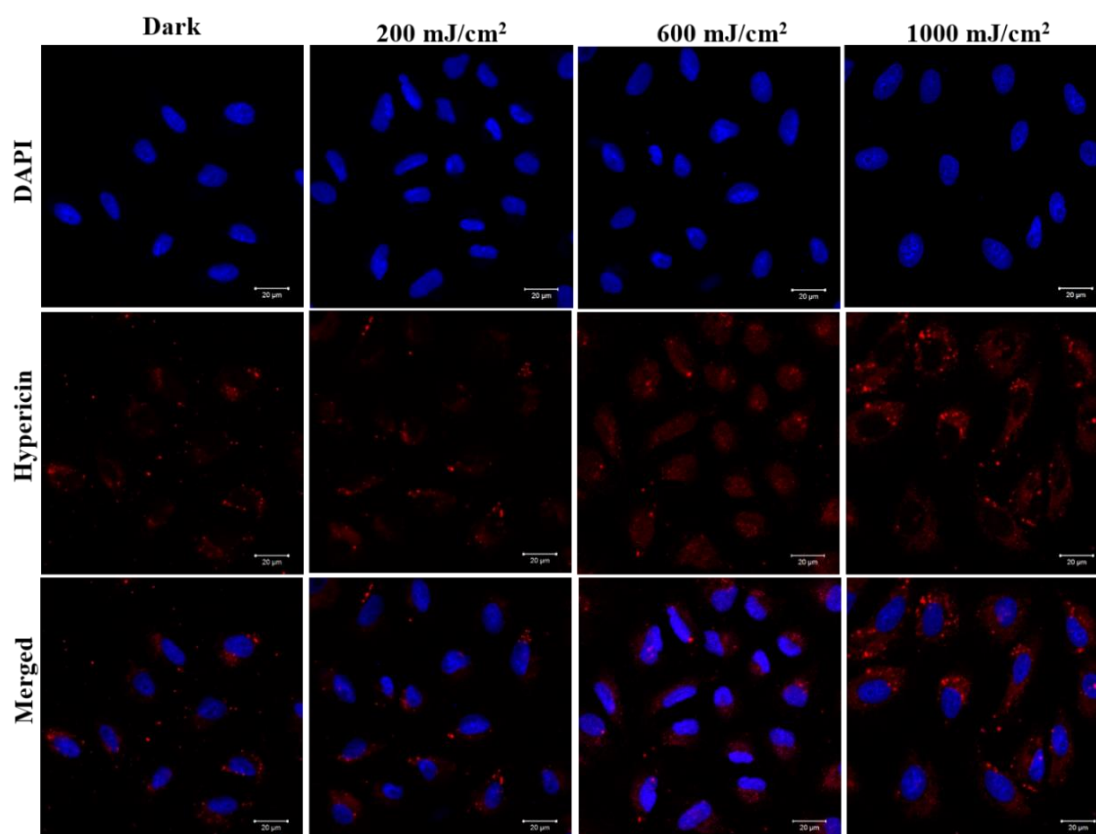


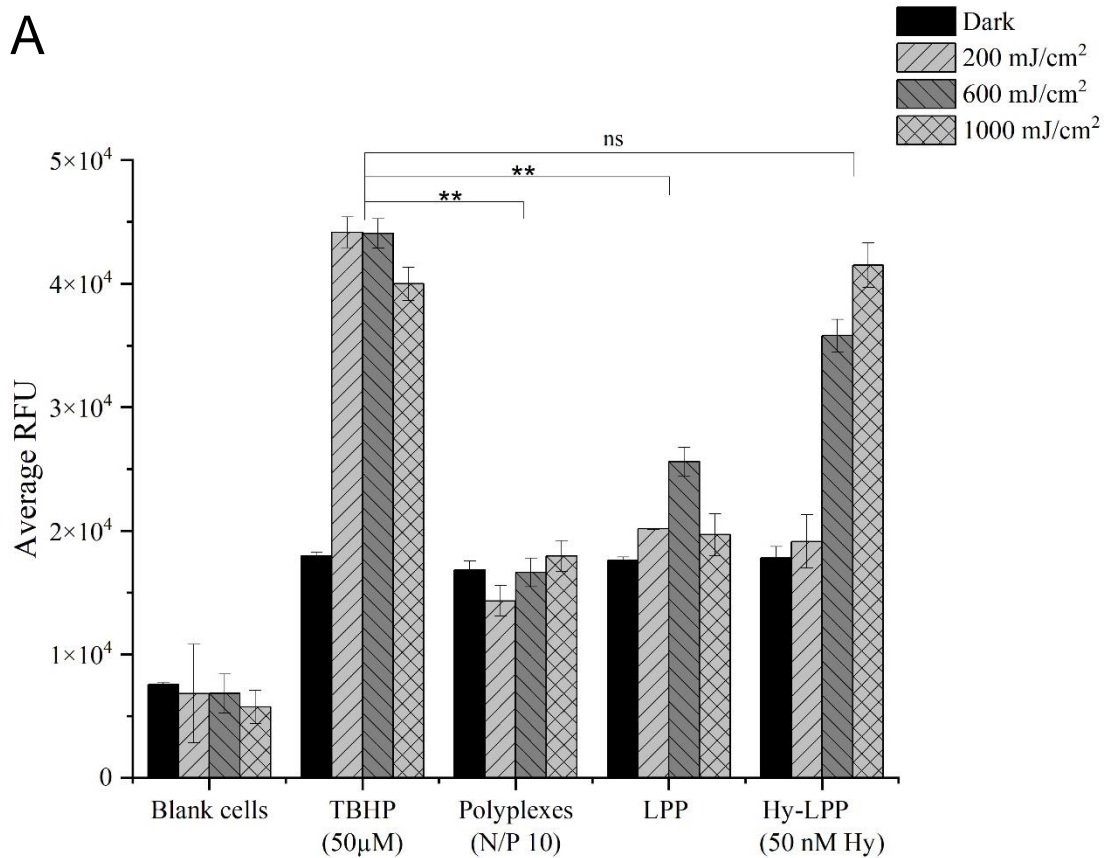
**Figure 40. Cellular uptake of hypericin lipopolyplexes.** HepG2 cells were incubated with the hypericin lipopolyplexes encapsulating 50 nM hypericin and 1 µg pDNA at 37°C for 2 h and exposed to photoirradiation at different light doses: 200 mJ/cm<sup>2</sup>, 600 mJ/cm<sup>2</sup> and 1000 mJ/cm<sup>2</sup>. DAPI stained nuclei are shown in blue and hypericin in the cytoplasm is shown in red fluorescence. (Scale bar = 20 µm)

#### 4.3.6 Intracellular reactive oxygen species measurements

The intracellular reactive oxygen species (ROS), produced by photoexcitation of intracellular hypericin, were measured for relative quantification of photochemical reaction. The results were compared with TBHP treated cells (positive control) and blank cells (negative control) (Figure 41). The relative fluorescence unit (RFU) measured in the different cells exhibited a pattern. IPEI/pDNA transfection without photoirradiation showed higher average RFU than blank cells. The result coincides with the findings that stated that PEI/DNA polyplex induces intracellular ROS generation upon irradiation.<sup>60, 157</sup> It was observed that the RFU value exhibited by the irradiated cells, incubated with Hy-LPP, was equivalent to average RFU values for positive control (TBHP treated cells). It was attributed to the photoexcitation of internalized hypericin (50 nM) which induces intracellular ROS generation<sup>66,164</sup> In presence of a photosensitizer, light promotes the

generation of reactive oxygen species in the cells; specifically, singlet oxygen ( $^1\text{O}_2$ ). DCFDA reagent, added to the cells, is oxidized by the photogenerated singlet oxygen to form DCF, a highly fluorescent compound inside the cells.<sup>165,176</sup> The generation of reactive oxygen species was found to be dependent on irradiation fluencies, as higher RFU was reported for 1000 mJ/cm<sup>2</sup> light dose.

The microscopic visualization of the non-irradiated cells incubated with LPP, and PP formulations showed no fluorescence whereas cells with Hy-LPP displayed negligible fluorescence. The irradiated cells incubated with Hy-LPP displayed more green fluorescence. The visualization of oval to spherical shaped cells indicated cytotoxicity by apoptosis, which attributed the effect of elevated ROS generation in HepG2 cells. It was reported elsewhere that sufficient light energy is a basic requirement for photosensitizers to easily generate ROS.<sup>153</sup> Therefore, the optimal light dose was determined to evaluate of the efficacy of PCI.



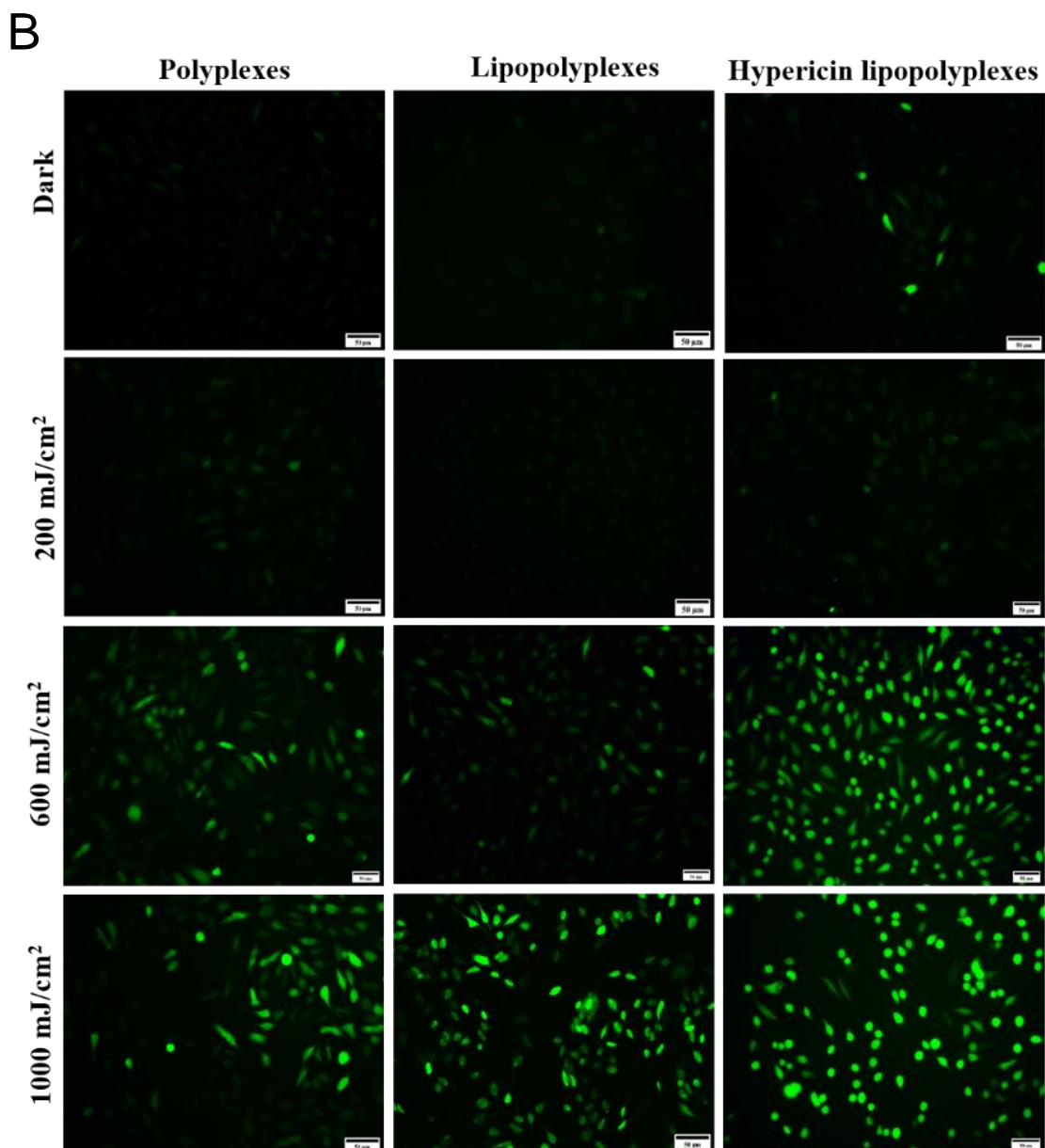


**Figure 41. Intracellular reactive oxygen species measurement.** (A) Quantitative measurements of relative fluorescence using FLUOstar multiplate reader for cells incubated with PP, LPP and Hy-LPP and irradiated or kept in dark conditions. The cells treated with TBHP (50  $\mu$ M) were considered a positive control and cells without treatment were considered as a negative control. The data are expressed as the mean  $\pm$  SD (n = 3). For statistical analysis, the results were compared against the results of non-irradiated cells (\*\*p<0.001) (B) Visualization of green fluorescence in the cells incubated at wavelength excitation/emission 480/520 nm using Olympus microscope with PP, LPP, Hy-LPP at different irradiation energies. (Scale bar = 50  $\mu$ m)

## 5. Result & Discussion - Selective phototransfection

### 5.1 Characterization of conjugated hypericin lipopolyplexes

#### 5.1.1 Average particle size and zeta potential

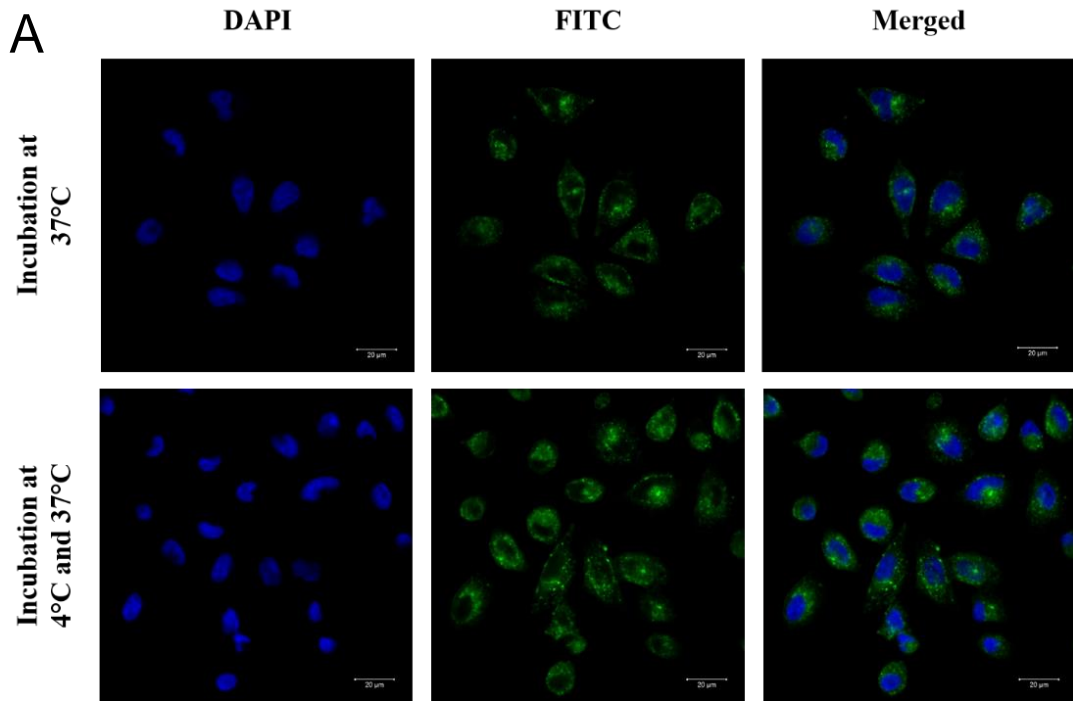
To obtain, a cancer cell-specific homing nanocarrier, the surface of hypericin liposomes were modified using anti-transferrin antibody. A rapid and simple coupling approach using DSPE-PEG terminus with cyanuric chloride as the linker moiety was adopted. The key for insertion of anti-transferrin antibody was basic pH of the reaction medium.<sup>177</sup> The prepared anti-transferrin conjugated hypericin liposomes (50 nM hypericin) were incubated with polyplexes to form conjugated hypericin lipopolyplexes. The formulation exhibited  $255 \pm 16$  nm average particle size and  $10.8 \pm 8.7$  mV zeta potential.

### 5.2 In-vitro cell culture evaluation

#### 5.2.1 TfR receptor expression in HepG2 cells

Transferrin is a bona fide cargo for the clathrin-mediated endocytosis pathway. Tf-fitc conjugate was prepared and its cellular uptake was assessed by fluorescence microscopy. The receptor-mediated endocytosis was visualized when cells were incubated with Tf-fitc conjugate at 4 °C (facilitating the ligand binding with the cells) followed by incubation at 37 °C (phase-chase period).<sup>178</sup> The localization of Tf-fitc conjugate near the membrane and the cytoplasm of the cells was evident (Figure 42). Its mean fluorescence intensity (n = 3) was found doubled than compared to cells incubated at 37 °C. The majority of the transferrin receptors (TfR) are localized in the cell-membrane interior.<sup>179</sup> The results attributed to the formation of clathrin-coated intracellular vesicles to transport both the Tf-fitc conjugate and internal receptor into the cell. The results showed that intracellular localization of Tf-fitc conjugate after 37 °C incubation indicated that the cellular uptake is an energy-dependent process.<sup>180</sup>





**B**

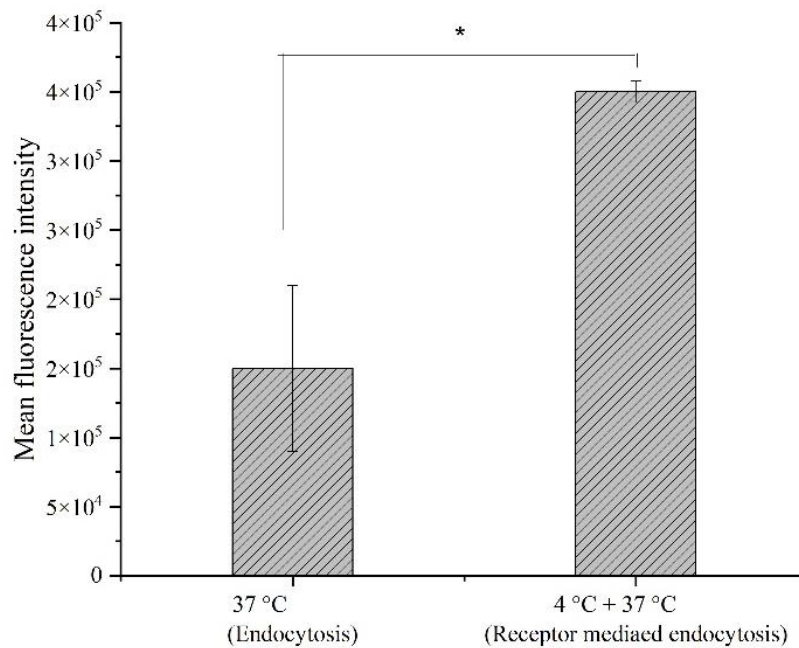


**Figure 42. Cellular binding and uptake of FITC-labelled transferrin conjugate.** (A) HepG2 cells were incubated with Tf-fitc conjugate (50  $\mu\text{g}/\text{mL}$ ) for 20 min at 4°C followed by washing with 1X PBS and incubation for 5 min at 37°C (phase-chase period). The cells incubated with conjugate at 37°C for 30 min were considered as a control group (Scale=20  $\mu\text{m}$ ) (B) Mean fluorescence intensity was calculated by ImageJ software. The data are expressed as the mean  $\pm$  SD (n = 3)

### 5.2.2 Ligand mediated cellular uptake

The cellular uptake of conjugated and non-conjugated hypericin lipopolyplexes (50 nM hypericin) was visualized under a microscope (Figure 43). The anti-transferrin antibody was utilized as a ligand for evaluation of receptor-mediated cellular uptake. The transferrin receptors are endocytosed by a clathrin-mediated endocytosis pathway (CME).<sup>181</sup> The cells, pretreated with chlorpromazine (a clathrin pathway blocker), were considered as a negative control group.

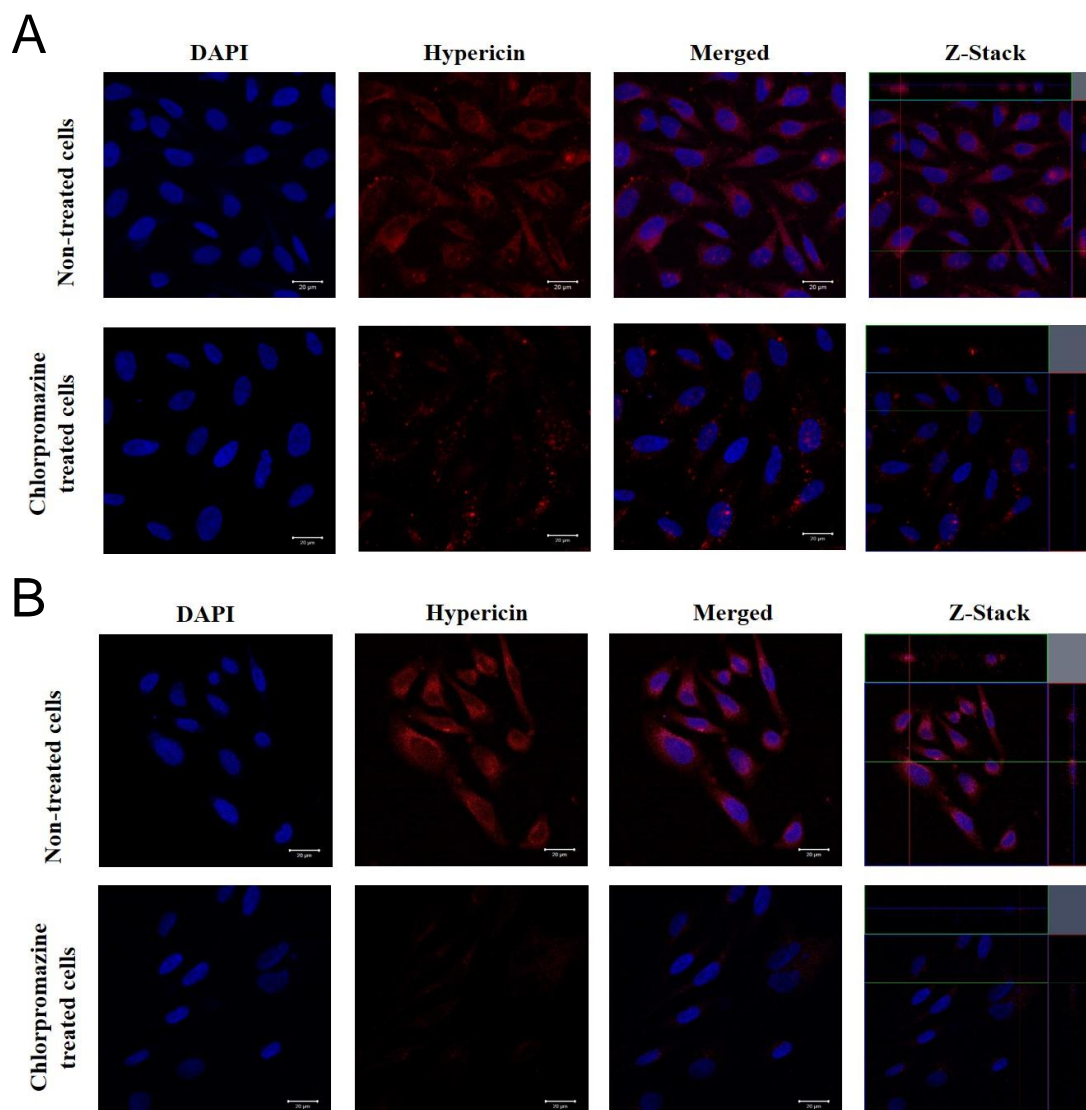


**Figure 43. Ligand mediated cellular uptake.** Selective cellular uptake of formulation via transferrin receptor in HepG2 cells. DAPI stained nuclei are shown in blue and hypericin in the cytoplasm is shown in red fluorescence (A) non-conjugated hypericin lipopolyplexes and (B) antibody conjugated hypericin lipopolyplexes containing 50 nM hypericin. The cells were pretreated with receptor pathway inhibitor 10 μM chlorpromazine in 3% BSA in PBS for 1 h at 37°C (lower panel) and the cells without pre-treatment were considered as control (Scale = 20 μm)

It was observed that the hypericin lipopolyplexes internalized in the chlorpromazine-treated cells whereas the anti-transferrin conjugated hypericin lipopolyplexes displayed no significant internalization. On the contrary, red fluorescence was observed throughout cytoplasm of non-treated cells. It was interpreted that the non-conjugated hypericin lipopolyplexes internalize via pathways other than CME, however, to a lesser extent.<sup>126,182</sup> However, the conjugated formulation showed selective cellular uptake in HepG2 cells via transferrin-receptor.<sup>180,182</sup>

### 5.2.3 GFP expression

After elucidation of cellular uptake pathway of anti-transferrin conjugated hypericin lipopolyplexes in HepG2 cells, formulations were further evaluated for transfection efficiency using pGFP gene (Figure 44). No significant difference was observed between different hypericin formulations in non-irradiated cells. It was observed that upon irradiation at 600 mJ/cm<sup>2</sup> light dose, anti-transferrin conjugated Hy-LPP were relatively more transfected as compared to control formulations i.e., non-conjugated Hy-LPP and polyplexes.

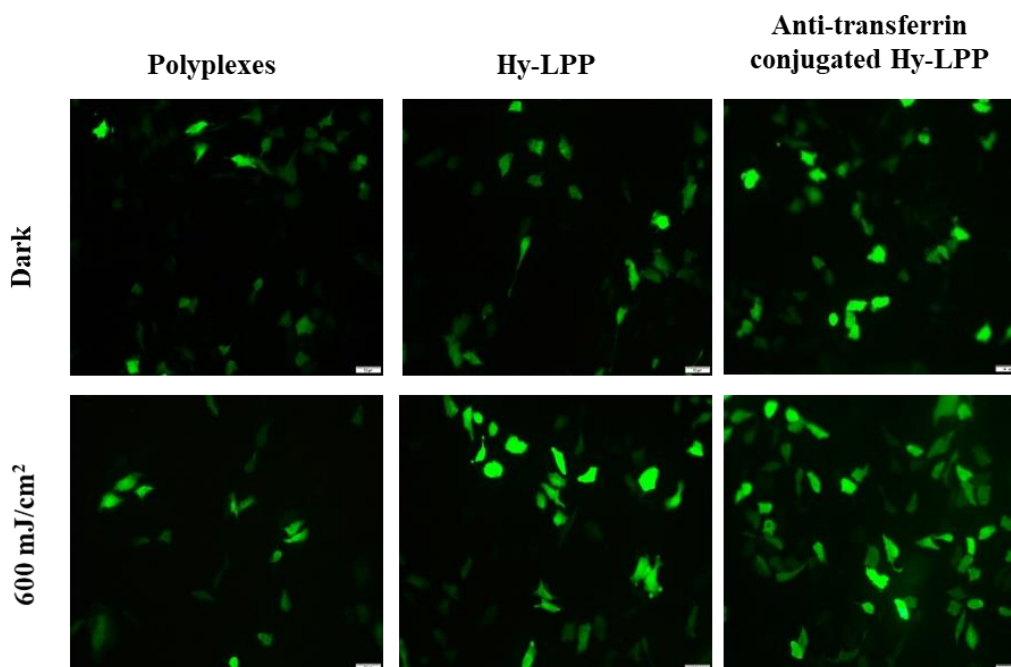


**Figure 44. Visualization of GFP expression.** HepG2 cells transfected with non-conjugated hypericin lipopolyplexes and anti-transferrin conjugated hypericin lipopolyplexes containing 1 µg pCMV-GFP and irradiated 600 mJ/cm<sup>2</sup> light dose. The cell kept in dark conditions were considered as a control in each group. (Scale = 50 µm)

The relatively higher green fluorescent protein was produced in the cell cytoplasm when irradiated at 600 mJ/cm<sup>2</sup> light dose. The higher GFP expression with conjugated Hy-LPP was associated with photoselective transfection of the formulation.<sup>184</sup> The photoirradiation of ligand-conjugated nanocarrier encapsulating photosensitizer and oligonucleotide encompasses multifunctionalities namely, targeted delivery and efficient transfection of genetic material.<sup>185,186</sup> The outcome coincides with the results of an in-vivo study where the transferrin-targeted siRNA polymer-based nanoparticle showed superior biodistribution and tumor accumulation as non-targeted formulations.<sup>187</sup>

## 6. Summary

In the present work, two methods for efficient gene transfer using lipopolyplexes as non-viral delivery systems were investigated. The aim was to develop a biocompatible and biodegradable non-viral vector for effective transfection in cancer cells. This novel therapeutic carrier for nucleic acid was engineered into trigger responsive formulation exploiting the potential of ultrasound or photoirradiation.

The introduction (Chapter 1) contains concepts, modalities, and functionalities of the project in which the physiological barriers, formulation-based challenges and recent advances in DNA-based therapeutics have been described. The introduction focuses on the current state of research on novel methods necessary to release the gene transfection systems from the endosome. The currently used lipid-based non-viral vectors are also contrasted. An overview of the various physical methods for gene therapy application is also provided. The basic physical principles of ultrasound and light as external trigger for gene delivery are precisely explained.

**Chapter 2** summarizes the methods and materials used. It covers different methodologies used in the development of the non-viral carriers. Preparation and characterization methods for ultrasound-active lipopolyplexes and hypericin lipopolyplexes were described in detail.

**Chapter 3** deals with the preparation and characterization of formulation, which can be applied as ultrasound imaging and as an efficient gene transfection system. Physicochemical characterization of ultrasound-active contrast vesicles using photon correlation spectroscopy revealed the formation of stable, monodisperse DPPC/CH/PEG40S lipid vesicles. A polydispersity index has proven that its particle size distribution was significantly improved by the presence of cholesterol. Inclusion of PEG40S in the phospholipid mixture of ultrasound-active contrast vesicles, contributed to develop an ultrasound contrast, which has been detected in-vitro by a fabricated tissue-flow model. The prepared non-lamellar phospholipid shell DPPC/CH/PEG40S is characteristic of ultrasound-active vesicle formation. Moreover, higher echogenicity was exhibited due presence of DPPG lipid in the phospholipid shell of

DPPC/CH/DPPG/PEG40S ultrasound-active contrast vesicles. The ultrasound contrast visualization was found equivalent to a standard ultrasound contrast agent, SonoVue<sup>®</sup>. The storage conditions showed no evident influence on the ultrasound contrast of these UCVs. The visualization of formulations shows detailed insight into surface morphology and particle size. The diameter obtained by atomic force microscopy coincided with their respective hydrodynamic particle size of the formulations. DPPC/CH/DPPG/PEG40S ultrasound-active vesicles were found monodispersed because of stronger interparticle repulsion owing to a higher magnitude of surface charge. Further, the physicochemical characterization of polyplexes (IPEI/pDNA complexes) using photon correlation spectroscopy and laser Doppler velocimetry has been studied. The polycationic complexes were later also evaluated by in-vitro cell culture model. Ultrasound-active lipopolyplexes were prepared using optimized polyplexes (optimized N/P ratio 12) and ultrasound-active contrast vesicles. The formulations having different liposome/PEI mass ratios were evaluated in SKOV-3 cell line. DPPC/CH/DPPG/PEG40S ultrasound-active lipopolyplexes possess minimum average particle size and carry a slightly positive charge. The optimized ternary formulation, having a diameter  $168.84 \pm 5.4$  nm and positive surface potential ensured cellular internalization of the formulation.

Influence of factors such as polymer concentration and lipid concentration on transfection efficiency and cell viability in SKOV-3 cells has been studied. The result of these experiments determined optimized N/P ratio for polyplexes and liposome/PEI mass ratios for lipopolyplexes. Compared to the polyplexes (IPEI/pDNA), the lipopolyplexes, especially those with liposome/PEI mass ratios 0.5, has shown an enormous increase in the luciferase expression. The lipid composition shields the positively charged PEI and hence facilitates cellular internalization. Further transfection studies of the ultrasound-active lipopolyplexes under influence of ultrasound treatment have been evaluated. An exposure to the low-frequency ultrasound showed 50-fold increased transfection efficiency for cells with higher post-transfection incubation time intervals. The results were confirmed by visualization of improved GFP expression in SKOV-3 cell line. Significant increased transfection efficiency of ultrasound-active lipopolyplexes with ultrasound treatment as compared to lipopolyplexes and polyplexes was observed. Moreover, ultrasound showed a positive influence in chlorpromazine-treated cells. The results have suggested that gene transfer in this method depends on the cellular

internalization process. Transfection in 3D cell culture has shown similar outcome which were visualized by GFP expression in the spheroids culture of SKOV-3 cells. In-vitro evaluation mainly focuses on the effect of ultrasound on cellular uptake and transfection efficiency of the non-viral vector.

**Chapter 4** elucidate the physicochemical characterization of a novel lipopolyplexes system for photochemical internalization of a gene. Hypericin, a hydrophobic photosensitizer, which can be readily adsorbed into cell membranes, forms aggregates in an aqueous phase. Therefore, a stable aqueous delivery system of the photosensitizer is a prerequisite. Passive encapsulation of hypericin, developed using the ethanol injection method, accounts for  $80.24 \pm 5.6$  % encapsulation efficiency. Physicochemical characterization of DPPC/CH/DSPE-PEG2000 hypericin liposomes has been determined using photon correlation spectroscopy, laser Doppler velocimetry and TEM. The formation of stable, monodisperse and negatively surface charge hypericin liposome was confirmed through the findings. The hydrodynamic diameter of hypericin liposomes, containing 200 nM hypericin, was  $196.5 \pm 10.21$  nm which coincided with the diameter obtained by atomic force microscopy  $214.8 \pm 10.32$  nm. Encapsulation of negatively charged hypericin raised the overall negative surface charge of liposomes from  $-14.3 \pm 2.60$  mV to  $-18.9 \pm 3.32$  mV.

Further, cationic polyplexes (N/P ratio 10, optimized by DNA migration assay) has been encapsulated in hypericin liposomes by virtue of electrostatic forces. Anionic hypericin liposomes, containing different hypericin concentrations, encapsulate cationic polyplexes (IPEI/pDNA; N/P ratio 10). The multicomponent hypericin lipopolyplexes were characterized by an average size, surface potential, surface morphology and entrapment efficiencies of biomolecules. The results concluded that hypericin lipopolyplexes were nanosized, non-spherical vesicles bearing a slightly positive charge. Gel electrophoresis and fluorescence quenching demonstrated efficient encapsulation of DNA in hypericin lipopolyplexes. A deeper insight into the co-encapsulation of both biomolecules into hypericin lipopolyplexes was assessed by gel-electrophoresis of photoirradiated hypericin lipopolyplexes. Unlike the distinct DNA migration bands from lysed formulation, no DNA migration bands were visible on the agarose bed from photoirradiated hypericin lipopolyplexes. The photoexcitation of entrapped hypericin did

not harm neighbouring pDNA. It has been attributed that DNA has been electrostatically complexed with polycationic polymer IPEI.

Biocompatibility and non-toxicity of hypericin liposomes for non-irradiated HepG2 cells was confirmed. However, hypericin dose- dependent cytotoxicity was apparent under influence of photoirradiation. In-vitro cell viability studies revealed that the induced cytotoxicity is dependent on the photochemical dose. The photochemical dose of hypericin has been subject to depend on the combination of light dose and hypericin concentration. Furthermore, the transfection efficiency of hypericin lipopolyplexes under influences of 200 mJ/cm<sup>2</sup>, 600 mJ/cm<sup>2</sup> and 1000 mJ/cm<sup>2</sup> light doses has been evaluated. Transfection efficiency of hypericin lipopolyplexes augmented significantly, while they induced minimal photocytotoxicity at a lower photochemical dose. Whereas an effective cell killing was caused by photodynamic activity of hypericin at higher photochemical dose. An elevated cellular uptake of Hy- LPP upon photoirradiation at 600 mJ/cm<sup>2</sup> light dose has been interpreted as light-induced facilitated intracellular trafficking. Moreover, transfected hypericin lipopolyplexes exhibited sufficient intracellular ROS generation which has been visualized (by optical microscopy) and quantified (by fluorescence spectroscopy). Thus, the increased transfection efficiency of the nanocarrier has been attributed to intracellular ROS generation, which has been governed by hypericin concentration and effective light dose.

In addition, **chapter 5** engaged the primary characterization of surface-modified anti-transferrin hypericin lipopolyplexes. The prepared conjugated hypericin lipopolyplexes have higher average particle size as compared to the non-conjugated formulation. The cellular internalization of fluorescent tagged holo-transferrin protein, a biomarker for clathrin-mediated endocytosis, weighed on transferrin receptor-mediated endocytosis in HepG2 cells. Further, the conjugated hypericin lipopolyplexes displayed substantial intracellular localization in the HepG2 cells. Although, no significant cellular uptake of conjugated formulation has been observed in the presence of chlorpromazine, clathrin-pathway inhibitor. It revealed that the selective cellular internalization of the nanocarrier occurs via transferrin receptor in the HepG2 cells. Additionally, the surface-modified hypericin lipopolyplexes showed a significant improved and light-induced GFP expression by targeted photochemical internalization process.



In summary, lipopolyplexes, the multicomponent formulation, were successfully developed and delivered using modern physical force i.e., ultrasound and light. The obtained results were promising for improved in-vivo gene transfer in cancer cells. Both formulations exhibited encapsulation of the nucleic acid and displayed physicochemical characteristics ideal for cellular internalization via passive targeting. The modified non-lamellar phospholipid shell imparted sonosensitivity to the formulation. The ultrasound improves the transfection efficiency while remaining biocompatible to cancer cells. On other hand, hypericin lipopolyplexes, ideal carrier for oligonucleotides such as therapeutic siRNA, promises an efficient gene knockdown by photochemical internalization while also exhibiting hypericin induced cytotoxicity by photodynamic activity of photosensitizer. Hence synergistic anticancer effect using siRNA-hypericin lipopolyplexes could be promised. Further, the anti-transferrin antibody conjugated Hy-LPP offers cell targeting for photochemical internalization of the lipopolyplexes and the photoirradiation enhances the in-vitro transfection efficiency of the formulation in cancer cells.

## 7. Zusammenfassung

In der vorliegenden Arbeit wurden zwei Methoden für einen effizienten Gentransfer unter Verwendung von Lipopolyplexen als nicht-virale Trägersysteme untersucht. Ziel war es, einen biokompatiblen und biologisch abbaubaren nicht-viralen Vektor für eine effektive Transfektion von Tumorzellen zu entwickeln. Dieser neuartige Wirkstoffträger für Nukleinsäuren wurde weiterhin so modifiziert, dass er durch Ultraschall oder Lichtbestrahlung aktiviert werden konnte.

Die Einleitung (Kapitel 1) enthält Konzepte, Modalitäten und Funktionalitäten des Projekts, in dem die physiologischen Barrieren, formulierungsbedingte Herausforderungen und die jüngsten Fortschritte bei DNA-basierten Therapeutika beschrieben werden. Die Einleitung konzentriert sich auf den aktuellen Stand der Forschung zu neuartigen Methoden, die notwendig sind, um Gentransfektionssysteme aus dem Endosom freizusetzen. Die derzeit verwendeten nicht-viralen Vektoren auf Lipidbasis werden gegenübergestellt. Außerdem wird ein Überblick über die verschiedenen physikalischen Methoden zur Anwendung in der Gentherapie gegeben. Die grundlegenden physikalischen Prinzipien von Ultraschall und Licht als externe Auslöser für die Genübertragung werden genau erläutert.

Kapitel 2 gibt einen Überblick über die verwendeten Methoden und Materialien. Es behandelt die verschiedenen Methoden, die bei der Entwicklung der nicht-viralen Träger verwendet werden. Präparations- und Charakterisierungsmethoden für ultraschallaktive Lipopolyplexe und Hypericin-Lipopolyplexe werden detailliert beschrieben.

Kapitel 3 befasst sich mit der Herstellung und Charakterisierung von Formulierungen, die sowohl für die Ultraschallbildgebung als auch als effizientes Gentransfektionssystem eingesetzt werden können. Die physikochemische Charakterisierung der ultraschallaktiven Kontrastvesikel mittels Photonenkorrelationsspektroskopie zeigte stabile, monodisperse DPPC/CH/PEG40S-Lipidvesikel. Durch die Anwesenheit von Cholesterin in der Lipiddoppelschicht verbesserte sich der Polydispersitätsindex (PDI). Die Aufnahme von PEG40S in die Phospholipidmischung der ultraschallaktiven Kontrastvesikel trug zur Entwicklung eines Ultraschallkontrasts bei, der in vitro durch

ein hergestelltes Gewebeflussmodell nachgewiesen wurde. Die hergestellte nicht-lamellare Phospholipidhülle DPPC/CH/PEG40S ist charakteristisch für die Bildung ultraschallaktiver Vesikel. Darüber hinaus wurde eine höhere Echogenität aufgrund des Vorhandenseins von DPPG-Lipid in der Phospholipidhülle der ultraschallaktiven DPPC/CH/DPPG/PEG40S-Kontrastvesikel festgestellt. Die Visualisierung des Ultraschallkontrasts wurde als gleichwertig mit einem Standard-Ultraschallkontrastmittel, SonoVue®, befunden. Die Lagerungsbedingungen zeigten keinen offensichtlichen Einfluss auf den Ultraschallkontrast dieser UCVs. Der mittels Rasterkraftmikroskopie ermittelte Partikeldurchmesser stimmte mit der jeweiligen hydrodynamischen Partikelgröße der Formulierungen überein. Darüber hinaus gibt die Visualisierung der Formulierungen einen detaillierten Einblick in die Partikelgrößenverteilung. Die ultraschallaktiven DPPC/CH/DPPG/PEG40S-Vesikel erwiesen sich als monodispers, da die Abstoßung zwischen den Partikeln aufgrund der höheren Oberflächenladung stärker war. Des Weiteren wurde die physikochemische Charakterisierung von Polyplexen (IPEI/pDNA-Komplexe) mittels Photonenkorrelationsspektroskopie und Laser-Doppler-Velocimetrie untersucht. Die polykationischen Komplexe wurden später auch in einem in-vitro-Zellkulturmodell untersucht. Ultraschallaktive Lipopolyplexe wurden unter Verwendung optimierter Polyplexe (N/P-Verhältnis 12) und ultraschallaktiver Kontrastvesikel hergestellt. Die Formulierungen mit unterschiedlichen Liposom/PEI-Massenverhältnissen wurden in der SKOV-3-Zelllinie untersucht. Die ultraschallaktiven DPPC/CH/DPPG/PEG40S-Lipopolyplexe haben eine minimale durchschnittliche Teilchengröße und sind leicht positiv geladen. Die ternäre Formulierung mit einem Durchmesser von  $168,84 \pm 5,4$  nm und einem positiven Oberflächenpotenzial gewährleistete die zelluläre Internalisierung der Formulierung.

Der Einfluss von Faktoren wie der Polymerkonzentration und der Lipidkonzentration auf die Transfektionseffizienz und die Zytotoxizität in SKOV-3-Zellen wurde untersucht. Die Ergebnisse dieser Experimente ergaben ein optimiertes N/P-Verhältnis für Polyplexe und Liposom/PEI-Massenverhältnisse für Lipopolyplexe. Im Vergleich zu den Polyplexen (IPEI/pDNA) zeigten die Lipopolyplexe, insbesondere diejenigen mit einem Liposom/PEI-Massenverhältnis von 0,5, eine enorme Steigerung der Expression des Luciferase-Gens. Die Lipidzusammensetzung schirmt das positiv geladene PEI ab und

erleichtert so die zelluläre Internalisierung. Weitere Transfektionsstudien der Polyplexe/Ultraschall-aktiven Vesikelkomplexe (Lipopolyplexe) wurden unter dem Einfluss von Ultraschallbestrahlung ausgewertet. Eine Exposition mit niederfrequenter Ultraschallbestrahlung zeigte eine 50-fach erhöhte Transfektionseffizienz für Zellen mit längeren Posttransfektions-Inkubationszeitintervallen. Die Ergebnisse wurden durch die Visualisierung der verbesserten GFP-Expression in der SKOV-3-Zelllinie bestätigt. Es wurde eine signifikant höhere Transfektionseffizienz von ultraschallaktiven Lipopolyplexen mit Ultraschallbestrahlung als von Lipopolyplexen und Polyplexen beobachtet. Außerdem zeigte die Ultraschallbestrahlung eine positive Wirkung auf Chlorpromazin-behandelte Zellen. Die Ergebnisse deuten darauf hin, dass der Gentransfer bei dieser Methode vom zellulären Internalisierungsprozess abhängt. Die Transfektion in 3D-Zellkulturen zeigte ähnliche Ergebnisse, die durch die GFP-Expression in den Sphäroiden von SKOV-3-Zellen sichtbar gemacht wurden. Die in-vitro-Bewertung konzentriert sich hauptsächlich auf die Wirkung von Ultraschall auf die zelluläre Aufnahme und die Transfektionseffizienz des nicht-viralen Vektors.

In Kapitel 4 wird die physikochemische Charakterisierung eines neuartigen Lipopolyplexsystems für die photochemische Internalisierung eines Gens erläutert. Hypericin, ein hydrophober Photosensibilisator, der leicht an Zellmembranen adsorbiert werden kann, bildet in einer wässrigen Phase Aggregate. Daher ist ein stabiles wässriges Verabreichungssystem für den Photosensibilisator eine Voraussetzung. Die passive Verkapselung von Hypericin, die mit der Ethanol-Injektionsmethode entwickelt wurde, weist eine Verkapselungseffizienz von  $80,24 \pm 5,6$  % auf. Die physikochemische Charakterisierung der DPPC/CH/DSPE-PEG2000-Hypericin-Liposomen wurde mit Hilfe von Photonenkorrelationsspektroskopie, Laser-Doppler-Velocimetrie und TEM bestimmt. Die Ergebnisse bestätigten stabile, monodisperse und negativ geladene Hypericin-Liposomen. Der hydrodynamische Durchmesser der Hypericin-Liposomen, die 200 nM Hypericin enthielten, betrug  $196,5 \pm 10,21$  nm, was mit dem durch Rasterkraftmikroskopie ermittelten Durchmesser von  $214,8 \pm 10,32$  nm übereinstimmte. Die Verkapselung von negativ geladenem Hypericin erniedrigte die Oberflächenladung der Liposomen von  $-14,3 \pm 2,60$  mV auf  $-18,9 \pm 3,32$  mV.

Außerdem wurden kationische Polyplexe (N/P-Verhältnis 10, optimiert durch den Gel-Retardierungs-Assay) mit negativ geladenen Hypericin-Liposomen komplexiert was zu Lipopolyplexen führte. Hypericin-Lipopolyplexe wurden bezüglich Größe, Oberflächenpotenzial, Morphologie sowie Verkapselungseffizienz charakterisiert. Die Ergebnisse zeigten, dass es sich bei den Hypericin-Lipopolyplexen um nanoskalige Formulierungen mit leicht positiver Ladung handelte, die als nicht kugelförmige Vesikel sichtbar wurden. Gel-Retardierungs-Assay und Fluoreszenzlöschung zeigten eine effiziente Verkapselung von DNA in Hypericin-Lipopolyplexen. Ein tieferer Einblick in die gemeinsame Verkapselung beider Biomoleküle in Hypericin-Lipopolyplexen wurde durch Gelelektrophorese von mit Licht bestrahlten Hypericin-Lipopolyplexen ermittelt. Im Gegensatz zu den ausgeprägten DNA-Migrationsbanden bei der Elektrophorese der lysierten Formulierung waren bei den lichtbestrahlten Hypericin-Lipopolyplexen keine DNA-Migrationsbanden im Agarose Gel sichtbar. Die Photoanregung des eingeschlossenen Hypericins hat die benachbarte pDNA, die mit dem polykationischen Polymer IPEI elektrostatisch komplexiert wurde, nicht beeinträchtigt.

Die Biokompatibilität und Nichttoxizität von Hypericin-Liposomen für nicht bestrahlte HepG2-Zellen wurde bestätigt. Unter dem Einfluss von Lichtstrahlung wurde jedoch eine dosisabhängige Zytotoxizität von Hypericin festgestellt. Die photochemische Dosis wurde durch die Kombination von Lichtdosis und Hypericin-Konzentration bestimmt. In vitro Studien zur Zellviabilität zeigten, dass die induzierte Zytotoxizität von der photochemischen Dosis abhängig ist. Darüber hinaus wurde die Transfektionseffizienz von Hypericin-Lipopolyplexen unter dem Einfluss von 200 mJ/cm<sup>2</sup>, 600 mJ/cm<sup>2</sup> und 1000 mJ/cm<sup>2</sup> Lichtdosen untersucht. Die Transfektionseffizienz von Hypericin-Lipopolyplexen erhöhte sich signifikant, während sie bei einer niedrigeren photochemischen Dosis nur eine minimale Phototoxizität verursachten. Bei einer höheren photochemischen Dosis führte die photodynamische Aktivität von Hypericin zu einer effektiven Zelltötung. Die erhöhte zelluläre Aufnahme von Hypericin-Lipopolyplexen bei einer Lichtbestrahlung mit einer Lichtdosis von 600 mJ/cm<sup>2</sup> wurde als lichtinduzierter erleichterter intrazellulärer Transport interpretiert. Darüber hinaus wiesen transfizierte Hypericin-Lipopolyplexe eine ausreichende intrazelluläre ROS-Bildung auf, die visualisiert (durch optische Mikroskopie) und quantifiziert (durch Fluoreszenzspektroskopie) werden konnte. Die erhöhte Transfektionseffizienz des

Nanoträgers wurde also auf die intrazelluläre ROS-Bildung zurückgeführt, die von der Hypericin-Konzentration und der effektiven Lichtdosis bestimmt wurde.

Darüber hinaus befasste sich Kapitel 5 mit der vorläufigen Charakterisierung von oberflächenmodifizierten Anti-Transferrin-Hypericin-Lipopolyplexen. Die hergestellten konjugierten Hypericin-Lipopolyplexe haben eine höhere durchschnittliche Partikelgröße als die nicht konjugierte Formulierung. Die konjugierten Hypericin-Lipopolyplexe zeigten eine deutliche intrazelluläre Lokalisierung. Allerdings wurde keine signifikante zelluläre Aufnahme der konjugierten Formulierung in Gegenwart von Chlorpromazin, einem Inhibitor des Clathrin-vermittelten Signalwegs, beobachtet. Des Weiteren wurde die zelluläre Internalisierung von Fluoreszenz-markiertem Holo-Transferrin-Protein, einem Biomarker für die Clathrin-vermittelte Endozytose, mit der Transferrin-Rezeptor-vermittelten Endozytose in HepG2-Zellen abgewogen. Die Ergebnisse bestätigten, dass die zelluläre Internalisierung des Nanocarriers über den Transferrin-Rezeptor in den HepG2-Zellen erfolgt. Zusätzlich zeigten die oberflächenmodifizierten Hypericin-Lipopolyplexe eine durch Lichtstrahlung induzierte signifikant verbesserte GFP-Expression in HepG2-Zellen.

Zusammenfassend lässt sich sagen, dass Lipopolyplexe erfolgreich entwickelt und mit Hilfe praktikabler physikalischer Methoden, bsw Ultraschall und Lichtexposition, angewendet wurden. Beide Formulierungen zeigten eine Verkapselung der Nukleinsäure und wiesen physikochemische Eigenschaften auf, die ideal für die zelluläre Internalisierung durch passives Targeting sind. Bei den ultraschallaktiven Lipopolyplexen zeigte sich, dass die Ultraschallexposition die Transfektionseffizienz verbessert und gleichzeitig biokompatibel mit den Zellen bleibt. Hypericin-Lipopolyplexe hingegen zeigten, dass die Lichtstrahlung zu einer erhöhten Transfektion durch photochemische Internalisierung führt und gleichzeitig eine minimale Zytotoxizität aufgrund der photodynamischen Aktivität des Photosensibilisators aufweist. Die Verkapselung von therapeutischen Oligonukleotiden verspricht eine synergistische krebshemmende Wirkung von Hypericin-Lipopolyplexen. Darüber hinaus zeigten mit Antikörper konjugierte Hypericin-Lipopolyplexe eine Zellspezifität (aktives Targeting) für die photochemische Internalisierung der Nukleinsäure. Zusammenfassend lässt sich sagen, dass beide Genträgersysteme hervorragend für einen effektiven in vivo Gentransfer für die Tumorthherapie geeignet sind.

## 8. Appendix

### 8.1 References

- 1) Patil S. et al., DNA-based therapeutics and DNA delivery systems: a comprehensive review. *The AAPS journal* 2005, (1), E61. DOI: 10.1208/aapsj070109.
- 2) Wirth T et al., Gene Therapy Used in Cancer Treatment. *Biomedicines* 2014, 2 (2), 149 -162. DOI: 10.3390/biomedicines2020149.
- 3) Shahryari A. et al., Engineering Gene Therapy: Advances and Barriers. *Advanced Therapeutics* 2021, (9), 2100040. DOI: 10.1002/adtp.202100040.
- 4) Jinturkar K. et al., Challenges and Opportunities in Gene Delivery. *Challenges in Delivery of Therapeutic Genomic and Proteomics* 2011, Chapter 2, 45-82.
- 5) Kulkarni J. et al., The current landscape of nucleic acid therapeutics. *Nature Nanotechnology* 2021, 16 (6), 630–643. DOI: 10.1038/s41565-021-00898-0.
- 6) Mohammed S. et al., Nonviral gene delivery: principle, limitations, and recent progress. *The AAPS journal* 2009, 11 (4), 671. DOI: 10.1208/s12248-009-9143-y
- 7) Sung Y. et al., Recent advances in the development of gene delivery systems. *Biomaterials Research* 2019, 23 (1), 8. DOI: 10.1186/s40824-019-0156-z.
- 8) Uherek C. et al., DNA-carrier proteins for targeted gene delivery. *Adv Drug Deliv Rev* 2000, 15 (44), 153-166. DOI: 10.1016/s0169-409x(00)00092-2.
- 9) Weeratna R. et al. Designing gene therapy vectors: avoiding immune responses by using tissue-specific promoters. *Gene Therapy* 2001, 8 (24), 1872–1878.
- 10) Butler J. et al., Enhancer-promoter specificity mediated by DPE or TATA core promoter motifs. *Genes and Development* 2001, 15, 2515-2519.
- 11) Zhang W. et al., The First Approved Gene Therapy Product for Cancer Ad-p53 (Gendicine): 12 Years in the Clinic. *Hum Gene Ther.* 2018, 29 (2), 160-179. DOI: 10.1089/hum.2017.218.
- 12) Holmlund J T. et al., Applying Antisense Technology. *Annals of the New York Academy of Sciences* 2003, 1002, 244-251. DOI: 10.1196/annals.1281.027.
- 13) Villalona-Calero M A. et al., A phase I/II study of LY900003, an antisense inhibitor of protein kinase C-alpha, in combination with cisplatin and gemcitabine in patients

- with advanced non-small cell lung cancer. *Clin Cancer Res.* 2004, 15 (10), 6086-6093. DOI: 10.1158/1078-0432.CCR-04-0779.
- 14) Jairath V. et al., Alicaforsen for the treatment of inflammatory bowel disease. *Expert Opin Investig Drugs.* 2017, 26 (8), 991-997. DOI: 10.1080/13543784.2017.1349753.
  - 15) Banerjee D, Genasense (Genta Inc). *Curr Opin Investig Drugs.* 2001, 2 (4), 574-580.
  - 16) Schoenmaker L. et al., mRNA-lipid nanoparticle COVID-19 vaccines: Structure and stability. *Int J Pharm.* 2021, (1873-3476 (Electronic)), 601:120586.
  - 17) Sriraman SK. et al., Barriers to drug delivery in solid tumors. *Tissue Barriers.* 2014, (2). DOI:10.4161/tisb.29528.
  - 18) Xie Y. et al., Targeted delivery of siRNA to activated T cells via transferrin-polyethylenimine (Tf-PEI) as a potential therapy of asthma. *Journal of control release.* 2016, 10 (229), 120-129. DOI: 10.1016/j.jconrel.2016.03.029.
  - 19) Liu C et al., Barriers and Strategies of Cationic Liposomes for Cancer Gene Therapy. *Mol Ther Methods Clin Dev* 2020, 18, 751-764. DOI: 10.1016/j.omtm.2020.07.015.
  - 20) Bingyang Shi et al., Challenges in DNA Delivery and Recent Advances in Multifunctional Polymeric DNA Delivery Systems. *Biomacromolecules* 2017, 18 (8), 2231–2246. DOI: 10.1021/acs.biomac.7b00803.
  - 21) Thomas O et al., Overcoming Physiological Barriers to Nanoparticle Delivery—Are We There Yet? *Front. Bioeng. Biotechnol.* 2019, 7, 415. DOI: 10.3389/fbioe.2019.00415.
  - 22) Boegh M et al., Mucus as a Barrier to Drug Delivery—Understanding and Mimicking the Barrier Properties. *Basic and Clinical Pharmacology and Toxicology.* 2015, 116, 179-186.
  - 23) Abbott NJ et al., Structure and function of the blood–brain barrier. *Neurobiol Dis.* 2010, 37 (1), 13–25.
  - 24) Kadry H et al., A blood–brain barrier overview on structure, function, impairment, and biomarkers of integrity. *Fluids Barriers of the CNS* 2020, 17. DOI: doi.org/10.1186/s12987-020-00230-3.
  - 25) Ballabh P et al., The blood–brain barrier: an overview: structure, regulation, and clinical implications. *Neurobiol Dis.* 2004, 16 (1), 1-13.
  - 26) Bastacky J et al., Alveolar lining layer is thin and continuous: low-temperature scanning electron microscopy of rat lung. *J Appl Physiol* 1995, 258, L134–147.



- 27) Geiser M et al., Update on macrophage clearance of inhaled micro- and nanoparticles. *J Aerosol Med Pulm Drug Deliv* 2010, 23, 207-217.
- 28) Shoyele S A et al., Particle engineering techniques for inhaled biopharmaceuticals. *Adv Drug Deliv Rev* 2006, 58, 1009-1029.
- 29) Francia V et al., Interactions at the cell membrane and pathways of internalization of nano-sized materials for nanomedicine. *Beilstein J Nanotechnol.* 2020, 11, 338-353. DOI: 10.3762/bjnano.11.25.
- 30) Chen K L et al., Nanoparticles meet cell membranes: probing nonspecific interactions using model membranes. *Environ Sci Technol.* 2014, 48, 873–880. DOI: 10.1021/es403864v.
- 31) Manzanares D et al., Endocytosis: The Nanoparticle and Submicron Nanocompounds Gateway into the Cell. *Pharmaceutics* 2020, 12 (4), 371
- 32) Longfa Kou et al., The endocytosis and intracellular fate of nanomedicines: Implication for rational design. *Asian Journal of Pharmaceutical Sciences* 2013, 8 (1), 1-10. DOI: 10.1016/j.ajps.2013.07.001.
- 33) Liu C et al., Barriers and Strategies of Cationic Liposomes for Cancer Gene Therapy. *Mol Ther Methods Clin Dev* 2020, 18(7), 51-764. DOI: 10.1016/j.omtm.2020.07.015.
- 34) Etoc F et al., Non-specific interactions govern cytosolic diffusion of nanosized objects in mammalian cell. *Nat. Mater.* 2018, 17.
- 35) Lukacs G L. et al., Size-dependent DNA mobility in cytoplasm and nucleus. *J. Biol. Chem* 2000, 275.
- 36) Pouton C W. et al., Key issues in non-viral gene delivery. *Adv Drug Deliv Rev.* 2001, 46 (1-3), 187-203. DOI: 10.1016/s0169-409x(00)00133-2.
- 37) Rettig G R et al., Non-viral gene delivery: from the needle to the nucleus. *Expert Opin Biol Ther.* 2007, 7 (6), 799-808. DOI: 10.1517/14712598.7.6.799.
- 38) Wiethoff C M et al., Barriers to nonviral gene delivery. *J Pharm Sci.* 2003, 92 (2), 203-217. DOI:10.1002/jps.10286.
- 39) Bally M B et al., Biological barriers to cellular delivery of lipid-based DNA carriers. *Adv Drug Deliv Rev.* 1999, 38 (3), 291-315. DOI: 10.1016/s0169-409x(99)00034-4.
- 40) Kamiya H et al., Intracellular trafficking and transgene expression of viral and non-viral gene vectors. *Adv Drug Deliv Rev* 2001, 52 (3), 153-164. DOI: 10.1016/s0169-409x(01)00216-2.

- 41) Scheule R K, The role of CpG motifs in immunostimulation and gene therapy. *Adv Drug Deliv Rev.* 2000, 44 (2-3), 119-134. DOI: 10.1016/s0169-409x(00)00090-9.
- 42) Yew N S et al., CpG-depleted plasmid DNA vectors with enhanced safety and long-term gene expression in vivo. *Mol Ther* 2002, 5 (6), 731-738.
- 43) Sullivan S M et al., Introduction to gene therapy and guidelines to Pharmaceutical development. In *Pharmaceutical gene delivery system*, 1st Edition ed.; Rolland, A. Ed.; CRC Press, 2003.
- 44) Degors I. et al., Carriers Break Barriers in Drug Delivery: Endocytosis and Endosomal Escape of Gene Delivery Vectors. *Accounts of Chemical Research* 2019, 52 (7), 1750-1760.
- 45) Grigsby C. et al., Balancing protection and release of DNA: tools to address a bottleneck of non-viral gene delivery. *Journal of the Royal Society, Interface* 2010, 7 (Suppl 1), S67-S82. DOI: 10.1098/rsif.2009.0260
- 46) Stenmark H et al., The Rab GTPase family. *Genome Biol.* 2001, 2 (5), reviews3007.3001–reviews3007.3007. DOI:10.1186/gb-2001-2-5-reviews3007.
- 47) Villarroel-Campos D et al., Rab-mediated trafficking role in neurite formation. *J Neurochem.* 2014, 129 (2).
- 48) Li X et al., The recycling endosome and its role in neurological disorders. *Prog Neurobiol.* 2012, 97 (2), 127–141. DOI: doi:10.1016/j.pneurobio.2011.10.002.
- 49) Sönnichsen B. et al., Distinct membrane domains on endosomes in the recycling pathway visualized by multicolor imaging of Rab4, Rab5, and Rab11. *The Journal of cell biology* 2000, (4), 901. DOI: 10.1083/jcb.149.4.901
- 50) Rennick, J.J. et al., Key principles and methods for studying the endocytosis of biological and nanoparticle therapeutics. *Nat. Nanotechnol.* 2021, 16, 266–276 (2021). DOI:10.1038/s41565-021-00858-8
- 51) Plummer M et al., Endocytic uptake pathways utilized by CPMV nanoparticles. *Molecular Pharmaceutics* 2013, 10 (1), 26-32. DOI:10.1021/mp300238w.
- 52) Yashunsky V. et al., Real-time monitoring of transferrin-induced endocytic vesicle formation by mid-infrared surface plasmon resonance. *Biophysical Journal* 2009, (4), 1003. DOI: 10.1016/j.bpj.2009.05.052
- 53) Daniel J. et al., Rafting with cholera toxin: endocytosis and trafficking from plasma membrane to ER. *FEMS microbiology letters* 2007, (2), 129–137. DOI: 10.1111/j.1574-6968.2006.00545.

- 54) Snapp, E et al., Design and use of fluorescent fusion proteins in cell biology. *Current protocols in cell biology* 2005, Chapter 21, 113. DOI: 10.1002/0471143030.cb2104s27
- 55) Shearer L J et al., Distribution and Co-localization of endosome markers in cells. *Heliyon*. 2019, (9), e02375. DOI:10.1016/j.heliyon.2019.e02375.
- 56) Oshiro-Júnior J. et al., Stimuli-responsive drug delivery nanocarriers in the treatment of breast cancer. *Current medicinal chemistry* 2020, 27 (15), 2494-2513.
- 57) Tian H. et al., pH-responsive zwitterionic copolypeptides as charge conversional shielding system for gene carriers. *Journal of Controlled Release* 2014, 174, 117-125. DOI:10.1016/j.jconrel.2013.11.008.
- 58) Yadav P. et al., Recent advances in nanocarriers-based drug delivery for cancer therapeutics: A review. *Reactive and Functional Polymers* 2021, 165, 104970. DOI:10.1016/j.reactfunctpolym.2021.104970.
- 59) Adelina-Gabriela Niculescu et al., New Applications of Lipid and Polymer-Based Nanoparticles for Nucleic Acids Delivery. *Pharmaceutics* 2021, (12), 2053. DOI: 0.3390/pharmaceutics13122053
- 60) Tros de Ilarduya C et al., Gene delivery by lipoplexes and polyplexes. *European Journal of Pharmaceutical Sciences* 2010, 40 (3), 159-170. DOI:10.1016/j.ejps.2010.03.019.
- 61) Zuhorn et al., Nonbilayer phase of lipoplex–membrane mixture determines endosomal escape of genetic cargo and transfection efficiency. *Molecular Therapy* 2005, 11 (5), 801-810. DOI:10.1016/j.ymthe.2004.12.018.
- 62) Mundra V et al., Design of nanocarriers for efficient cellular uptake and endosomal release of small molecule and nucleic acid drugs. *Front. Chem. Sci. Eng* 2014, 8 (4), 387-404
- 63) Forrest M. L et al., On the Kinetics of Polyplex Endocytic Trafficking: Implications for Gene Delivery Vector Design. *Molecular Therapy* 2002, 6 (1), 57-66. DOI:10.1006/mthe.2002.0631.
- 64) Berg K et al., A. Photochemical internalization: a novel technology for delivery of macromolecules into cytosol. *Cancer Res.* 1999, 59 (0008-5472 (Print)), 1180-1183.
- 65) Panje C. M. et al., Ultrasound-Mediated Gene Delivery with Cationic Versus Neutral Microbubbles: Effect of DNA and Microbubble Dose on In Vivo Transfection Efficiency. *Theranostics* 2012, 2 (11), 1078-1091, DOI: 10.7150/thno.4240.

- 66) Alice Abu Dayyih et al., Thermosensitive liposomes encapsulating hypericin: Characterization and photodynamic efficiency. *International Journal of Pharmaceutics* 2021, 609, 121195.
- 67) Younis M et al., Gene Therapy for Hepatocellular Carcinoma: Highlighting the Journey from Theory to Clinical Applications. *Advanced Therapeutics* 2020, (11), 2000087. DOI:10.1002/adtp.202000087
- 68) Ueno S et al., Development of ErbB2-Targeting Liposomes for Enhancing Drug Delivery to ErbB2-Positive Breast Cancer. *Pharmaceutics* 2020, 12(6) (1999-4923 (Print)), 585. DOI:10.3390/pharmaceutics12060585.
- 69) Balazs DA et al., Liposomes for use in gene delivery. *J Drug Deliv.* 2011, 326497. DOI: 10.1155/2011/326497.
- 70) T. Bus et al., The great escape: how cationic polyplexes overcome the endosomal barrier. *Journal of Materials Chemistry B* 2018, 6, 6904 - 6918
- 71) Hoffmann M et al., Complex Size and Surface Charge Determine Nucleic Acid Transfer by Fusogenic Liposomes. *Int J Mol Sci.* 2020, 21 (6), 2244. DOI: 10.3390/ijms21062244.
- 72) Simões S et al., Cationic liposomes for gene delivery. *Expert Opinion on Drug Delivery* 2005, (2), 237. DOI:10.1517/17425247.2.2.237.
- 73) Y. Xia et al., Effect of surface properties on liposomal siRNA delivery. *Biomaterials* 2016, 79, 56-68.
- 74) Lombardo D et al., Methods of Liposomes Preparation: Formation and Control Factors of Versatile Nanocarriers for Biomedical and Nanomedicine Application. *Pharmaceutics* 2022, 14 (3), 543. DOI: 10.3390/pharmaceutics14030543
- 75) Singh P et al., Lipoplex-based therapeutics for effective oligonucleotide delivery: a compendious review. *Journal of Liposome Research* 2020, 30 (4), 313-335. DOI: 10.1080/08982104.2019.1652645.
- 76) Kim B et al., DOTAP/DOPE ratio and cell type determine transfection efficiency with DOTAP-liposomes. *Biochim. Biophys. Acta*, 2015, 1848, 1996-2001. DOI:10.1016/j.bbamem.2015.06.020
- 77) Ellens H et al., Membrane fusion and inverted phases. *Biochemistry* 1989, 28 (9), 3692-3703. DOI: 10.1021/bi00435a011.

- 78) Engelhardt K. et al., Transfection Studies with Colloidal Systems Containing Highly Purified Bipolar Tetraether Lipids from *Sulfolobus acidocaldarius*. *Archaea* 2017; 8047149. DOI:10.1155/2017/8047149.
- 79) Wong A et al., DNA Internalized via Caveolae Requires Microtubule-dependent, Rab7-independent Transport to the Late Endocytic Pathway for Delivery to the Nucleus. *Journal of Biological Chemistry* 2007; 282 (31), 22953-22963. DOI:10.1074/jbc.M611015200.
- 80) Granot Y. et al., Delivering the right message: Challenges and opportunities in lipid nanoparticles-mediated modified mRNA therapeutics-An innate immune system standpoint. *Semin Immunol* 2017; 34 (1096-3618 (Electronic)), 68-77.
- 81) Shepherd S et al., Scalable mRNA and siRNA Lipid Nanoparticle Production Using a Parallelized Microfluidic Device. *Nano Letters* 2021, 21 (13), 5671-5680. DOI:10.1021/acs.nanolett.1c01353.
- 82) Hou X. et al., Lipid nanoparticles for mRNA delivery. *Nat Rev Mater* 2021, 6, 1078–1094. DOI:10.1038/s41578-021-00358-0.
- 83) Kim J et al., Self-assembled mRNA vaccines. *Adv. Drug Deliv. Rev* 2021, 170.
- 84) Leung K et al., Microfluidic mixing: a general method for encapsulating macromolecules in lipid nanoparticle systems. *J. Phys. Chem. B.* 2015, 119, 8698–8706.
- 85) Olbrich C et al., Cationic solid-lipid nanoparticles can efficiently bind and transfect plasmid DNA. *J Control Release.* 2001, 77 (3), 345-355. DOI: 10.1016/s0168-3659(01)00506-5
- 86) Shidhaye S et al., Solid Lipid Nanoparticles and Nanostructured Lipid Carriers. *Innovative Generations of Solid Lipid Carriers. Current Drug Delivery* 2008, 5.
- 87) Sentjurc M et al., Effect of colloidal carriers on ascorbyl palmitate stability. *Eur. J. Pharm. Sci* 2003, 19 (4).
- 88) Tenchov R et al., Lipid Nanoparticles—From Liposomes to mRNA Vaccine Delivery, a Landscape of Research Diversity and Advancement. *ACS Nano* 2021, 15 (11), 16982–17015.
- 89) Tabatt K et al., Transfection with different colloidal systems: comparison of solid lipid nanoparticles and liposomes. *J Control Release.* 2004, 97 (2), 321-332. DOI:10.1016/j.jconrel.2004.02.029.

- 90) Dolatabadi J et al., Solid Lipid Nanoparticles as Efficient Drug and Gene Delivery Systems: Recent Breakthroughs. *Adv Pharm Bull.* 2015, 5 (2), 151-159. DOI:10.15171/apb.2015.022.
- 91) Kneuer C et al., The influence of physicochemical parameters on the efficacy of non-viral DNA transfection complexes: a comparative study. *J Nanosci Nanotechnol.* 2006, 6 (9-10), 2776-2782. DOI: 10.1166/jnn.2006.409.
- 92) Hall A. et al., Polyplex Evolution: Understanding Biology, Optimizing Performance. *Molecular therapy : the journal of the American Society of Gene Therapy* 2017; 25 (7), 1476-1490. DOI: 10.1016/j.ymthe.2017.01.024
- 93) Hanzlíková M et al., The role of PEI structure and size in the PEI/liposome-mediated synergism of gene transfection. *Plasmid* 2009, 61 (1), 15-21.
- 94) Kunath K et al., The Structure of PEG-Modified Poly(Ethylene Imine)s Influences Biodistribution and Pharmacokinetics of Their Complexes with NF- $\kappa$ B Decoy in Mice. *Pharm Res* 2002, 19, 810–817. DOI: doi.org/10.1023/A:1016152831963.
- 95) Kursá M et al., Novel Shielded Transferrin–Polyethylene Glycol–Polyethylenimine/DNA Complexes for Systemic Tumor-Targeted Gene Transfer. *Bioconjugate Chem* 2003, 14 (1), 222–231.
- 96) Chytlá A et al., nA. High-level expression of palmitoylated MPP1 recombinant protein in mammalian cells. *Membranes* 2021, 11.
- 97) Schäfer J et al., Liposome–polyethylenimine complexes for enhanced DNA and siRNA delivery. *Biomaterials* 2010, 31 (26), 6892-6900. DOI:10.1016/j.biomaterials.2010.05.043.
- 98) Tariq I et al., A promising nanocarrier for enhanced gene delivery with minimal cytotoxicity. *European Journal of Pharmaceutics and Biopharmaceutics* 2019, 135, 72-82. DOI:10.1016/j.ejpb.2018.12.013.
- 99) Chen W et al., Lipopolyplex for Therapeutic Gene Delivery and Its Application for the Treatment of Parkinson's Disease. *Frontiers in aging neuroscience* 2016, 8, 68-68. DOI: 10.3389/fnagi.2016.00068 PubMed.
- 100) García L. et al., Serum-resistant lipopolyplexes for gene delivery to liver tumour cells. *European Journal of Pharmaceutics and Biopharmaceutics* 2007, 67 (1), 58-66. DOI:10.1016/j.ejpb.2007.01.005.

- 101) Ewe A et al., Liposome-polyethylenimine complexes (DPPC-PEI lipopolyplexes) for therapeutic siRNA delivery in vivo. *Nanomedicine* 2017, 13 (1), 209-218. DOI: 10.1016/j.nano.2016.08.005.
- 102) Ewe A et al., Storage stability of optimal liposome-polyethylenimine complexes (lipopolyplexes) for DNA or siRNA delivery. *Acta Biomater* 2014, 10, 2663–2673. DOI:10.1016/j.actbio.2014.02.037.
- 103) Zuhorn IS et al., Phase behavior of cationic amphiphiles and their mixtures with helper lipid influences lipoplex shape, DNA translocation, and transfection efficiency. *Biophys J.* 2002, 83 (4), 2096 - 2108. DOI:10.1016/S0006-3495(02)73970-2.
- 104) Pelisek J et al., Optimized lipoplexes formulations for gene transfer to human colon carcinoma cells under in vitro conditions. *J. Gene Med* 2006, 8, 186-197. DOI:10.1002/jgm.836.
- 105) Luis Brito L et al., Poly( $\beta$ -amino ester) and Cationic Phospholipid-Based Lipopolyplexes for Gene Delivery and Transfection in Human Aortic Endothelial and Smooth Muscle Cells. *Biomacromolecules* 2008, 9 (4), 1179-1187. DOI:10.1021/bm7011373.
- 106) Wang B et al., Chitosan enhanced gene delivery of cationic liposome via non-covalent conjugation. *Biotechnol Lett* 2012, 34, 19-28. DOI:10.1007/s10529-011-0748-8.
- 107) Mahmoudi A et al., Preparation and in-vitro Transfection Efficiency Evaluation of Modified Cationic Liposome-polyethyleneimine-plasmid Nanocomplexes as a Novel Gene Carrier. *Current Drug Delivery* 2014, 11 (5). DOI:10.2174/1567201811666140616160237
- 108) Perche F et al., Selective gene delivery in dendritic cells with mannosylated and histidylated lipopolyplexes. *Journal of Drug Targeting* 2011, 19 (5), 315-325. DOI:10.3109/1061186X.2010.504262.
- 109) Reza K et al., Cationic liposomes-polyallylamine-plasmid nanocomplexes for gene delivery. *Journal of Experimental Nanoscience* 2014, 9 (10), 1026-1034. DOI:10.1080/17458080.2013.771245
- 110) Ma K et al., Development of a successive targeting liposome with multi-ligand for efficient targeting gene delivery. *J. Gene Med* 2011, 13, 290-301.

- 111) Song H et al., Cationic lipid-coated PEI/DNA polyplexes with improved efficiency and reduced cytotoxicity for gene delivery into mesenchymal stem cells. *International Journal of nanomedicine* 2012, 7, 4637.
- 112) VILLEMEJANE J et al., Physical methods of nucleic acid transfer: general concepts and applications. *British journal of pharmacology* 2009, 157 (2), 207-219. DOI: 10.1111/j.1476-5381.2009.00032.
- 113) Newman C et al., Gene therapy progress and prospects: Ultrasound for gene transfer. *Gene Ther* 2007, 14 (6), 465 –475. DOI: 10.1038/sj.gt.3302925.
- 114) Cool S. K. et al., Enhancing Nucleic Acid Delivery with Ultrasound and Microbubbles. In *Nanotechnology for Nucleic Acid Delivery: Methods and Protocols*, Ogris, M., Oupicky, D. Eds.; Humana Press, 2013, pp 195-204.
- 115) Kiessling F et al., Recent advances in molecular, multimodal and theranostic ultrasound imaging. *Advanced Drug Delivery Reviews* 2014, 72, 15-27. DOI:10.1016/j.addr.2013.11.013.
- 116) Hyvelin J. M et al., Characteristics and Echogenicity of Clinical Ultrasound Contrast Agents: An In Vitro and In Vivo Comparison Study. *Journal of Ultrasound in Medicine* 2017, 36 (5), 941-953. DOI:10.7863/ultra.16.04059.
- 117) Yin T et al., Nanobubbles for enhanced ultrasound imaging of tumors. *International journal of nanomedicine* 2012, 7, 895-904. DOI:10.2147/IJN.S28830.
- 118) Canavese G et al., Nanoparticle-assisted ultrasound: A special focus on sonodynamic therapy against cancer. *Chemical Engineering Journal* 2018, 340, 155-172. DOI:10.1016/j.cej.2018.01.060.
- 119) Tian Y et al., New Aspects of Ultrasound-Mediated Targeted Delivery and Therapy for Cancer. *Int J Nanomedicine* 2020, 15, 401-418.
- 120) Høgset A et al., Photochemical internalisation in drug and gene delivery. *Advanced drug delivery reviews* 2004, 56 (1), 95-115.
- 121) Berstad M et al., Photochemical internalization (PCI) of HER2-targeted toxins: Synergy is dependent on the treatment sequence. (12), 1849.
- 122) Selbo P et al., Photochemical Internalisation: A Novel Drug Delivery System. *Tumor Biology* 23 (2), 103-112. DOI: 10.1159/000059713.
- 123) Oliveira S et al., Photochemical internalization enhances silencing of epidermal growth factor receptor through improved endosomal escape of siRNA. *Biochimica et Biophysica Acta (BBA)- Biomembranes* 2007, 1768 (5), 1211-1217.



- 124) Feng L et al., Cisplatin-Prodrug-Constructed Liposomes as a Versatile Theranostic Nanoplatfom for Bimodal Imaging Guided Combination Cancer Therapy. *Advanced Functional Materials* 2016, (13), 2207-2217.
- 125) Adigbli K et al., Photochemical internalisation of chemotherapy potentiates killing of multidrug-resistant breast and bladder cancer cells. *British Journal of Cancer* 2007, 97(4), 502-512. DOI: 10.1038/sj.bjc.6603895.
- 126) Pinnapireddy S R et al., Composite liposome-PEI/nucleic acid lipopolyplexes for safe and efficient gene delivery and gene knockdown. *Colloids and Surfaces B: Biointerfaces* 2017, 158, 93-101.
- 127) Raval N et al., Method and its Composition for encapsulation, stabilization, and delivery of siRNA in Anionic polymeric nanoplex: An In vitro- In vivo Assessment. *Scientific Reports* 2019, 9 (1), 16047. DOI: 10.1038/s41598-019-52390-4.
- 128) Brüßler J. et al., Correlation of structure and echogenicity of nanoscaled ultrasound contrast agents in vitro. *Colloids and Surfaces B: Biointerfaces* 2014, 117, 206-215. DOI:10.1016/j.colsurfb.2014.02.029.
- 129) Plenagl N. et al., Photodynamic therapy - hypericin tetraether liposome conjugates and their antitumor and antiangiogenic activity. *Drug Deliv.* 2019, 26(1), 23-33. DOI: 10.1080/10717544.2018.1531954.
- 130) Ewe A. et al., A novel tyrosine-modified low molecular weight polyethylenimine (P10Y) for efficient siRNA delivery in vitro and in vivo. *Journal of Controlled Release* 2016, 230, 13-25. DOI: 10.1016/j.jconrel.2016.03.034.
- 131) Tariq I. et al., Lipodendriplexes mediated enhanced gene delivery: a cellular to pre-clinical investigation. *Scientific Reports* 2020, 10 (21446). DOI: 10.1038/s41598-020-78123-6.
- 132) Ali S. et al., Lipoparticles for Synergistic Chemo-Photodynamic Therapy to Ovarian Carcinoma Cells: In vitro and in vivo Assessments. *Int J Nanomedicine*. 2021, 11;16 (1178-2013 (Electronic)), 951-976. DOI: 10.2147/IJN.S285950.
- 133) Gucwa A. et al., UIM domain-dependent recruitment of the endocytic adaptor protein Eps15 to ubiquitin-enriched endosomes. *BMC Cell Biol* 2014, 15 (34). DOI: 10.1186/1471-2121-15-34.
- 134) Marxer E. et al., Development and characterization of new nanoscaled ultrasound active lipid dispersions as contrast agents. *European journal of pharmaceutics and*

- biopharmaceutics: official journal of Arbeitsgemeinschaft für Pharmazeutische Verfahrenstechnik e.V 2010, 77, 430-437. DOI: 10.1016/j.ejpb.2010.12.007.
- 135) Owen, J. et al., The Role of PEG-40-stearate in the Production, Morphology, and Stability of Microbubbles. *Langmuir* 2019, 35 (31), 10014 - 10024. DOI: 10.1021/acs.langmuir.8b02516.
  - 136) Abdalkader, R et al., The development of mechanically formed stable nanobubbles intended for sonoporation-mediated gene transfection. *Drug Deliv.* 2017, 24 (1), 320-327. DOI:10.1080/10717544.2016.1250139.
  - 137) Kurosaki, T. et al., Development of anionic bubble lipopolyplexes for efficient and safe gene transfection with ultrasound exposure in mice. *Journal of Controlled Release* 2014, 176, 24-34. DOI:10.1016/j.jconrel.2013.12.023.
  - 138) Kapoor M. et al., Physicochemical characterization of anionic lipid-based ternary siRNA complexes. *Biochimica et biophysica acta* 2012, 1818 (7), 1603-1612. DOI: 10.1016/j.bbamem.2012.03.013.
  - 139) Brüßler, J. et al., Nanoscaled ultrasound contrast agents for enhanced sonothrombolysis. *Colloids and Surfaces B: Biointerfaces* 2018, 172, 728-733. DOI:10.1016/j.colsurfb.2018.09.037.
  - 140) Suzuki, R. et al., Gene delivery by combination of novel liposomal bubbles with perfluoropropane and ultrasound. *Journal of Controlled Release* 2007, 117 (1), 130-136. DOI:10.1016/j.jconrel.2006.09.008.
  - 141) Yoon, S. et al., Acoustic-transfection for genomic manipulation of single-cells using high frequency ultrasound. *Scientific Reports* 2017, 7 (1), 5275. DOI: 10.1038/s41598-017-05722-1.
  - 142) Dewitte, H. et al., The potential of antigen and TriMix sonoporation using mRNA-loaded microbubbles for ultrasound-triggered cancer immunotherapy. *Journal of Controlled Release* 2014, 194, 28-36. DOI:10.1016/j.jconrel.2014.08.011.
  - 143) Omata D. et al., Bubble Liposomes and Ultrasound Promoted Endosomal Escape of TAT-PEG Liposomes as Gene Delivery Carriers. *Molecular Pharmaceutics* 2011, 8 (6), 2416-2423. DOI: 10.1021/mp200353m.
  - 144) Ibsen S. et al., A novel nested liposome drug delivery vehicle capable of ultrasound triggered release of its payload. *Journal of controlled release* 2011, 155 (3), 358–366. DOI:10.1016/j.jconrel.2011.06.032.

- 145) Amin U et al., Ultrasound-Responsive Smart Drug Delivery System of Lipid Coated Mesoporous Silica Nanoparticles. *Pharmaceutics* 2021, 13 (9), 1396. DOI: 10.3390/pharmaceutics13091396.
- 146) Wang, M. et al., Sonoporation-induced cell membrane permeabilization and cytoskeleton disassembly at varied acoustic and microbubble-cell parameters. *Scientific Reports* 2018, 8 (1), 3885. DOI: 10.1038/s41598-018-22056-8.
- 147) Lentacker I. et al., Ultrasound Exposure of Lipoplex Loaded Microbubbles Facilitates Direct Cytoplasmic Entry of the Lipoplexes. *Molecular Pharmaceutics* 2008; 6 (2), 457. DOI:10.1021/mp800154s.
- 148) Fraire C. et al., Vapor nanobubble is the more reliable photothermal mechanism for inducing endosomal escape of siRNA without disturbing cell homeostasis. *Journal of Controlled Release* 2020; 319, 262-275. DOI: 10.1016/j.jconrel.2019.12.050.
- 149) Yasunaga M. et al., Continuous long-term cytotoxicity monitoring in 3D spheroids of beetle luciferase-expressing hepatocytes by nondestructive bioluminescence measurement. *BMC Biotechnology* 2017; 17 (1), 54. DOI: 10.1186/s12896-017-0374-1.
- 150) Langhans A. et al., Three-Dimensional in Vitro Cell Culture Models in Drug Discovery and Drug Repositioning. *Frontiers in Pharmacology* 2018; 9 (6), Review. DOI: 10.3389/fphar.2018.00006.
- 151) Mellor R. et al., Optimising non-viral gene delivery in a tumour spheroid model. *The Journal of Gene Medicine* 2006; 8 (9), 1160-1170. DOI: 10.1002/jgm.947
- 152) Song Y. et al., Identification of hepatic fibrosis inhibitors through morphometry analysis of a hepatic multicellular spheroids model. *Scientific Reports* 2021; 11 (1), 10931. DOI: 10.1038/s41598-021-90263-x.
- 153) Sardoiwala M. et al., Hypericin-Loaded Transferrin Nanoparticles Induce PP2A-Regulated BMI1 Degradation in Colorectal Cancer-Specific Chemo-Photodynamic Therapy. *ACS Biomaterials Science & Engineering* 2020, (5), 3139. DOI: 10.1021/acsbiomaterials.9b01844.
- 154) Kimberly J. et al., Impact of lipid nanoparticle size on mRNA vaccine immunogenicity. *Journal of Controlled Release* 2021, 335, 237-246. DOI: 10.1016/j.jconrel.2021.05.021.
- 155) Liposomes and The Use of Zeta Potential Measurements to Study Sterically Stabilized Liposomes. Malvern Panalytical. AZoNano. 2019.

- 156) Selbo P. et al., Photochemical internalization provides time- and space-controlled endolysosomal escape of therapeutic molecules. *Journal of Controlled Release* 2010, 148, 2-12.
- 157) Arnida N. et al., PEGylated gene nanocarriers based on block cationomers bearing ethylenediamine repeating units directed to remarkable enhancement of photochemical transfection. *Journal of Controlled Release* 2006, (115), 208-215
- 158) Rezaee M et al., Progress in the development of lipopolyplexes as efficient non-viral gene delivery systems. *Journal of Controlled release* 2016, 236, 1-14.
- 159) Bofinger R et al., Development of lipopolyplexes for gene delivery: A comparison of the effects of differing modes of targeting peptide display on the structure and transfection activities of lipopolyplexes. *Journal of Peptide Science* 2018, 24 (e3131). DOI: 10.1002/psc.3131.
- 160) Zarei H. et al., Multifunctional peptides based on low molecular weight protamine (LMWP) in the structure of polyplexes and lipopolyplexes: Design, preparation and gene delivery characterization. *Journal of Drug Delivery Science and Technology* 2021, 62, 102422. DOI: 10.1016/j.jddst.2021.102422.
- 161) Deepagan V. et al., In situ diselenide-crosslinked polymeric micelles for ROS-mediated anticancer drug delivery. *Biomaterials* 2016, 56-66. DOI: 10.1016/j.biomaterials.2016.06.044.
- 162) Park S. et al., The transfection efficiency of photosensitizer-induced gene delivery to human MSCs and internalization rates of EGFP and Runx2 genes. (27), 6485. DOI:10.1016/j.biomaterials.2012.05.040.
- 163) Lind P. et al., Efficacy of pegylated liposomal doxorubicin in patients with advanced hepatocellular carcinoma. *Acta Oncologica* 2007, (2), 230-233. DOI: 10.1080/02841860600693473.
- 164) Abdelsalam A. et al., Surface tailored zein as a novel delivery system for hypericin: Application in photodynamic therapy. *Material Science and Engineering: C* 2021, 112420. DOI: 10.1016/j.msec.2021.112420.
- 165) Shao C. et al., Facile fabrication of hypericin-entrapped glyconanoparticles for targeted photodynamic therapy. *Int J Nanomedicine*. 2018, 13, 4319-4331. DOI: 10.2147/IJN.S161262.

- 166) Liu L. et al., Effect of Extracellular Matrix Coating on Cancer Cell Membrane Encapsulated Polyethyleneimine/DNA Complexes for Efficient and Targeted DNA Delivery In Vitro. *Molecular Pharmaceutics* 2021, 18 (7), 2803-2822
- 167) Hsueh-Lin Lu et al., Dendrimer phthalocyanine-encapsulated polymeric micelle-mediated photochemical internalization extends the efficacy of photodynamic therapy and overcomes drug-resistance in vivo. *Journal of Controlled Release* 2011, 155, 458-464.
- 168) Marit Hellum A. et al., Photochemically enhanced gene delivery with cationic lipid formulations *Photochem. Photobiol. Sci.* 2003, 407–411.
- 169) Nomoto T et al., Three-layered polyplex micelle as a multifunctional nanocarrier platform for light-induced systemic gene transfer. *Nature Communication* 2014, 5 (1), 3545. DOI: 10.1038/ncomms4545.
- 170) Jerjes W. et al., Photochemical Internalization for Intracellular Drug Delivery. From Basic Mechanisms to Clinical Research. *J Clin Med* 2020, 9 (2), 528. DOI: 10.3390/jcm9020528.
- 171) Gargouri M. et al., Photochemical internalization for pDNA transfection: Evaluation of poly(d,l-lactide-co-glycolide) and poly(ethylenimine) nanoparticles. *International Journal of Pharmaceutics* 2011, 403, 276-284.
- 172) Agostinis P. et al., Hypericin in cancer treatment: more light on the way. *The International Journal of Biochemistry & Cell Biology* 2002, 34, 221–241.
- 173) Jayakumar M. et al., Near-infrared-light-based nano-platform boosts endosomal escape and controls gene knockdown in vivo. *ACS Nano* 2014, 27 (8(5)), 4848-4858. DOI:10.1021/nn500777n.
- 174) Chen W. et al., Photoresponsive endosomal escape enhances gene delivery using liposome–polycation–DNA (LPD) nanovectors. *Journal of Materials Chemistry B* 2018, (32), 5269. DOI: 10.1039/c8tb00994e m3
- 175) Chen W. et al., Light-Triggerable Liposomes for Enhanced Endolysosomal Escape and Gene Silencing in PC12 Cells. *Molecular Therapy: Nucleic Acids* 2017, 7 DOI:10.1016/j.omtn.2017.04.015.
- 176) Li K T et al., The effect of aloe emodin–encapsulated nanoliposome-mediated r-caspase- 3 gene transfection and photodynamic therapy on human gastric cancer cells. *Cancer Medicine* 2015, 5 (2), 361–369. DOI:10.1002/cam4.584.

- 177) Anabousi S. et al., Assessing transferrin modification of liposomes by atomic force microscopy and transmission electron microscopy. *Eur J Pharm Biopharm.* 2005, (2), 295. DOI: 10.1016/j.ejpb.2004.12.009.
- 178) Noguchi, Y., et al., A cell based assay for evaluating binding and uptake of an antibody using hepatic nonparenchymal cells. *Sci Rep* 2021, 11, 8383.
- 179) Deshpande P. et al., Transferrin and octaarginine modified dual-functional liposomes with improved cancer cell targeting and enhanced intracellular delivery for the treatment of ovarian cancer. *Drug Delivery* 2018, (1), 517. DOI: 10.1080/10717544.2018.1435747.
- 180) Xiao X. et al., Antibody incubation at 37°C improves fluorescent immunolabeling in free-floating thick tissue sections. *Biotechniques* 2017, 62(3), 115-122. DOI: 0.2144/000114524.
- 181) Luo M. et al., Systematic Evaluation of Transferrin-Modified Porous Silicon Nanoparticles for Targeted Delivery of Doxorubicin to Glioblastoma. *ACS Applied Materials & Interfaces.* 2019, (37), 33637. DOI:10.1021/acsami.9b10787.
- 182) Shah H. et al., Development and Characterization of Ultrasound Activated Lipopolyplexes for Enhanced Transfection by Low Frequency Ultrasound in In Vitro Tumor Model. *Macromolecular Bioscience* 2020, (12), 2000173. DOI:10.1002/mabi.202000173.
- 183) Loomis K. et al., Specific targeting to B cells by lipid-based nanoparticles conjugated with a novel CD22-ScFv. *Exp Mol Pathol* 2010, 88(2), 238-249. DOI:10.1016/j.yexmp.2010.01.006
- 184) Abela, R., et al. Radiation improves gene delivery by a novel transferrin-lipoplex nanoparticle selectively in cancer cells. *Cancer Gene Ther* 2008, 15, 496–507.
- 185) Gierlich P. et al., Ligand-Targeted Delivery of Photosensitizers for Cancer Treatment. *Molecules* 2020, 25, 5317. DOI:10.3390/molecules25225317.
- 186) Kloeckner J. et al., Photochemically Enhanced Gene Delivery of EGF Receptor-targeted DNA Polyplexes. *Journal of Drug Targeting* 2004, 12 (4), 205-213. DOI:10.1080/10611860410001723090.
- 187) Wei L. et al., Brain tumor-targeted therapy by systemic delivery of siRNA with Transferrin receptor-mediated core-shell nanoparticles. *Int J Pharm.* 2016, (1), 394. DOI: 10.1016/j.ijpharm.2016.06.127.

## 8.2 Abbreviation

AAVs	Adeno-associated viruses
AFM	Atomic force microscopy
BCA	Bicinchoninic acid
BSA	Bovine serum albumin
CMV	Cytomegalovirus
CPZ	Chlorpromazine
CSLM	Confocal Scanning Laser Microscopy
DAPI	4',6-diamidino-2-phenylindole
DCFA	2',7' –dichlorofluorescin diacetate
DCFH	2', 7' –dichlorofluorescein
DMEM	Dulbecco's Modified Eagle Medium (cell culture medium)
EL	Empty liposomes
EPR	Enhanced permeability and retention effect
FCS	Fetal Bovine Serum
FITC	Fluorescein isothiocyanate
FTIR	Fourier-Transform Infrared Spectroscopy
GFP	Green fluorescent protein
HEPES	(4-(2-hydroxyethyl)-1-piperazineethanesulfonic acid )
Hy-LPP	Hypericin lipopolyplexes
HyL	Hypericin liposomes

LDH	Lactate dehydrogenase
LED	Light emitting diodes
LNP	Lipid nanoparticle
IPEI	Linear polyethylimine
LPP	Lipopolyplexes
MTT	[3-(4,5-s-dimethylthiazol-2-yl)-2,5-diphenyl tetrazolium bromide]
NIR	Near infrared light
NMR	Nuclear magnetic resonance
ODN	Oligonucleotide
PBS	Phosphate buffer
PCI	Photochemical internalization
pCMV-GFP	Plasmid for GFP expression
pCMV-Luc	Plasmid for Luciferase expression
PCS	Photon correlation spectroscopy
pDNA	Plasmid DNA
PEG	Polyethyleneglycol
PP	Polyplexes
PS	Photosensitizer
RFU	Relative fluorescent unit
ROS	Reactive oxygen speices



RPMI	Roswell Park Memorial Institute (Cell culture medium)
SDS	Sodium dodecyl sulfate
SUVs	Small unilamellar vesicles
TAE	Tris-acetate-EDTA buffer
TBHP	Tert-Butyl hydroperoxide
TEM	Transmission electron microscopy
Tf	Transferrin
Tf-fitc	FITC labelled holo-transferrin
Tf-Hy-LPP	Transferrin conjugated hypericin lipopolyplexes
UCA	Ultrasound contrast agent
UCVs	Ultrasound contrast vesicles
UV	Ultraviolet light
US	Ultrasound

## 8.3 Research Output

### 8.3.1 Publication

1. In-vitro photoselective transfection by codelivery of photosensitizer and nucleic acid in HepG2 cells using hypericin lipopolyplexes. Shah H, Dayyih AA, Amin MU, Engelhardt K, Pinnapireddy SR, Preis E, Bakowsky U. (in progress)
2. Development and Characterization of Ultrasound Activated Lipopolyplexes for Enhanced Transfection by Low Frequency Ultrasound in in-Vitro Tumor Model. Shah H, Tariq I, Engelhardt K, Bakowsky U, Pinnapireddy SR. *Macromolecular Bioscience*. 2020; 20(12). doi: 10.1002/mabi.202000173.

### 8.3.2 Conference and Workshops

1. CRS Germany Local Chapter, organized by CRS Germany and LMU Munich. Biomedical Center Munich., 20/02/2020 – 21/02/2020
2. Cell culture Under Flow, Workshop ibidi GmbH Gräfelfing, 26/11/2019 – 27/11/2019
3. Workshop on Zetasizer Ultra by Malvern Pananalytical Fachbereich Chemie, Philipps University Marburg, 14/11/2019
4. Writing Lab- Academic writing style for Life and Natural science by MARA Marburg University Research Academy, Philipps University Marburg, 24/11/2018

## 8.4 Curriculum Vitae

Name: Hirva Shah

Birth-date: 24.09.1989

Birth-place: Gujarat, India

Nationality: India

### ***EXPERIENCE***

10/2022 – till present Marburg	<b>Scientist</b> CSL Behring Innovative GmbH
07/2013 – 06/2017 Gujarat, India	<b>Assistant lecturer</b> S.N.L.P. College of Pharmacy Gujarat Technological University
01/2013 - 05/2013 Gujarat, India	<b>Master Thesis</b> S.K.P.C. Pharmaceutical education and research Ganpat University
05/2010 – 08/2010 Gujarat, India	<b>Internship</b> Cadila Healthcare Ltd

---

### ***EDUCATION***

06/2018 – present Marburg	<b>Doctoral study</b> Institute of Pharmazeutical Technology and Biopharmacy, Philipps University Marburg
11/2017 – 08/2018 Bad Homburg	<b>Language school</b> Internationaler Bund (IB)- Hessen
07/2011 – 05/2013 Gujarat, India	<b>Master of Pharmacy (M.Pharm)</b> S.K.P.C. Pharmaceutical education and research Ganpat University (Major subject: Pharmaceutical technology)

09/2007 – 04/2011

**Bachelor of Pharmacy (B.Pharm)**

Gujarat, India

Veer Narmad South Gujarat University

---

2005 -2007

**High school**

Gujarat, India

**Shardayatan**

Gujarat Higher Secondary Education Board

---

***Languages***

**Gujarati** (native language)

**English** (proficient)

**German** (proficient)

---

***Computer-based skills***

MS Office, Design-Expert Stat-Ease®, EndNote,  
Origin, GraphPad, Inkspace, GIMP

---